# MELTING OF D-R MATERIALS IN STEELMAKING SLAGS

by

KHATIBOLESLAM SADRNEZHAAD

B.S., Arya-Mehr University of Technology

Tehran, Iran

1974

Submitted in partial fulfillment of the requirements

for the degree of

DOCTOR OF PHILOSOPHY

at the

Massachusetts Institute of Technology

February 1979

Signature of Author .....
Department of Materials Science and Engineering
January 12, 1979

Certified by .....
.....
Thesis Supervisor

Accepted by .....
.....
Chairman, Departmental Committee on Graduate Students

# ABSTRACT

## MELTING OF D-R MATERIALS IN STEELMAKING SLAGS

by

KHATIBOLESLAM SADRNEZHAAD

Submitted to the Department of Materials Science and Engineering on January 12, 1979 in partial fulfillment of the requirements for the degree of Doctor of Philosophy.

Methods of melting Direct Reduced Iron (DRI) in arc electric furnaces may be optimized through a quantitative analysis of the details of the final reduction-heat transfer systems involved.

The rates of melting of metallized particles immersed in hot liquid slags as influenced by various system variables were investigated. Such variables as (a) the physical and chemical properties of the particles, (b) the rate of ultimate reduction of the direct reduced materials, (c) the evolution of gas formed in the particles, and (d) the conditions of the molten bath of slag all affect the rate of transfer of heat from the bath into the particles.

The rates of evolution and analysis of gas from D-R materials of various degrees of metallization ranging from 86 to 94 percent were determined by heating these materials in an extraction bomb and measuring the rate of flow and composition of the gas evolved.

A simple computer model was developed which predicts the rate of evolution of the gas, the movement of solid-liquid slag interface, and the variation of the temperature within a DRI pellet immersed into the molten slag.

Using this simulation model, the melting time of D-R materials of different sources fed into an electric-steelmaking slag was calculated. The most critical parameters for efficient operation of the DRI-Steelmaking systems were determined.

Thesis Supervisor: John F. Elliott
Title: Professor of Metallurgy

# TABLE OF CONTENTS

TABLE OF CONTENTS (Cont'd.)

TABLE OF CONTENTS (Cont'd.)

TABLE OF CONTENTS (Cont'd.)

TABLE OF CONTENTS (Cont'd.)

TABLE OF CONTENTS (Cont'd.)

# LIST OF TABLES

LIST OF TABLES (Cont'd.)

## LIST OF FIGURES

LIST OF FIGURES (Cont'd.)

LIST OF FIGURES (Cont'd.)

LIST OF FIGURES (Cont'd.)

LIST OF FIGURES (Cont'd.)

LIST OF FIGURES (Cont'd.)

ACKNOWLEDGEMENTS

The author wishes to express his sincere appreciation to Professor John F. Elliott for his supervision, guidance, and constant encouragement throughout the course of this study.

The author also wishes to thank Professors Warren R. Rohsenow, Borivaje B. Mikic and Kenneth A. Smith for their very helpful discussions on the treatment of the effects of local gas evolution and free and forced convection on the Nusselt number of the slag bath.

Thanks are also due to members of the Chemical Metallurgy for the many useful exchanges of ideas.

The National Science Foundation is gratefully acknowledged for their financial support.

# CHAPTER I

## INTRODUCTION

Electric steelmaking with direct reduced iron (DRI) has proved a possible substitution method for conventional steelmaking processes such as scrap-remelting or the blast furnace-BOF process. Although much has been written on the general performance of the electric arc bath as a medium for melting DRI, yet the practice of iron and steel manufacturing suffers from a lack of quantitative information on the behavior of the DRI melting system.

The purpose of this study is to determine the roles that various parameters play until the prereduced iron particles fed into the electric arc bath are totally melted and to analyze the operational conditions under which the rate of production of steel may be enhanced.

The question to be answered is therefore: What are the optimum properties of materials and operational conditions under which the rate of melting of DRI may be maximized? Because of the technical difficulties in running experimental tests at relatively high temperatures corresponding with typical practical DRI melting systems and substantial differences in conditions and properties of various materials employed in such systems, it is desirable to develope a general model that can utilize the available information to reasonably predict the melting time of DRI particles charged into a steelmaking furnace. Simple experimental tests are designed to collect the information that is essential to building such a model. The tests are conducted at temperatures below the melting point of DRI materials. Simple assumptions are made to

extrapolate the model predictions up to the complete melting of the charged particles.

The melting of inert metallic spheres in ferrous silicate slags has earlier been studied by Nauman[58] who has developed a computer model for prediction of the melting rate of cold spheres immersed in slags. He has, however, neglected the variations of the thermal properties of the materials involved as temperature rises. Such variations have a significant effect on the rate of heating and melting of particles in slags. The thermal conductivities of iron and nickel spheres used by Nauman[58] for heat transfer studies, for instance, drop to one and two third of their initial values when the temperature of the immersed object rises 1000°C, while that of the slag shell doubles for a similar temperature change (cf. Table 5-3 and Appendix D).

The chemical reactions that result in the final reduction of D-R pellets immersed in liquid slags result in further changes of the thermal properties of the pellets. The enthalpies of the reduction reactions will be added to the heat capacity of D-R pellets while the changes of the chemical composition and porosity affects the thermal conductivity of the pellets. The evolution of the gases formed in DRI pellets increases the porosity of the shell of slag that may freeze on the pellets and changes the thermal conductivity of the shell.

The conditions of the liquid slags used as media for heating and melting of DRI pellets and growth of the shell of solid slag on periphery of the immersed pellets are influeced by the evolution of gas from the pellets into the slag (chap. VI). As will be seen later, the formation of gas, the condition of the bath, the exchange of heat,

and the solidification and melting of liquid and solid phases all are interrelated.

The gas evolution and heat transfer processes are analyzed separately to identify the appropriate interrelations. The results of these analyses are then synthesized to determine the nature of the overall system and the influence of various parameters on the behavior of the system. The focus of the studies has always been on the properties and behavior of materials involved in the DRI melting system, such as: (a) D-R particles that are utilized as the charge to the steelmaking furnace, (b) the solid and liquid phases that function as the medium for the transfer of heat, and (c) the gases that form in the particles and evolve into the liquid bath during the melting process.

The evolution of gas from pellets was studied by determining the volume and analysis of the gases evolved during heating of DRI particles. Changes in properties of the DRI particles such as chemical composition, thermal diffusivity, and melting temperature were evaluated from the above information. These results were incorporated into a dynamic model that simulates the behavior of direct reduced pellets immersed in a hot liquid environment such as a steelmaking slag. The model was tested against the experimental results and was used to determine the parameters that may be influential in optimization of the DRI-electric steelmaking practice.

# CHAPTER II

## LITERATURE SURVEY

Areas relevant to the heating and melting of DRI materials in steelmaking slags are catalogued in three articles:

A. Steelmaking with D-R Spong Iron as compared to other steelmaking methods such as scrap remelting or conventional blast furnace-BOF process,

B. Simulation Models used to predict the course of events during the melting of cold particles charged into a steelmaking furnace,

C. Thermal Conductivity of Slags serving as a principal medium for heating DRI materials.

### A. Steelmaking with D-R Sponge Iron

In steelmaking via direct reduction, the total removal of oxygen from iron-bearing minerals is achieved during two stages:

1. primary reduction of ore into sponge iron,

2. final reduction and melting of the sponge in a steelmaking furnace.

Commercial methods developed to achieve the former stage--known as direct reduction--are described in Section 1. The nature of the direct reduced materials is discussed in Section 2. Final reduction and melting of the sponge iron products in an arc electric furnace as an alternative to conventional processes is discussed in Section 3.

### 1. Direct Reduction of Ore

Numerous processes for reducing the iron rich ores without a melting stage have been developed since 1950. Several of them are now in operation. There is an extensive number of papers written about development, operation, and advantages of these processes.[1-25]

Table 2-1 Principal Features of D-R Processes.[1-25]

| Process | Retort | Shaft, Countercurrent | | |
|---|---|---|---|---|
| | HYL | MIDREX | PUROFER | ARMCO |
| Reductant | Gas | Gas, recuperative | Gas, regenerative | gas |
| Product | Pellet | Pellet, Lump Ore | Briquette | Pellet, Lump Ore |
| Reduction Temp., °C | 1000-1100 | 875 | 1000 | 900 |
| % Met. | 83-90 | 92-96 | 92-95 | 92-95 |
| %C | 1.5-2.2 ($Fe_3C$) | 0.7-2.0 ($Fe_3C$) | 1.4 | - |
| Operation period, hr | 12 | 6 | - | - |
| Year of commercialization | 1955 | 1969 | 1976 | 1972 |
| Capacity in operation, 1000 ton/yr | 150-600 | 200-600 | 150-350 | 380 |
| Sponsor | HYL, Mexico | Midland-Ross, U.S. | Thyssen-Purofer, Germany | Armco, U.S. |
| Other features | 4 independent reactors in series | Two unit operation<br>1. gas reformer<br>2. furnace | Hot briquetting of products | Once-through flow of reducing gas |

Basic features of the best known direct reduction techniques that have practically been implemented are summarized in Tables 2-1 and 2-2.

As is illustrated in the tables, direct reduction of ore is accomplished either by a stream of reducing gas ($CO+H_2$) or by direct contact of ore with solid carbon. The specifications of the direct reduction fuels have been studied by a number of authors.[1,5,26,27] The majority of direct reduction processes involve gaseous reduction of agglomerated ore at about 1000°C or less. The ore is heated in a reduction furnace (Retort, Shaft or Fluidized Bed) and reduced with a flow of preheated reducing gas (cf. Tables 2-1 and 2-2).

In the solid reduction processes, a mixture of coal and limestone (or dolomite) is fed with iron ore into a sloping rotary kiln in which a long constant temperature zone of about 1000°C is maintained by means of a series of air injectors positioned along the kiln (Table 2-2). The addition of limestone is to scavenge the sulfur content of the coal.

2. Nature of D-R Materials

The quality of direct reduced materials has a substantial effect on both direct reduction and steelmaking processes. The criteria for desirable physical and chemical specifications of these materials for both cases are given.[26-31]

a. Physical Character

Metallized materials in the iron and steel industry are produced in four different shapes: pellets, briquettes, sinter, and lump ore.[30] These materials are produced by agglomeration and subsequent direct reduction of fine ores, flue dust, ore concentrates, ore fines, and

Table 2-2 Principal Features of D-R Processes.[1-25]

| Process | Fluidized Bed | | Rotary Kiln | | |
|---|---|---|---|---|---|
| | FIOR | HIB | SL/RN | KRUPP | ACCAR |
| Reductant | Gas, recirculation | Gas | Coal | Coal | Coal, oil, gas |
| Product | Briquette | | Pellet, Fine Ore | Pellet, Lump Ore | |
| Reduction Temp., °C | 600 | 700 | 1000 | 950-1050 | 1000 |
| % Met. | 88-93 | 70-75 | 92-95 | 98 | 92-95 |
| %C | $\leq$2.0 | 1.0 | Low | - | 0-1 |
| Operation period, hr | - | - | 5 | - | - |
| Year of commercialization | 1966 | 1973 | 1960 | 1973 | 1976 |
| Capacity in operation, 1000 ton/yr | 400 | 650 | 60-400 | 150 | 80-400 |
| Sponsor | Exxon, U.S. A.G. McKee | U.S. Steel | Canada Steel | Crupp, S. Africa | Allis-Chalmers, Canada |
| Other features | 4 pressurized reactors in series, ore fines 0.04 to 9.5 mm | Used as feed of blast furnace, ore fines | Coal volatiles combusted with air in the kiln to produce heat | countercurrent gas flow, good temp. control in kiln | Fuel flexibility |

other iron-bearing particles of small size into granular, coarse particles of relatively high permeability. Depending on the type of the raw material and the direct reduction process employed, the density and the specific area of the products vary from 1.5 to 4.0 $g/cm^3$ and 0.5 to 4.0 $m^2/g$, respectively.[29]

For efficient operation of various direct reduction processes, certain physical specifications such as size, shape, density, porosity and mechanical strength must be met. Elliott[1] has described the desirable size of the ore feeds of several direct reduction techniques. George and Meadowcroft[28] have discussed the essential characteristics of SL/RN pellets utilized in Stelco blast furnaces. Their results show that the optimum pellet size for SL/RN process is 0.6-1 cm in diameter. They indicate that the degree of metallization of materials produced by the SL/RN process is independent of the particle size. For small size particles, better mixing of the charge with the solid reductant should lead to a greater production rate. However, the formation and growth of accretions on the wall of the kiln will be promoted, once the size of particles is under 0.2 cm. To scale off such accretions, the kiln should periodically be bored out. Besides, for particle sizes of less than 0.6 cm, the tendency for sulfur pickup will be enhanced.

The optimum ASTM tumbler index for proper operation of blast furnace and kiln without formation of accretions on the wall of the kiln is suggested by the above authors to be 95 percent + 0.6 cm particles after tumbling. The equivalent compression strength is given as 200 Kg/pellet for 1.3 cm pellets.

b. Chemical Character

The level to which iron oxides can be reduced by various direct reduction processes is given in Tables 2-1 and 2-2. This level is usually expressed in terms of the percentage of the total iron that may be present in reduced form and is called the degree of metallization. The chemical composition of the metallized charge affects the quality of the steel product. The levels of sulfur, phosphorus, acidic gangue, and acidic binders in the metallized iron must be low to decrease the required amount of fluxes (burnt lime) necessary for removal of these constituents from the steel by slagging.[1]

The effect of the silica content of the ore on the power consumption of the electric arc furnace is given by George, et al.[28] For a low power dissipation, they have suggested a maximum of 3.5 percent silica in the prereduced pellet.

One of the difficulties in using prereduced materials is their susceptibility to reoxidation even at atmospheric temperatures.[32,33] The heat of oxidation is usually stored in the D-R particles, due to their low thermal conductivity and accelerates the rate of reoxidation. The stability of metallized materials depends upon the nature of the direct reduction employed for their production. It is well known, for instance, that metallized materials reduced at the higher temperatures are less susceptible to reoxidation.[34,35]

To reduce the rate of reoxidation of D-R materials, they may be compacted into high density briquettes.[36,37] Besides, they must be stored under dry and, if convenient, inert atmospheres. Carburizing the surface of particles is also a way of decreasing their susceptibility

to reoxidation.

3. Electric Steelmaking Practice

Three-phase direct arc furnaces have been used during the past twenty years for production of plain carbon steels by melting scrap and iron-rich ores.[38,43] In these furnaces, the arcs are struck between the charge and three vertical electrodes. The detailed description of the electric furnace operation is given by a number of authors.[30,38,39]

Electric steelmaking processes are generally divided into two categories, (a) acid practice, and (b) basic practice.

The physical and chemical character of the charge and its arrangement in the furnace can affect the melting time and the lining life of the hearth. A mixed feed of fairly uniform density, with a mixture of medium and light scrap will present an ideal charge of fairly uniform resistivity.[38,43] On top-charge furnaces, it is desirable to locate some heavy scrap low in the charge under the electrodes to prevent the bottom of the hearth from being damaged by the arcs. The total operation requires about 3 hours from tap to tap for a 100-ton capacity furnace.[43]

The most successful application of basic arc practice is the continuous feeding of DRI materials into the pool of slag and metal with or without use of scrap, while maintaining full power supply and adjusting the composition and temperature of the bath.[39-42] A combination of DRI and scrap is in many cases charged to the electric furnace.[43] Because of the lower cost of DRI, it is however desirable to use as much sponge as possible. Various methods may be used to charge metallics

continuously into the furnace. Celada and Quintero[43] have described different techniques employed by HyLSA and the results obtained. They have fed DRI materials into the furnace by several methods such as: continuous loading through the wall,continuous loading through the roof using one hole directed to the center of the delta, and continuous loading through the roof using one and two holes directed between the electrodes and the wall. They have also used batch type feeding of scrap and DRI as described previously.

Much has been written about the use of DRI metallics as a principal charge to the electric arc furnace and as a way of diminishing the cost of the steel products and increasing the production rates.[43-52]

Continuous charging of direct reduced materials of low degrees of metallization presents a vigorous boil in the slag that may result in production of a foamy slag. Such a slag can shield the walls and roof of the furnace from the intense radiation of the arcs.[1,39] The evolved CO in this case decreases the density of the slag and increases its volume. The excess of slag can flow out of the furnace from the openings made for removal of the slag. The continuous utilization of the radiated heat, for melting DRI materials can furthermore reduce wear on the lining that may occur in the normal scrap melting practice.[33,38]

The results of Sibakin et al.[39] show that a reduction in refractory consumption of 27 percent can be obtained, once the sponge materials are continuously charged into the arc furnace. These results also show that using about 75 percent DRI can reduce the operation time of the arc furnace from three hours, for a total scrap load, to as little as

1.5 - 2 hours. This reduction is equivalent to an increase in production rate of up to 50 percent with a reduction in power consumption of 40 KWh/ton. This improvement is attributed to the simultaneous charging and refining operation, low content of tramp elements in the charge, and reduction in the number of recharges and the amount of heat dissipation associated with swinging aside the top of the furnace.

Post and Ameling[34] have reported several improvements in operation of Hamburger Stahlwerke's electric furnaces such as productivity increase, increase in the proportion of power-on time, decrease of electrode consumption, yield increase, and decrease in lime consumption as a result of continuous feeding of highly metallized Midrex pellets. Utilization of such materials has enabled them to produce high quality steel grades while using cheap scrap grades as a supplementary charge to the furnace. They have suggested an optimum degree of metallization of about 93 to 94 percent for minimum energy consumption and higher than 94 percent for optimum production rate.

Electric steelmaking with DRI materials has several other advantages relative to the other steelmaking processes, too. The low content of tramp elements, for example, allows the steelmaker to use DRI for producing a wide variety of steels. However, there are also a number of restrictions to the increase in DRI utilization due to the limited supplies of high quality ores that can meet the minimum standards for production of DRI materials suitable for arc furnace, and the limited availability of natural gas and electric power.[1]

Compared with traditional blast furnace-BOF practice, direct reduction-arc furnace operation requires a lower investment cost per ton

Table 2-3 Important Features of DRI-Steelmaking Practice.[5,27,45,54]

| ADVANTAGE | | DISADVANTAGE |
|---|---|---|
| Compared to BOF-Blast | Compared to Scrap-Arc | Comp. to Scrap-Arc |
| 1. Low capital cost (32% less than Blast-BOF for 1 million ton/year capacity). | 1. Possibility of continuous feeding | 1. Low iron content as compared to slag. |
| 2. Low level of air pollution. | 2. Consistency of chemical analysis. | 2. Low packing density. |
| 3. Low production cost (8% less than Blast-BOF). | 3. Low and known tramp elements (Cu, Sn, Ni, Pb, etc.). | 3. Low quality product when high S and P ores used. |
| 4. High flexibility in locating plants. | 4. Less fluctuations in price of raw materials. | |
| 5. Less sensitive to cost of fuel than Blast-BOF (1/4 of cost of billets as compared to 1/3). | 5. Easy handling. | |
| | 6. Less noise. | |
| | 7. Better protection of refractory as a result of formation of frothy slag due to the evolved bubbles. | |
| | 8. Possibility of shortening of Arc-refining period due to the uniformity of physical and chemical properties. | |
| | 9. Production of high quality steel. | |
| | 10. Possibility of using various raw materials. | |
| | 11. Lower production cost (23% less than scrap-Arc). | |

of steel.[5,27,46] Nevertheless, a direct reduction steelmaking plant is well able to produce as much as half a million tons of steel per year, while a relatively large blast furnace is likely to have an annual capacity of two to four million tons of pig iron.[5] These figures indicate that a considerable potential exists for substituting direct reduction steelmaking methods for the traditional ones, especially for smaller production units.

The production and consumption of direct reduced iron has increased rapidly during the past decade. While in 1970 the capacity of direct reduction plants was slightly more than a million ton, in 1980 this amount will exceed 30 million tons.[2,5,44] Yet, greater growth in production of DRI is expected to be achieved in the foreseeable future. Such growth may diminish the enhanced demand for the world supply of scrap that may become chronic in the future.

The important features of DRI-arc steelmaking practice as compared to the other steelmaking processes are summarized in Table 2-3.

B. Heat Transfer Models

Numerical models based on heat conduction equations have been widely used to describe the temperature fields inside an object being heated, in terms of time and space.[55-60] To develop such models, the pertinent partial differential equations and their boundary conditions are translated into finite-difference equations and are solved by a high-speed computer.

An example of such models is the one developed by Elliott and Nauman.[57,58] To formulate the finite difference equations, the above

authors have used the simplified form of the general heat conduction equation in spherical coordinates for one-dimensional heat flow:

$$\frac{1}{r^2}\frac{\partial}{\partial r}\left(r^2\frac{\partial T}{\partial r}\right) = \frac{1}{\alpha}\frac{\partial T}{\partial t} \qquad (2.1)$$

where $\alpha$, T, t, and r are thermal diffusivity, temperature, time, and distance from the origin of the coordinates, respectively. Employing the dominant boundary conditions, they have been able to solve this equation for the temperature distribution in a cold solid sphere immersed in a hot liquid environment.

As a result of the transfer of heat into the sphere, a shell of solid slag freezes on its surface, once the sphere is submerged into the bath. This shell grows to a certain thickness initially, and will remelt later. If the liquid medium has a sufficiently high temperature, the original sphere also will melt, eventually.

For the heat transfer conditions illustrated in Figure 2-1, the boundary conditions may be described with the following equations:

$$T = T_\ell \qquad r = L \qquad (2.2)$$

$$\bar{h}(T_\infty - T_\ell) = k\left(\frac{\partial T}{\partial r}\right)_L - \Delta H.\rho.\frac{\partial L}{\partial t} \qquad (2.3)$$

$$k\left(\frac{\partial T}{\partial r}\right)_{R+} = k\left(\frac{\partial T}{\partial r}\right)_{R-} \qquad r = R \qquad (2.4)$$

$$T = T_\infty \qquad r = \infty \qquad (2.5)$$

$$\frac{\partial T}{\partial r} = 0 \qquad r = 0 \qquad (2.6)$$

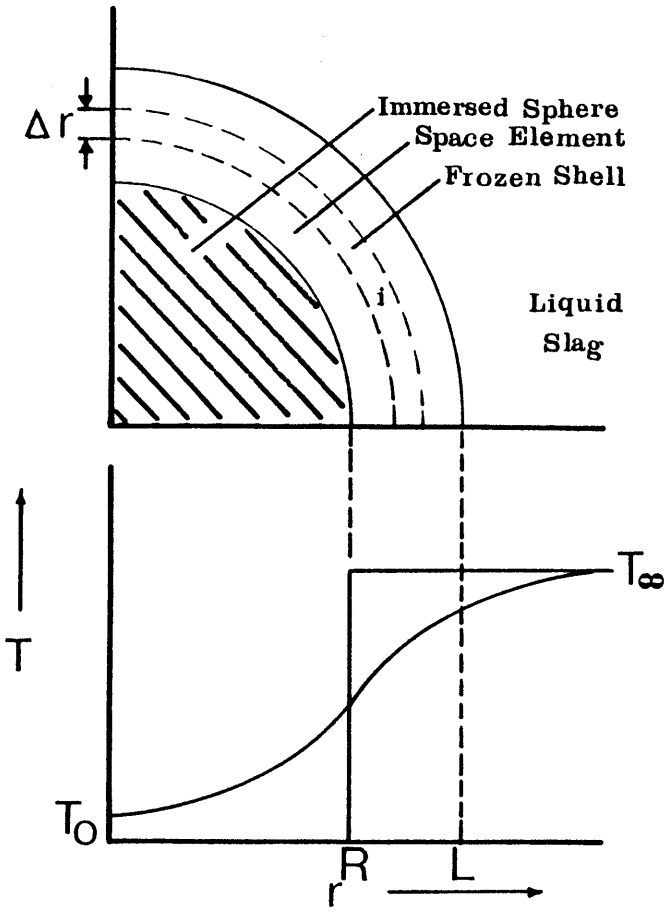


Fig. 2-1 Temperature Profile for Cold Sphere Immersed in Hot Liquid Slag.

where $\rho$, k, $\Delta H$, and $T_\ell$ are density, thermal conductivity, heat of fusion and the liquidus temperature of the slag respectively, $T_\infty$ is the real temperature of the bulk slag, R is the radius of the sphere, $\bar{h}$ is the average heat transfer coefficient and L is the distance from the center of the sphere to the solid-liquid interface. Initially, there is no frozen shell of slag and the temperature throughout the slag is constant, $T_\infty$. Converting the partial derivatives to finite difference ratios, Equations (2.1) to (2.6) can be written in the form of finite-difference-equations. The new equations will yield both the future temperature of each space interval along the radius of the particle, $T_{i,j+1}$, and the position of the liquid-solid interface, $L_{j+1}$, at a time t after the present time j $\Delta t$:

$$T_{i,j+1} = T_{i,j} + \alpha \frac{\Delta t}{\Delta r} \cdot \frac{A_i}{V_i} (T_{i+1,i} - T_{i,j}) + \alpha \frac{\Delta t}{\Delta r} \cdot \frac{A_{i-1}}{V_i} (T_{i-1,j} - T_{i,j}) \qquad (2.7)$$

$$L_{j+1} = L_j + \frac{k}{\rho \Delta H} \cdot \frac{\Delta t}{\rho_j} (T_{i-1,j} - T_\ell) + \frac{\bar{h}}{\rho \Delta H} \Delta t (T_\infty - T_\ell) \qquad (2.8)$$

where $A_i$ and $V_i$ are mean surface area and mean space volume of element i. The value of $\ell_j$ is chosen to be less than $\Delta r$ and is used to indicate the movement of the interface between space intervals:

$$L_j = i \, \Delta r + \ell_j \qquad (2.9)$$

Starting with the specified initial conditions, the above equations can be used to compute both the temperature distribution throughout the body

and the position of the interface at any time by a step-by-step computation.

A study on the transient transfer of heat to cylindrical iron specimens immersed in carbon saturated liquid iron has been made by Kim and Pehlke.[67] They developed a numerical model for transfer of heat, solidification and remelting of a carbon-rich crust of iron on the surface of specimen similar to the one developed for spherical particles.[57]

Ehrich, Chuang, and Schwerdtfeger[60] have solved Equations (2.1) to (2.6) by using the method of Green's function and have calculated the melting time of a sphere of a pure metal immersed in its own melt. They have converted Fourier's second law, Equation (2.1), and the boundary conditions to integral equations and solved them by numerical technique.

George and Damle[61] have solved the same equations with the method of lines for conditions of combined heat transfer and solidification in spheres, and have tested their numerical results against known data. Grimado and Boley[62] have used the embedding technique to solve the spherical heat conduction problem, while Pedroso and Domoto[63] have obtained the perturbation solution of the problem by using a series expantion of the general solution and substituting in the equations of heat transfer. Hung and Shih[64] have similarly obtained perturbation solutions of inward and outward solidification of a saturated liquid in spherical and cylindrical containers. Their quasi-steady state approximations have been comparable to the other perturbation solutions and have been found satisfactory for practical applications. Chuang and

Ehrich[65] have solved the transient diffusion problem with moving boundary in spherical coordinates by applying the Green's function to convert the governing transfer equations to an integral form. A comparison of their approximate solutions with the computer results has proved the validity of their method. The solidification of cylinders and spheres of metals has also been studied by Kern and Wells.[66] Based on the assumption of a linear temperature profile in the solidified shell, they have developed a model that predicts the movement of the solidification front as a function of time.

Although the above procedures have been able to yield approximate analytical solutions to the heating and melting of spherical objects immersed in hot fluids for a series of specific conditions, there is not an exact solution as yet available that satisfies the conditions governing the system. Besides, the basic assumptions concerning the constant thermo-physical properties of materials that are always postulated through developing these solutions introduce a number of restrictions on the applicability of the results. Only numerical techniques seem to be capable of giving valid solutions to the heating and melting systems of the real case, at the present time.

C. Thermal Diffusivity of Slags

Thermal properties of oxide phases present as the slag in pyrometallurgical processes have an impact upon the transfer of heat to the particles immersed in the slag. Yet, very little is known about the thermal properties of these phases.

The only definitive measurements of the thermal diffusivity of synthetic steelmaking slags have been made by Fine, Enge and Elliott,[69]

Foo and Elliott,[70] and Nauman, Foo and Elliott.[71] For measuring the thermal conductivity of such slags, conventional methods are not applicable due to the highly corrosive nature of these slags at the relatively high temperatures at which the tests must be made. These temperatures range from 1200 to 1600°C. Elliott[68] has described the experimental problems associated with thermal diffusivity measurements for liquid silicate slags. Fine, et al.[69] have measured the effective diffusivities of slags with basicities (lime/silica ratio) of 1.0 and 1.5, and FeO contents of up to 25 percent in the silicate. The results of their studies have been fitted to an equation relating basicity, FeO content and temperature to the apparent thermal diffusivity of the synthetic oxides:

$$\alpha_{eff} = 0.001(1.5-0.5B) + 0.018(T/1500)^3/(\%FeO)^{0.8} \quad (cm^2/sec) \qquad (2.10)$$

Equation (2.10) is valid for temperatures ranging from the liquids temperature of the slag to 1750°K.

The measurements of Fine, et al.[69] and Foo[70] show that the effective thermal diffusivities of glasses whose compositions are similar to metallurgical slags range from 0.002 to 0.008 $cm^2/sec$. The values obtained for igneous rocks[73,74] and typical coal ash slags[75] are in the same range.

Gibby and Bates[73] used a high temperature laser pulse technique to measure the thermal diffusivity of basalt. Murse and McBirney[74] measured the thermal conductivity of a synthetic lunar rock by employing a radial heat-flow technique. Both results showed that the thermal diffusivity of the rocks decreases as the temperature increases around the melting

point.

Bates[75] used the high temperature laser pulse technique to measure the thermal diffusivity of several coal ash slags. Fujisaw, et al.[76] measured the thermal diffusivity of $Mg_2SiO_2$, $FeSiO_4$ and NaCl at high pressures and temperatures. They studied the effects of olivine-spinel phase transition on thermal diffusivity of $Fe_2SiO_4$.

The works of Bates[75] indicated that in addition to the composition, the microstructure of the samples of solid slags may also have a substantial effect on the thermal diffusivities of such samples.

# CHAPTER III

# EXPERIMENTAL

A general discussion of the experimental program designed to study the DRI melting process is given in Section A. The arrangements used to determine the volume and composition of the gases that evolve from DRI and the equilibrium phase changes in D-R particles are described in Sections B and C. The apparatus employed for measurement of the rate of transfer of heat from a hot bath of slag to the immersed particles is described in Section D. The information obtained on the nature of gas evolution in liquid slags is given in Section E.

## A. Experimental Program

Two major areas are recognized for investigation of the melting process of DRI particles in steelmaking slags: (a) evolution of gas as a result of the final reduction of DRI and (b) the exchange of heat between the liquid slag and immersed particles. The evolution of gas from DRI was investigated by heating D-R materials of different sources either in sealed containers or in hot liquid slags and measuring the rate and composition of the gases evolved.

Since the chemical composition of D-R materials affects their properties and the rate of evolution of gas from DRI, and D-R particles are subject to reoxidation during shipping, storage and handling, a set of experimental tests is necessary to determine their precise chemical composition periodically. The oxygen content of DRI samples was determined by reducing them under hydrogen (III.B.2.a). The least carbon content of the samples and the maximum volume of the gases that can

evolve from D-R materials were determined by heating DRI under helium at constant temperature and pressure (III.B.2.b). The maximum gas volumes determined by these tests were utilized as a base-line for comparison with results of the gas evolution experiments described in Section III.B.3.

The temperatures at which phase transformations occur in D-R materials are necessary to determine the thermal properties of these materials. These temperatures were estimated from the evolution results and verified by analyzing D-R materials thermally (III.C).

The heat transfer studies in liquid slags were necessary to determine the effects of the evolution of gas and the change of properties of materials on the thickness of the frozen shell of slag and on the rate of heating of immersed stationary particles. Solid nickel and sintered iron spheres were employed because they were previously utilized by other investigators[57-59] for similar studies. Direct reduced pellets were utilized to determine the evolution of gas and the effects of the change of chemical composition and the change of thermal properties of the specimens on the heating rate of the immersed particles.

The nature of gas bubbles evolved from the immersed particles was studied to obtain the information necessary for estimating the change of properties of the liquid slag that surrounds a particle (Appendix I) and the contribution of the local bubbling on transfer of heat into the immersed particles (V.D.3).

B. Extraction of Gas from DRI

Samples with different oxygen and carbon contents were heated under both constant and varying temperature circumstances to study the

Table 3-1 Conditions of Extraction Tests.

| Temperature | Constant | | Variable |
|---|---|---|---|
| | Hydrogen | Helium | |
| Type of D-R material* | All | All except A and F | All |
| Test temp., °C | 950 | 400-1100 | 25-1400 |
| Grain size, mm | 0.6, 1,2 | 0.6, 1,2,3 | 1,2 |
| Temp. rate, °C/min | 0 | 0 | 50 - 1000 |

*See Tables 3-2, 4-1 and 4-2 for chemical analysis of DRI samples.

formation of gas as a result of the final reduction of prereduced sponge iron. The effects of the rate at which the temperature of the samples increased, the size differences of DRI grains, and the chemical composition of D-R materials on the rate of evolution of gas from the samples were determined. The pertinent experimental conditions are listed in Table 3-1.

1. Preparation of Materials

The extraction experiments were carried out on three types of commercially produced materials:

1. HYL Pellets
2. Midrex Pellets
3. Midrex Lump Ore

The chemical analyses of these materials are shown in Table 3-2. The figures in parentheses are calculated from the other figures. It is to be noted that an increase in the oxygen content of a sample results in a decrease in the degree of metallization. The degree of metallization of the samples employed in the experiments ranged between 85 to 95 percent.

Since the above materials had been produced in large quantities, they varied in their chemical composition, size, shape and density. Therefore, to get a uniform distribution of particles in a batch of samples, they were finely crushed and evenly blended. These small sized samples of crushed materials were used in extraction experiments. Their typical sizes were 0.6, 1, 2 and 3 millimeters in diameter.

Table 3-2 Chemical Analyses of Prereduced HYL and MIDREX Materials Reported by Manufacturer.

| Pellet Type | HYL | | | | MIDREX | | |
|---|---|---|---|---|---|---|---|
| | A | B | C | D | E | F | Lump Ore |
| $Fe_{Total}$ | - | - | - | - | 91.2 | 85.3 | 93.8 |
| $Fe_{Met}$ | - | - | - | - | 86.3 | 78.2 | 86.2 |
| % Met | 91.89 | 87.21 | 92.31 | 86.59 | 94.6 | 91.7 | 92.0 |
| S. Dev. | 0.56 | 0.28 | 0.72 | 0.17 | - | - | - |
| % O | (2.23) | (3.45) | (2.11) | (3.61) | 1.48 | 2.14 | 2.17 |
| % C | 1.67 | 2.21 | 1.93 | 2.22 | 1.78 | 0.90 | 1.00 |
| S. Dev. | 0.05 | 0.04 | 0.04 | 0.02 | - | - | - |
| % Gangue | - | - | - | - | 5.54 | 11.66 | 3.03 |

2. Sample Analysis

Analytical tests were carried out on DRI crushed samples by heating them under hydrogen or inert helium atmosphere at a constant temperature. The purpose of the former was to find the oxygen content of DRI materials while that of the latter was to determine the least available carbon content of the samples and the maximum volume of the total gas that could be produced because of carbon-oxygen reduction reactions. A comparison of the results of hydrogen extraction tests with the analysis of the samples reported by the manufacturer is made in Tables 4-1 and 4-2. Similarly, a comparison of the results of helium extractions with those of the variable temperature extractions (sec. III.B.3) is made in Section IV.A.2.

a. Hydrogen Extraction

Samples of crushed DRI were completely reduced by a stream of purified hydrogen to determine their oxygen content. The samples were placed inside a Vycor capsule (Figure 3-1) and heated up to 950°C. They were held at this temperature for a period of 10 hours, during which complete reduction of the samples was achieved (cf. sec. IV.A.1.a). A horizontal resistance furnace was used to generate the required heat.

The exhaust gas was passed through Ascarite and Phosphoric Oxide columns where $CO_2$ and $H_2O$ were collected, respectively. The numbers of moles of $CO_2$, $H_2O$, and CO in the exhaust were determined from the weight gains of these columns and the weight loss of the sample, under the assumption that $CO_2$, $H_2O$ and CO were the only products of the final reduction of the sample. From a total mass balance, the reacting contents of oxygen and carbon were computed for the sample. A sample

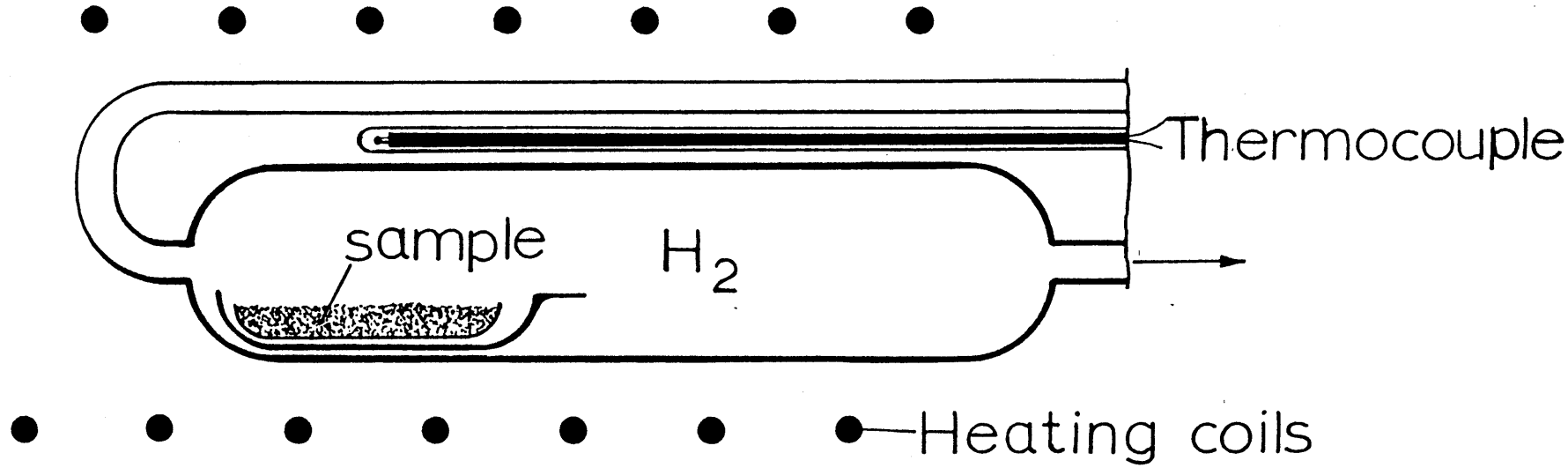


Fig. 3-1 .Capsule for Hydrogen and Helium Extraction of DRI.

calculation is described in Appendix A.

b. Helium Extraction

Crushed DRI grains were also reduced under inert helium atmosphere. The experimental procedure was similar to that of hydrogen extraction except that the capsule was flushed with helium before and after the heating period for about one minute. The reaction tube was only purged when the sample was at room temperature to avoid reoxidation of DRI apparently due to the very low partial pressure of oxygen in the helium stream. The capsule was heated uniformly to avoid the decomposition of CO to $CO_2$ and carbon at the cold sites of the capsule.

3. Bomb Extraction

The volume and composition of gases evolved from D-R materials were determined by heating a bed of crushed DRI in a sealed bomb, collecting $CO_2$ and $H_2O$ and measuring the rate of flow of CO. The experimental set-up is described in the following section.

a. Furnace Arrangements

Samples of crushed DRI were charged into cylindrical steel "bombs" such as the one shown in Figure 3-2 and reduced. Heat was supplied by induction through a graphite susceptor. Suitable connections were employed to conduct the gaseous products out of the bomb for analysis and volumetric measurements. The bomb was made of a 9cm x 1.3 cm I.D. iron pipe which was reamed with a 1.5 cm drill. It was closed at the top by a 0.6 x 0.3 cm iron bushing and at the bottom by a 1.5 x 1.5 cm iron plug which were welded to the pipe. Copper coils were used to water-cool the gas conduit that directed the exhaust out of the bomb.

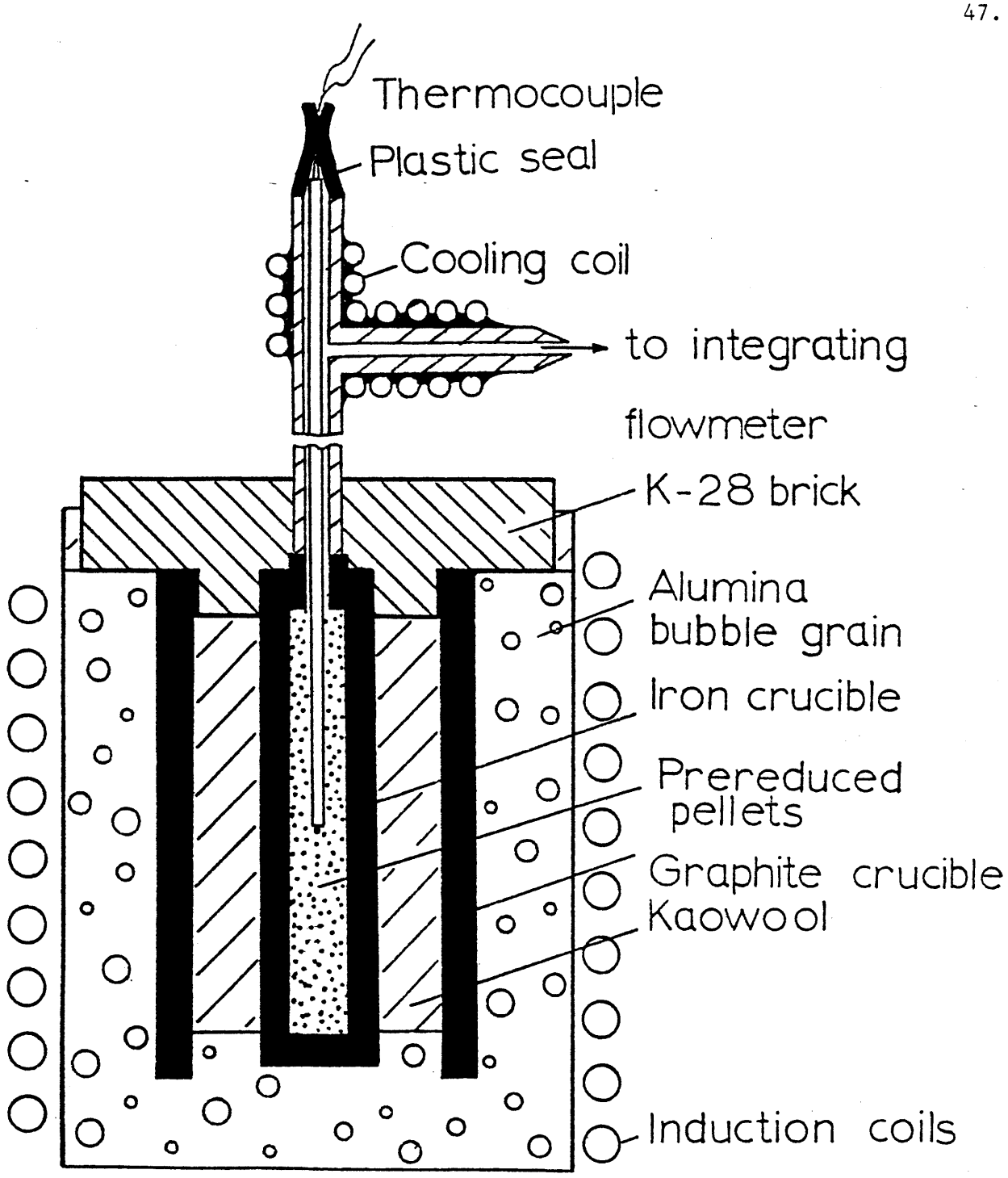


Fig. 3-2 Experimental Assembly for Bomb Extraction of DRI.

A Platinum/Platinum-Rhodium thermocouple was used to measure the temperature of charge. A short-length of Vincon PVC tubing was clamped around the thermocouple wires to seal the assembly at the exit. The thermocouple bead was positioned at the geometric center of the charge. A predetermined temperature profile was used to control the rise of temperature of the charge. The induction heating permitted relatively precise control of the rate at which the sample was heated, but it was difficult to obtain a smooth temperature profile when the rate of increase of temperature exceeded 1000°C/min.

In practice, it was found that optimum results could be obtained when the reactor was insulated externally. For insulation, alumina bubble grains, Kaowool and K-28 bricks were utilized as shown in Figure 3-2. In this case, even at a high temperature, local melting of the crucible was avoided; moreover, the charge reacted uniformly and did not reduce or melt locally.

It was assumed that there was no large temperature gradient in the charge and that the temperature detected by the thermocouple was a measure of the real temperature of the sample.

As a result of the abundance of both iron and carbon in the reaction medium, the thermocouple bead was usually contaminated during an extraction experiment. This contamination slowed the time response of the thermocouple and caused fusion of the thermocouple bead at high temperatures. After each experiment, therefore, the thermocouple bead was replaced to avoid the introduction of error in temperature measurement.

Various other techniques were also tried. None of them, however, solved the problem. For example, using a closed-end, single-bore,

alumina protection tube had a side effect of slowing the time response of the thermocouple to an even greater degree. Using a thin platinum foil to protect the thermocouple bead, was not helpful either because of the contamination and partial fusion of this foil during the experiment.

The emission from a heating bomb was basically composed of the gases produced during the final stage reduction of the prereduced charge. In the following section, the method employed to determine the composition and the volumetric rate of evolution of the gaseous emission is described.

b. Composition and Rate of Gas

The gases from the bomb were conducted through $CO_2$ and $H_2O$ absorbent columns, where $CO_2$ and $H_2O$ were collected. After absorption of these components, the gas stream was passed through an integrating flowmeter, described in Appendix B, to measure the volumetric rate. The total volume of each component was then determined from the weight gain of the absorbent columns and the information obtained from the volumetric measurements, based on the assumption that $CO_2$, $H_2O$ and CO were the only components of the evolved gas.

The above method was used to determine the analysis of the released gas for a number of experiments. Employing the procedure described in Appendix C, the rate of formation of gas as a function of the temperature of the sample could be determined for all of the bomb extraction tests. From this rate the total volume of gas was calculated.

4. Correction Factor

In order to determine the necessary correction factors, a number of experiments were run with blank boats in the case of hydrogen and helium extractions, and with empty reactors in the case of bomb extractions.

Table 3-3 Typical Corrections for Extraction Tests.

| Extraction | $H_2O$ ($cm^3/g$) | $CO_2$ ($cm^3/g$) | Total gas vol. ($cm^3/g$) | Flow rate ($cm^3/g.min$) |
|---|---|---|---|---|
| $H_2$ | 3.0-6.0 | -.3 - -1.4 | 2.7 - 4.6 | - |
| He | 0.1-0.5 | 0.1 - 0.4 | 0.1 - 0.9 | - |
| Bomb | - | - | 1.3 | 0.1 - 1.0 |

Suitable corrections for results of each case were made.

Typical results of the blank extractions are summarized in Table 3-3. These results (for hydrogen and helium extractions) were usually a function of many factors, such as air humidity, room temperature, and reaction tube cleanliness, all of which changed from time to time. For this reason, the blank tests were repeated regularly and the results were corrected for the measured values.

C. Thermal Analysis of DRI

D-R materials were thermally analyzed to specify the phase changes that occur when they are heated. For this purpose a one-gram sample of crushed DRI was charged into a 6 mm diameter alumina crucible imbedded in a high-temperature refractory cement. A similar one-gram sample of reagent grade alumina powder was loaded up into an identical Alumina crucible placed at a symmetrical position next to the prereduced sample in the refractory. The refractory was surrounded by a graphite susceptor and heated by induction. Two Pt-Pt 10% Rh thermocouples were used to measure the temperature of the sample and of the reference, as shown in Figure 3-3.

A plot was made of the temperature of the charge vs. the temperature difference between the sample and the reference. Because of the absorption of heat during a phase transition, this plot showed a change in slope when a phase transformation occurred. The initial and final temperatures of solid-solid and solid-liquid transformations were determined from the resulting curves.

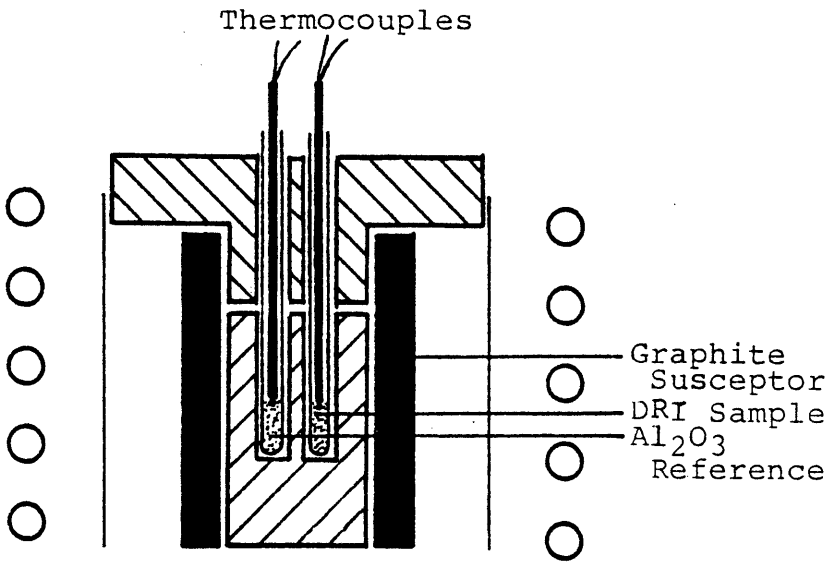


Fig. 3-3 Assembly for Differential Thermal Analysis of DRI Materials.

D. Heating Particles in Slag

A small experimental furnace was used to study the nature of the DRI melting process. The method employed was similar to the one described in reference 58. It consisted of submerging a cold metal ball into a hot pot of molten slag. The dimensions of this vessel were large enough to assume wall effects insignificant. The temperature of the submerged object was recorded continuously and was used later to study the heating process of the particle.

When the cold ball was plunged into the bath, a layer of slag that was adjacent to the particle solidified on the surface of the particle. This layer was melted later when the temperature of the surface of particle was hot enough that the flux of heat from the solid-liquid slag interface to the particle was less than that from the bulk liquid to the interface.

A study was made of the effects of gas evolution on the thickness of the solidified shell of slag. The immersed particle was withdrawn from the bath at specified times. The slag skull was broken into pieces and its thickness was measured at various points by callipers. The mean shell thickness and its standard deviation were then determined. Liquid nitrogen was used to cool the particle after each measurement. It took much longer to cool the particle in air. Cooling in water was not also applicable because of the evaporation of the remained moisture during the subsequent test. The effects of temperature and composition of the liquid bath on the thickness of the shell of slag were also determined.

The experimental equipment and method that were employed for heat transfer studies are described in the following sections.

1. Slag Bath

The liquid slag was contained in a steel crucible 14 cm I.D. and 20 cm high. This pot was fabricated from a 20-cm long section of in schedule 40 steel pipe to which an 8-mm thick steel plate was welded on the bottom. A similar steel plate was the lid for the crucible. A 5-cm hole was machined at the center of the lid to permit insertion of the metal particles into the slag (Figure 3-4).

The slags were made of reagent grade powders of various oxides blended by tumbling. Their chemical composition was selected from those given by Nauman.[58] Slag A was selected because of its low melting temperature which allowed its easy handling. Slag B was used to test the effect of various constituents which are usually present in steelmaking slags. It was also a typical copper smelting slag. Slag C was a typical steelmaking slag and was used to calculate the melting time of D-R pellets fed into arc furnace. The chemical composition of the slags was calculated based on quantities of the powders mixed and is given in Table 3-4.

The slag was heated indirectly by an induction generator (TOCCO 50 KW model). The crucible was shielded on the external surface by winding thin steel plate around it to heat the slag evenly. This plate prevented the formation of an electrical arc at the welding zone of the iron pipe and thereby extended the life-time of the crucible.

The temperature of the slag was measured either by an optical pyrometer sighting on the internal surface of the crucible or a Pt-Pt 10% Rh thermocouple inserted in an alumina protection tube. The thermocouple bead was positioned at the same depth of slag as that of the center

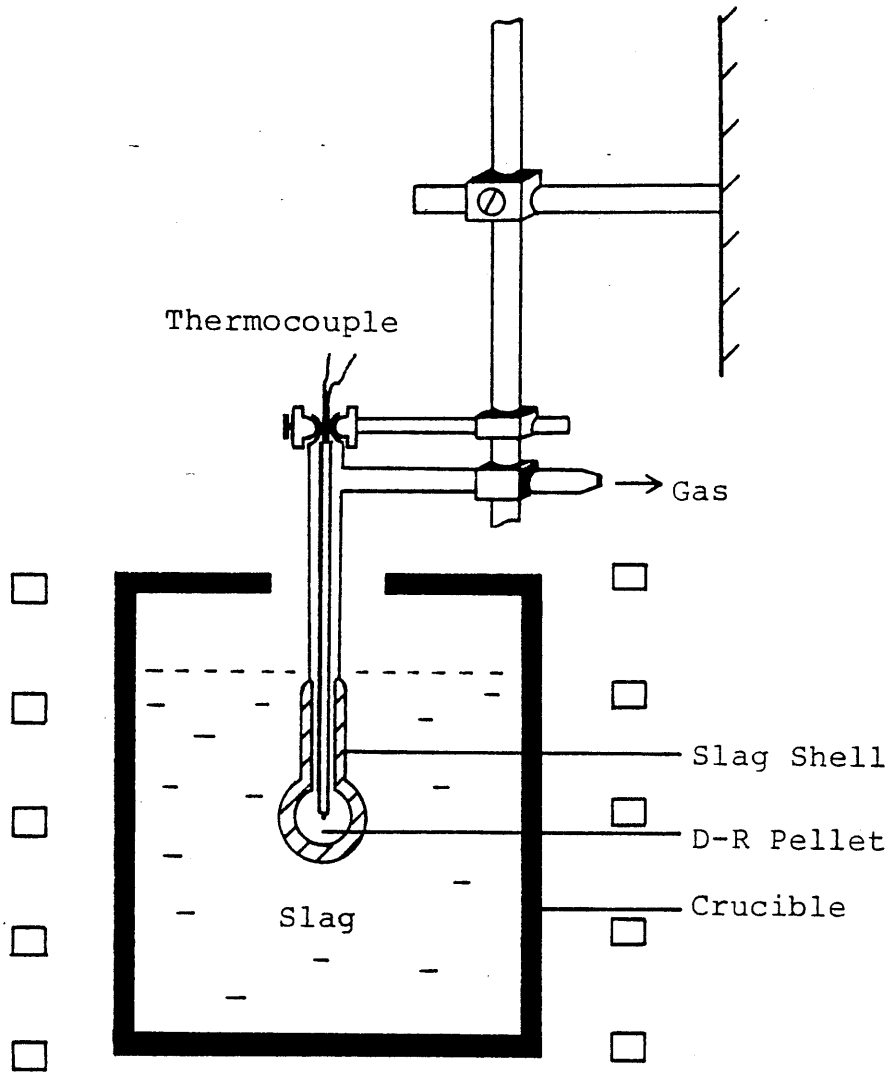


Fig. 3-4 Experimental Furnace for Heat Transfer Studies.

Table 3-4 Chemical Composition of Slags* and Heats of Fusion of Materials.

| Component | Weight Percent | | | $\Delta H_m$[77] |
|---|---|---|---|---|
| | A | B | C# | Cal/g |
| $Fe_{total}$ | 48.0 | 35.0 | 11.0 | - |
| "FeO" | 60.5 | 40.5 | 14.2 | 108.7 |
| $Fe_2O_3$ | 1.4 | 5.0 | - | 142.5 |
| $SiO_2$ | 38.1 | 40.5 | 31.4 | 34.0 |
| CaO | - | 7.0 | 31.4 | 339.0 |
| $Al_2O_3$ | - | 5.0 | 12.5 | 255.0 |
| MgO | - | 1.0 | 10.5 | 53.1 |
| S | - | 1.0 | - | 10.5 |

*Also used by Nauman.[58]

#Synthetic Steelmaking Slag.

of the immersed particle. This depth was usually around 4-7 cm. The total depth of the liquid bath was at least twice the depth of immersion of the particle.

2. Test Specimen

Three kinds of particles attached to steel tubing stems were used for heat transfer studies. The supporting stem was fixed to a movable steel rod. This rod slid vertically upon a rack which was tightly fixed to an aluminum frame. Loosening the screw of this rack allowed the particle to move into the slag. When the particle reached the desired depth, the assembly was fixed at that position by tightening this screw again. The same procedure was repeated to remove the specimen from the slag when the measurements were finished.

The temperature of the particle was measured with a thermocouple that was placed within the supporting stem and whose Pt/Pt 10% Rh tip was located at the bottom of the thermocouple insertion well and protected by a 0.025 mm thick platinum foil. The thermocouple wires were passed thru a short-length of Vincon PVC tubing clamped around the wires tightly and then connected to a cold junction ice-bath and finally to a strip-chart recorder. The supporting tube was air-cooled at the upper part (opposite to the specimen) to avoid overheating the tightly clamped seal. The assembly is shown in Figure 3-4.

a. Nickel Sphere

Cast nickel balls of 1.84 and 3.00 cm diameters with and without gas parts served as the heating object for heat transfer studies. These particles were produced by precision casting of pure molten nickel into preheated investment molds. A well was bored along the radial direction

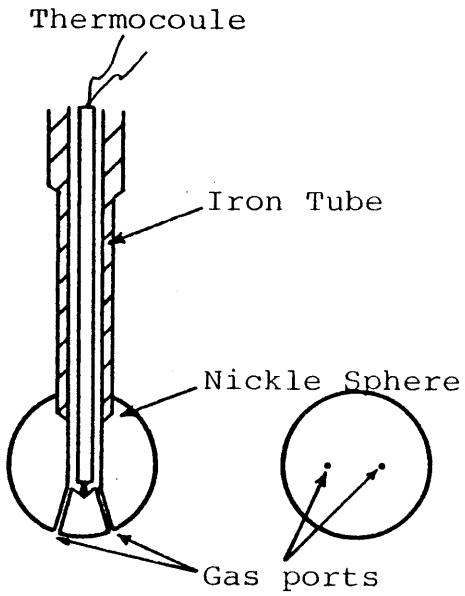


Fig. 3-5 Cast Nickel Sphere (Rad., 9mm) and Thermocouple Assembly. Diameter of Gas Ports, 0.7 mm.

of each specimen for the thermocouple insertion and a supporting tube was welded to each of them. Two 0.7 mm diameter holes were bored from surface toward the center of the small spheres, three were made for the large ones for simulation of gas evolution from the spheres into the slag during forced bubbling experiments. The design of the particles is shown in Figures 3-5 and 3-6.

b. Sintered Sphere

Porous iron spheres, 3 cm in diameter, were produced by sintering 40 mesh iron filings imbedded inside investment molds. The filings were first packed into the spherical cavity of the mold, then an iron tubing indented at the end was mounted vertically in the mold while the indented part was surrounded by the iron filings. Before mounting the stem, a steel rod shielded by an inflammable piece of tape was inserted into the stem so that the tip of the rod was at the center of the packed filings. The assembly was heated to 950°C and held at this temperature for two hours to sinter the powder. The tape was burnt up during this period leaving a blind hole for the thermocouple inside the sphere. The mold was then left to cool off. The particle was removed from the mold and carefully cleaned at last.

A difficulty in making a sintered sphere was to fix the stem firmly in the porous body. This difficulty was usually accompanied by uneven density and permeability of the particle especially around the stem. Permeability of a particle was particularly important in the forced bubbling studies. Packing the gap between the stem and the mold after the cavity was filled with 40 mesh filings and the stem was mounted by 100-mesh iron powder solved the problem. The fine powder was sintered

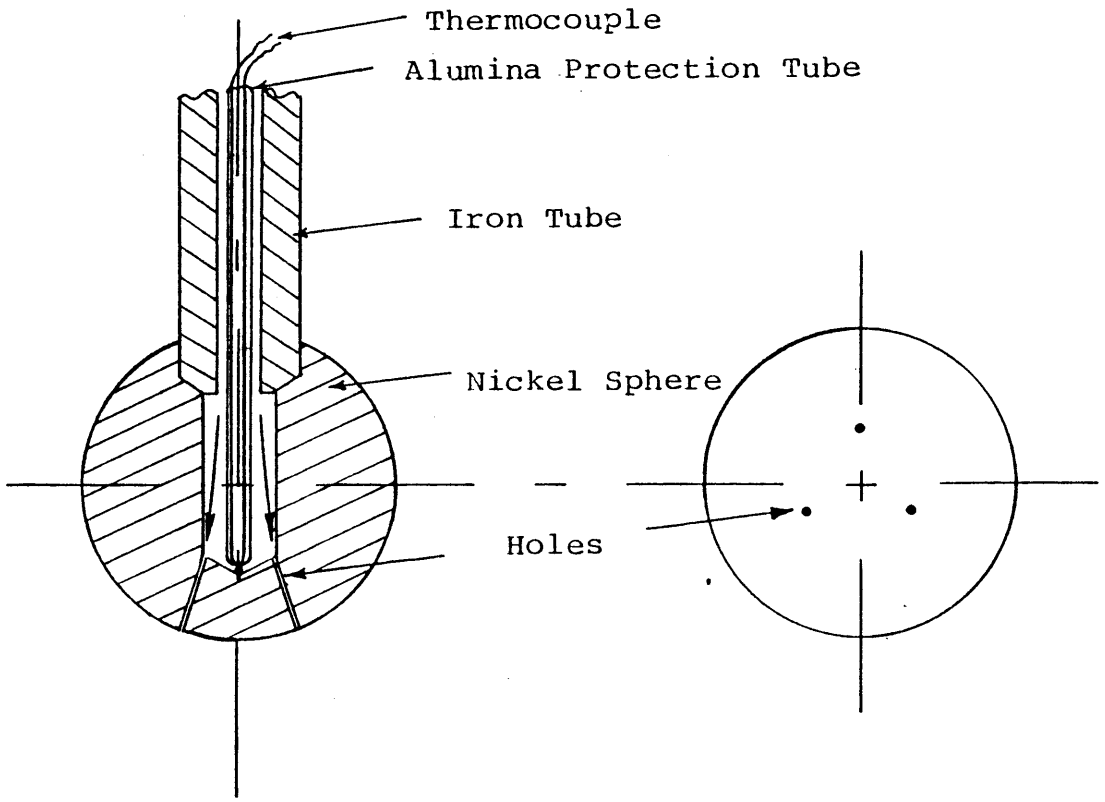


Fig. 3-6 Cast Nickel Sphere (Rad., 15 mm) and Thermocouple Assembly. Diameter of Gas Ports, 0.7 mm.

to the stem when heated. While improving the attachment of the iron ball to the stem, it eliminated the excess permeability of the sinter at the joining area.

c. Prereduced Pellet

A blind hole 3 mm in diameter was first bored into a DRI pellet for thermocouple insertion. The pellet was then attached to the support structure in the following way: (a) it was pierced 5 mm deep with a 7 mm drill, (b) two 0.7 mm openings were made in the pellet, connecting the bottom of the thermocouple well to the external surface of the pellet, (c) a piece of steel wire was passed through these openings attaching the pellet to a 5.3 mm I.D. iron nipple. The free ends of this wire were passed up the support nipple. At the top of this nipple, they were held in place by a short length of iron pipe that was pounded into an iron bushing connected to the nipple at the top. This piece-pipe was tapered to fit the bushing and notched to prevent shearing of the wire ends. A pellet attached to its support structure is schematically shown in Figure 3-7.

Special attention was paid during drilling to avoid oxidation or contamination of the pellets. They were drilled slowly and neatly, in order to keep them cold and clean.

3. Bubbling in Slag

Effect of evolution of gas on the rate of heating of immersed particles was simulated either by forcing nitrogen thru gas ports of nickle particles and porous surface of sintered spheres or heating a partially metallized pellet in hot slag and measuring the temperature of the specimens and the thickness of the shell of slag frozen on the

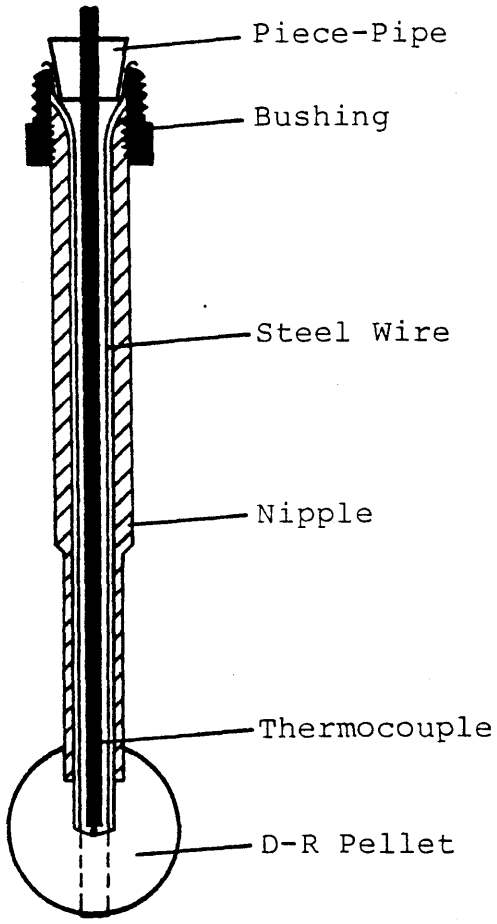


Fig. 3-7 DRI Pellet with Supporting Stem.

particles. The nature of gas bubbling was investigated.

a. Forced Bubbling

Cast nickel and sintered iron spheres were used as the heating specimen in these studies. Nitrogen was used as the bubbling gas. Its flow rate and pressure were measured by a capillary flowmeter and a mercury manometer, respectively. This rate ranged from zero to 1.2 liters per minute (0-6 ℓ/min at slag temperature). Monitoring pressure allowed gas flow rate to remain nearly constant. The effects of forced bubbling on the rate of rise of temperature of various particles were determined.

b. Free Bubbling

Free bubbling was produced as a result of the evolution of gas when a D-R pellet was heated in a bath of hot slag. Because of variation in the physical and chemical specifications of pellets, it was difficult to produce comparable data. Nevertheless, a number of heat transfer measurements were made with and without evolution of gas from DRI pellets. In the former the gases formed in the pellet evolved into the slag whereas in the latter they were sucked out from the supporting tube for volumetric measurements. The results obtained for different pellets were compared.

c. Nature of Gas Evolution

Motion pictures were taken of the surface of the liquid slag B when agitated by rising gas bubbles. Since the liquid was not transparent, it was not possible to observe the gas bubbles when forming or ascending thru the slag. A Glycerin-10% water solution was therefore used to determine the physical specifications of the evolving bubbles. The

Table 3-5 Data on Gas Evolution in Glycerin - 10% Water Solution.

| Gas Rate $cm^3$/min. port | Gas | Average Dia. of Bubbles, mm | Velocity cm/sec | Frequency bubble/sec | Mean Dia. Calculated, mm |
|---|---|---|---|---|---|
| 338 | He | 7.2 | 21 | 13.6 | 9.3 |
| 589 | $N_2$ | 9.3 | 24 | 14.0 | 11.0 |
| 909 | He | 10.9 | 25 | 15.5 | 12.23 |
| 1307 | He | 11.6 | 26 | 16.1 | 13.7 |
| Jet Action* | | | | | |
| 2020 | $N_2$ | 12.1 | 32 | 21.4 | 14.4 |
| 2789 | $N_2$ | 14.9 | 33 | 27.5 | 14.8 |

*Two single-bubbles immediately after formation join together making a larger bubble. The data is given for the latter.

viscosity of this solution was the same as that of the liquid slag (2 poise).[92] Motion pictures were taken from the surface and the bulk of this solution, while gas bubbles were evolving from a 3-cm diameter nickel sphere into the solution. These pictures were compared with those taken from the surface of liquid slag. The size of the bubbles when they burst at the surface of the liquids was almost the same.

Size, velocity and frequency of evolution of the bubbles determined from the pictures taken from Glycerin-water solution are given in Table 3-5. The observations show that at high gas rates (2.8 ℓ/min. port) two single-bubbles leaving a gas port make a single-bubble of considerably larger size by joining togehter. Also, the rising gas bubbles shield the surface of the immersed sphere partially.

# CHAPTER IV

# RESULTS

Illustrative results of the experiments are divided into three categories: (1) information on volume and composition of gases from D-R materials, (2) results of phase transformation studies, and (3) data obtained from heat transfer measurements in hot slags.

## A. Formation of Gas in DRI

Results of the experimental studies on formation of gas in DRI are presented under constant and variable temperature extractions. Sample examples are described.

### 1. Constant Temperature Extraction

The oxygen contents of DRI samples that react with hydrogen or carbon during hydrogen extraction tests are given in Tables 4-1 and 4-2. The size of the grains and the analyses of the materials reported by manufacturer are also specified.

The exhaust of the hydrogen extraction capsule contained $H_2$, $H_2O$, CO and $CO_2$, while that of the helium extraction capsule contained He, CO, $CO_2$ and a small amount of water vapor that did not exceed 1.5 cubic centimeter of cold gas per gram of DRI. The reduction reactions that occur during final reduction of samples under hydrogen and helium are described in Chapter VI.

The composition of the gases produced during He extraction tests was determined as a function of the temperature of the capsule. The oxygen and carbon contents of the samples that reacted during a test were deduced from these data. Since the carbon contents of a number of samples exceed the balance of oxygen for complete reduction of DRI, the

Table 4-1 Chemical Composition of HYL Pellets*.

| Size mm | Pellet Type | G | A | B | C | D | H |
|---|---|---|---|---|---|---|---|
| | % Met | (94.3) | (93.6) | (89.9) | (93.9) | (89.4) | (93.0) |
| Hydrpgen Extraction 1¢ | %O | | | 3.28 | 2.22 | 3.19 | 2.43 |
| | S.D. | | | 0.26 | 0.07 | 0.11 | 0.32 |
| | % C | | | 2.23 | 1.57 | 2.08 | 1.40 |
| | S.D. | | | 0.17 | 0.08 | 0.08 | 0.34 |
| Hydrpgen Extraction 2χ | %O | 2.01 | 2.17 | 3.24 | 2.14 | 3.05 | |
| | S.D. | 0.32 | 0.22 | 0.29 | 0.03 | 0.12 | |
| | %C | 1.06 | 1.18 | 2.44 | 1.50 | 2.04 | |
| | S.D. | 0.22 | 0.10 | 0.21 | 0.06 | 0.08 | |
| Analysis # | (% O) | | (2.23) | (3.45) | (2.11) | (3.61) | |
| | %C | | 1.67 | 2.21 | 1.93 | 2.22 | |
| | S.D. | | 0.05 | 0.04 | 0.04 | 0.02 | |

*Figures within parantheses are calculated from the data on chemical analysis of DRI based on the assumption that the pellets contain 5% Gangue.

#Reported by manufacturer.

¢ 16-18 mesh screens with openings of 1190-1000 microns.

χ8-10 mesh screen with openings of 2.0 - 2.38mm.

Table 4-2. Chemical Composition of MIDREX materials.

| | Size mm | Pellet type | E | E (0.6 mm) | F | Lump Ore |
|---|---|---|---|---|---|---|
| | | % Met | 94.6 | | 91.7 | 92.0 |
| Hydrogen Extraction[1] | | % O | 1.99 | 1.90 | 2.55 | 1.85 |
| | | S.D. | 0.05 | 1.12 | 0.17 | 0.10 |
| | | % C | 1.38 | 1.38 | 0.93 | 1.07 |
| | | S.D. | 0.01 | 0.13 | 0.13 | 0.05 |
| Hydrogen Extraction[2] | | % O | 1.87 | | | |
| | | S.D. | - | | | |
| | | % C | 1.35 | | | |
| | | S.D. | - | | | |
| Analysis[#] | | % O | 1.48 | | 2.14 | 2.17 |
| | | % C | 1.78 | | 0.90 | 1.00 |
| | | % Gangue | 5.54 | | 11.66 | 3.03 |

[#] Reported by manufacturer.

quantities obtained from extraction tests may be less than the total carbon content of the samples.

a. Period of Total Reduction

The time necessary for reduction reactions to approach an equilibrium state was about 10 hours and was chosen as the standard period for long term reduction of DRI samples.

In Figure 4-1, the rates of reduction of the 1 mm size samples of types B and E at 750°C are plotted against the reaction time. From this figure, % O/% C ratio for the long-term (10 hours) extraction of type B pellets is 1.8. This ratio is 1.5 for type E. The volume fraction of $CO_2$ is therefore no more than 0.36 for type B and no more than 0.13 for type E pellets, at 750°C. A plot is made of the total volume of the gases evolved (CO, $CO_2$, $H_2O$) from these samples as a function of the extraction time in Figure 4-2.

b. Long-Term Helium Extraction

Results of the 10-hour reduction of type B pellets under a helium atmosphere and at various temperatures are shown in Table 4-3. The percentages of oxygen and carbon that have undergone reaction are given in this table. The results show that above 700°C, CO is the major component of the exhaust while $CO_2$ and $H_2O$ partial volumes decrease as temperature rises. These results are explained in terms of the equilibria of the reactions in Chapter VI. Similar data for various DRI samples with different chemical compositions are given in Tables 4-4 to 4-8. The total oxygen and carbon contents of the samples shown in parentheses are selected from the data of Tables 4-1 and 4-2.

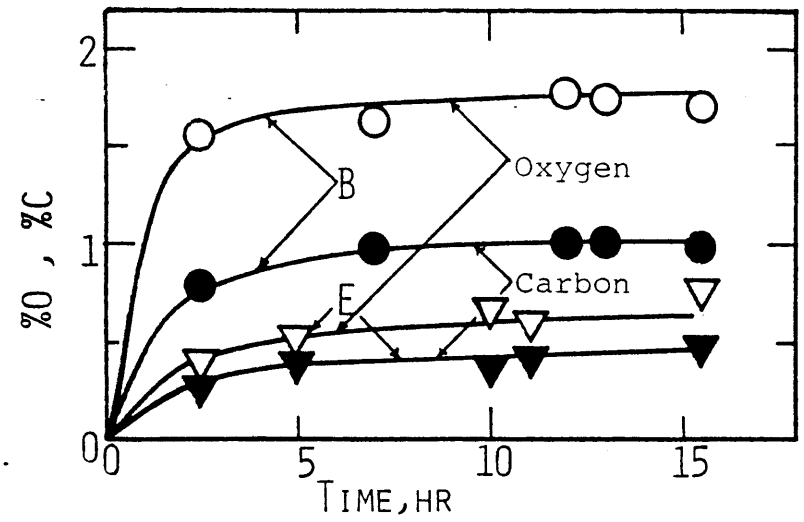


Fig. 4-1 Percentage of Reacting Oxygen and Carbon of Types B and E Pellets vs. Period of Helium Extraction. Temp. of Furnace, 750°C. Particle Size, 1 mm.

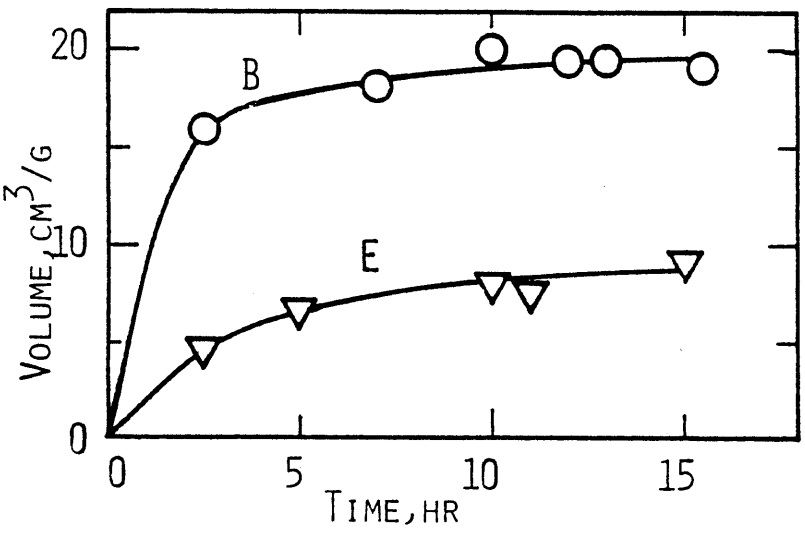


Fig. 4-2 Total Volume of Released Gas During Helium Extraction of Types B and E Pellets. Temp. of Furnace, 750°C. Particle Size, 1 mm.

Table 4-3 Results of the Extraction for Type B Pellets (%O = 3.26, %C = 2.21)*.

| T(°C) | Size (mm) | %O | %C | $CO/CO_2$ | V($Cm^3/g$) $H_2O$ | $CO_2$ | CO |
|---|---|---|---|---|---|---|---|
| 505 | 2 | 0.08 | 0.00 | 0.0 | 0.2 | 1.2 | 0.0 |
| 583 | 2 | 0.67 | 0.29 | 0.5 | 0.4 | 3.6 | 1.8 |
| 673 | 2 | 1.38 | 0.70 | 1.2 | 0.3 | 6.0 | 7.1 |
| 727 | 1 | 1.65 | 0.90 | 1.7 | 1.3 | 3.1 | 15.6 |
| 746 | 1 | 2.06 | 1.13 | 1.8 | 0.3 | 7.5 | 13.6 |
| 768 | 2 | 2.00 | 1.17 | 2.8 | 0.3 | 5.8 | 16.1 |
| 840 | 2 | 2.22 | 1.44 | 6.1 | 0.3 | 3.8 | 23.2 |
| 891 | 1 | 2.75 | 1.78 | 5.8 | 0.4 | 4.9 | 28.3 |
| 935 | 2 | 2.48 | 1.65 | 6.9 | 0.0 | 3.9 | 27.0 |
| 985 | 2 | 3.12 | 2.07 | 6.7 | 0.1 | 5.1 | 33.5 |

*The chemical compositions are selected from the data of Table 4-1.

The total volumes of gas are plotted against the temperature of the capsule in Figures 4-3 and 4-4. The effects of the size of the samples on these volumes are also shown. As is seen, the results of the 2 mm size samples do not differ appreciably from those of the 1 mm ones. However, the spread of the data obtained from the extraction of the 3 mm size samples is substantially wider than that of the others. This difference is probably due to the lack of homogeneity in chemical composition of the 3 mm crushed materials.

To prove that the total volume of the evolved gas is basically controlled by the chemical composition of the charge, 30% totally reduced type D pellets were mixed with 70% non-reduced ones to prepare a new sample (designated H in Table 4-1) with the same composition as that of type C. The results of hydrogen extraction for this sample (H) is given in Table 4-1. As is seen, the oxygen content of sample H is about 10% more than that of type C pellets.

The data obtained from helium extraction of sample H are illustrated in Table 4-5 and Figure 4-3. These data show that the total volume of the extracted gas and the content of oxygen removed from the sample are also about 10 percent higher than that of type C. This result indicates that the total volume of the evolved gas is nearly proportional to the oxygen content of DRI materials, if there is sufficient carbon available to react with the oxygen.

The results of helium extraction tests (Figures 4-3 and 4-4 show that the evolution of gas from DRI starts around 500°C, continues proportional with temperature and slows down as the temperature exceeds

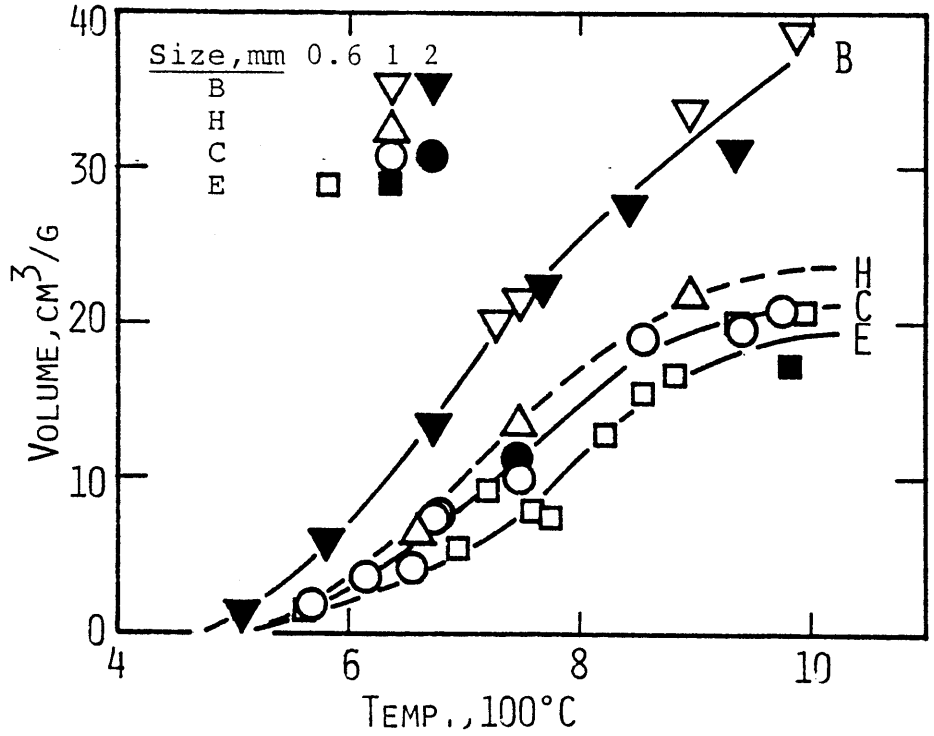


Fig. 4-3 Total Volume of Gases Evolved During He Extraction of D-R Materials.

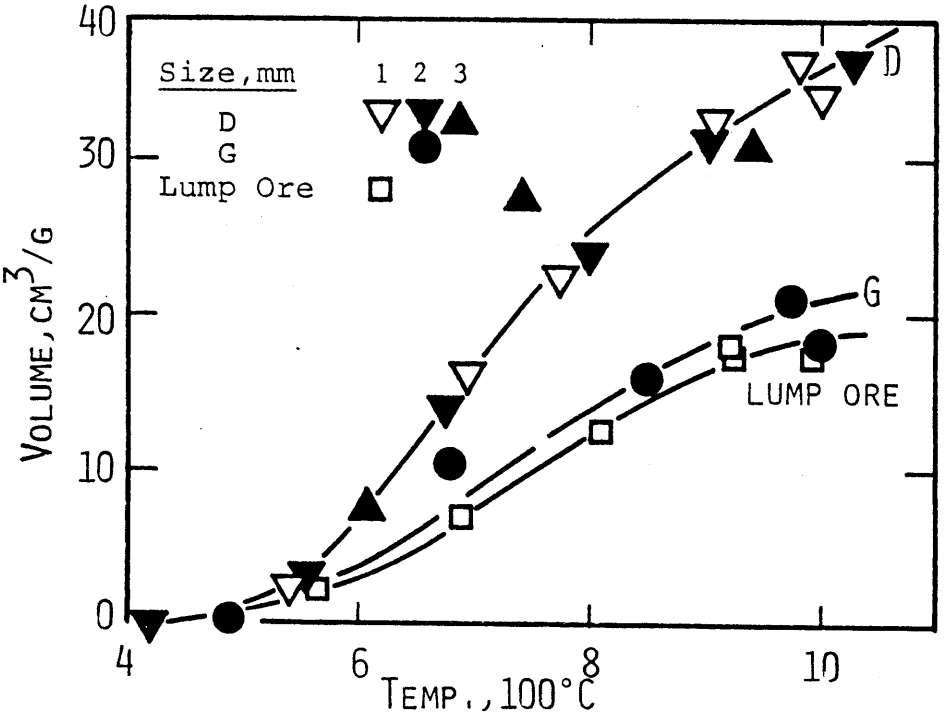


Fig. 4-4 Total Volume of Gases Evolved During He Extraction of D-R Materials.

Table 4-4 Results of the Extraction for Type D pellets (%O = 3.12, %C = 2.22).

| T(°C) | Size (mm) | %O | %C | $CO/CO_2$ | V($cm^3/g$) $H_2O$ | $CO_2$ | CO |
|---|---|---|---|---|---|---|---|
| 420 | 2 | 0.00 | 0.00 | 0.0 | 0.1 | 0.2 | 0.0 |
| 543 | 1 | 0.35 | 0.11 | 0.0 | 0.5 | 2.5 | 0.0 |
| 553 | 2 | 0.40 | 0.15 | 0.2 | 0.2 | 2.5 | 0.4 |
| 608 | 3 | 0.88 | 0.40 | 0.5 | 0.0 | 4.9 | 2.6 |
| 673 | 2 | 1.45 | 0.73 | 1.1 | 0.2 | 6.4 | 7.3 |
| 695 | 1 | 1.64 | 0.83 | 1.3 | 0.9 | 6.7 | 8.8 |
| 737 | 3 | 2.64 | 1.53 | 2.2 | 0.0 | 9.1 | 19.6 |
| 774 | 1 | 1.95 | 1.19 | 3.7 | 0.2 | 4.7 | 17.5 |
| 803 | 2 | 2.02 | 1.28 | 4.5 | 0.1 | 4.3 | 19.5 |
| 903 | 2 | 2.53 | 1.67 | 6.3 | 0.0 | 4.3 | 26.9 |
| 908 | 1 | 2.62 | 1.71 | 6.0 | 0.1 | 4.6 | 27.4 |
| 940 | 3 | 2.55 | 1.57 | 4.8 | 1.4 | 5.0 | 24.3 |
| 978 | 1 | 2.96 | 1.95 | 6.2 | 0.0 | 5.1 | 31.4 |
| 997 | 1 | 2.77 | 1.79 | 6.2 | 0.8 | 4.7 | 28.7 |
| 1028 | 2 | 2.89 | 1.94 | 7.8 | 0.2 | 4.1 | 32.0 |

Table 4-5 Results of He Extraction for Type C Pellets (%O = 2.18, %C = 1.93).

| T(°C) | Size (mm) | %O | %C | $CO/CO_2$ | V($cm^3/g$) $H_2O$ | $CO_2$ | CO |
|---|---|---|---|---|---|---|---|
| 565 | 1 | 0.24 | 0.05 | 0.0 | 0.8 | 1.7 | 0.0 |
| 615 | 1 | 0.51 | 0.14 | 0.0 | 0.9 | 3.6 | 0.0 |
| 651 | 1 | 0.47 | 0.23 | 0.9 | 0.0 | 2.3 | 2.0 |
| 662* | 1 | 0.67 | 0.30 | 0.9 | 0.9 | 2.9 | 2.7 |
| 674 | 1 | 0.72 | 0.35 | 1.3 | 0.7 | 2.9 | 3.6 |
| 676 | 1 | 0.70 | 0.35 | 1.7 | 0.8 | 2.5 | 4.1 |
| 746 | 1 | 0.88 | 0.53 | 3.3 | 0.1 | 2.3 | 7.7 |
| 746* | 1 | 1.08 | 0.70 | 3.0 | 1.0 | 2.0 | 10.1 |
| 747 | 2 | 0.94 | 0.60 | 5.1 | 0.1 | 1.8 | 9.4 |
| 853 | 1 | 1.52 | 0.96 | 6.7 | 1.1 | 2.3 | 15.5 |
| 890* | 1 | 1.70 | 1.08 | 4.5 | 0.2 | 3.4 | 16.7 |
| 937 | 1 | 1.56 | 1.07 | 9.7 | 0.0 | 2.2 | 17.8 |
| 971 | 1 | 1.65 | 1.12 | 8.5 | 0.0 | 2.4 | 18.7 |

*Results of He Extraction of Type H Pellets.

Table 4-6 Results of He Extraction for Type G Pellets (%O = 2.01, %C = 1.06).

| T(°C) | Size (mm) | %O | %C | $CO/CO_2$ | V($cm^3$/g) | | |
|---|---|---|---|---|---|---|---|
| | | | | | $H_2O$ | $CO_2$ | CO |
| 487 | 2 | 0.09 | 0.04 | 0.0 | 0.0 | 0.9 | 0.0 |
| 683 | 2 | 0.99 | 0.58 | 2.1 | 0.0 | 3.5 | 7.4 |
| 849 | 2 | 1.27 | 0.77 | 4.2 | 0.6 | 2.8 | 11.7 |
| 970 | 2 | 1.72 | 1.13 | 6.1 | 0.0 | 3.1 | 17.9 |
| 997 | 2 | 1.46 | 0.96 | 6.5 | 0.1 | 2.4 | 15.6 |

Table 4-7 Results of He Extraction for Type E Pellets (%O = 1.92, %C = 1.78).

| T(°C) | Size (mm) | %O | %C | $CO/CO_2$ | V($cm^3/g$) $H_2O$ | $CO_2$ | CO |
|---|---|---|---|---|---|---|---|
| 558 | 0.6 | 0.22 | 0.07 | 0.0 | 0.3 | 1.3 | 0.1 |
| 691 | 0.6 | 0.53 | 0.31 | 2.6 | 0.0 | 1.8 | 4.6 |
| 718 | 1 | 0.81 | 0.49 | 3.6 | 0.2 | 2.0 | 7.1 |
| 823 | 0.6 | 1.04 | 0.69 | 6.7 | 0.0 | 1.8 | 11.2 |
| 854 | 1 | 1.23 | 0.80 | 7.6 | 0.6 | 1.7 | 13.2 |
| 882 | 1 | 1.31 | 0.90 | 9.9 | 0.0 | 1.7 | 15.2 |
| 933 | 0.6 | 1.54 | 1.03 | 10.0 | 0.5 | 1.8 | 17.5 |
| 982 | 1 | 1.34 | 0.94 | 13.4 | 0.0 | 1.4 | 16.1 |
| 996 | 0.6 | 1.55 | 1.07 | 11.7 | 0.1 | 1.6 | 18.4 |

Table 4-8. Results of He Extraction for Lump Ores (%O = 1.85, %C = 1.00).

| T(°C) | Size (mm) | %O | %C | $CO/CO_2$ | V($cm^3/g$) $H_2O$ | $CO_2$ | CO |
|---|---|---|---|---|---|---|---|
| 559 | 1 | 0.29 | 0.12 | 0.3 | 0.1 | 1.8 | 0.5 |
| 692 | 1 | 0.65 | 0.36 | 2.2 | 0.2 | 2.1 | 4.6 |
| 808 | 1 | 1.04 | 0.66 | 5.2 | 0.1 | 2.0 | 10.4 |
| 917 | 1 | 1.49 | 0.95 | 5.0 | 0.0 | 3.0 | 15.1 |
| 923 | 1 | 1.53 | 0.97 | 4.7 | 0.0 | 3.2 | 15.0 |
| 993 | 1 | 1.63 | 0.94 | 5.0 | 0.0 | 5.5 | 12.1 |

900°C. At about 1200°C, the reactions become almost complete and the gas evolution stops. It is also shown that the total volume of gas decreases as the oxygen content of a sample falls off.

2. Variable Temperature extraction

To study the nature of the DRI melting process, we need to know the quantity and composition of the gases that evolve during heating of prereduced materials. Such information can be utilized to determine the changes of properties of materials and to develop a mathematical model for predicting the behavior of the melting system. The rates of evolution and composition of gases are determined by extracting DRI in a bomb and are used to evaluate the total volume of the gases evolved from DRI.

a. Gas Evolution History

The rate of evolution of gas during the bomb extraction of DRI was measured and plotted against the temperature of the center of the charge. This rate was integrated to obtain the total volume of the released gas. The effects of size, composition and the rate of rise of temperature of DRI on the rate and volume of the gases evolved were determined.

The measured temperature of the charge usually fluctuated around the predetermined temperature profile. The results of the bomb extractions were corrected for the actual rate of change of temperature of the sample by multiplying the measured gas rate with a correction factor. The method of derivation of this factor and a sample example of the procedure used to analyze the results of the bomb extractions are described in Appendix C.

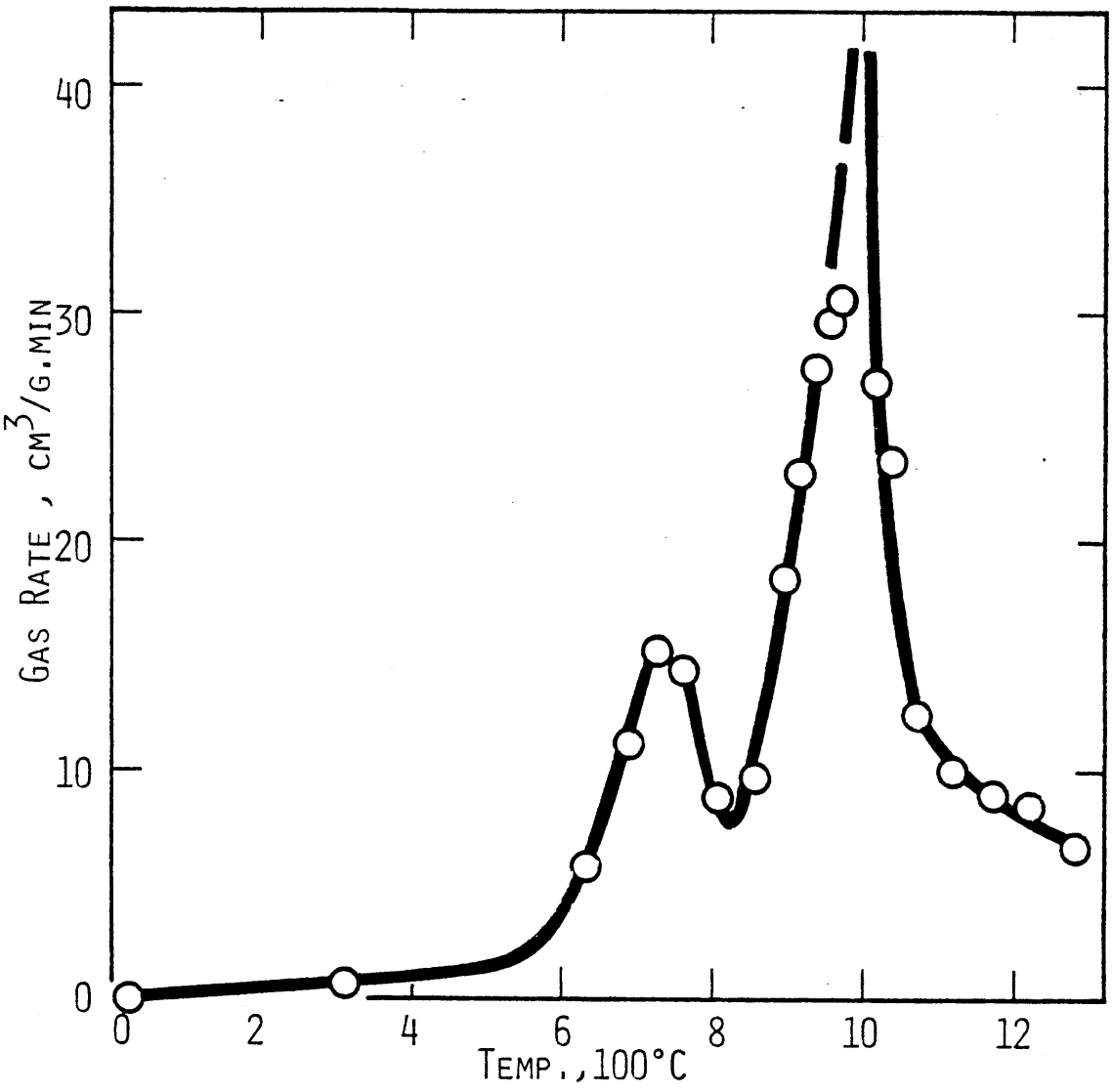


Fig. 4-5 Gas Evolution from Type B Pellets. Temp. Rate, 250°C/min. Particle Size, 1 mm.

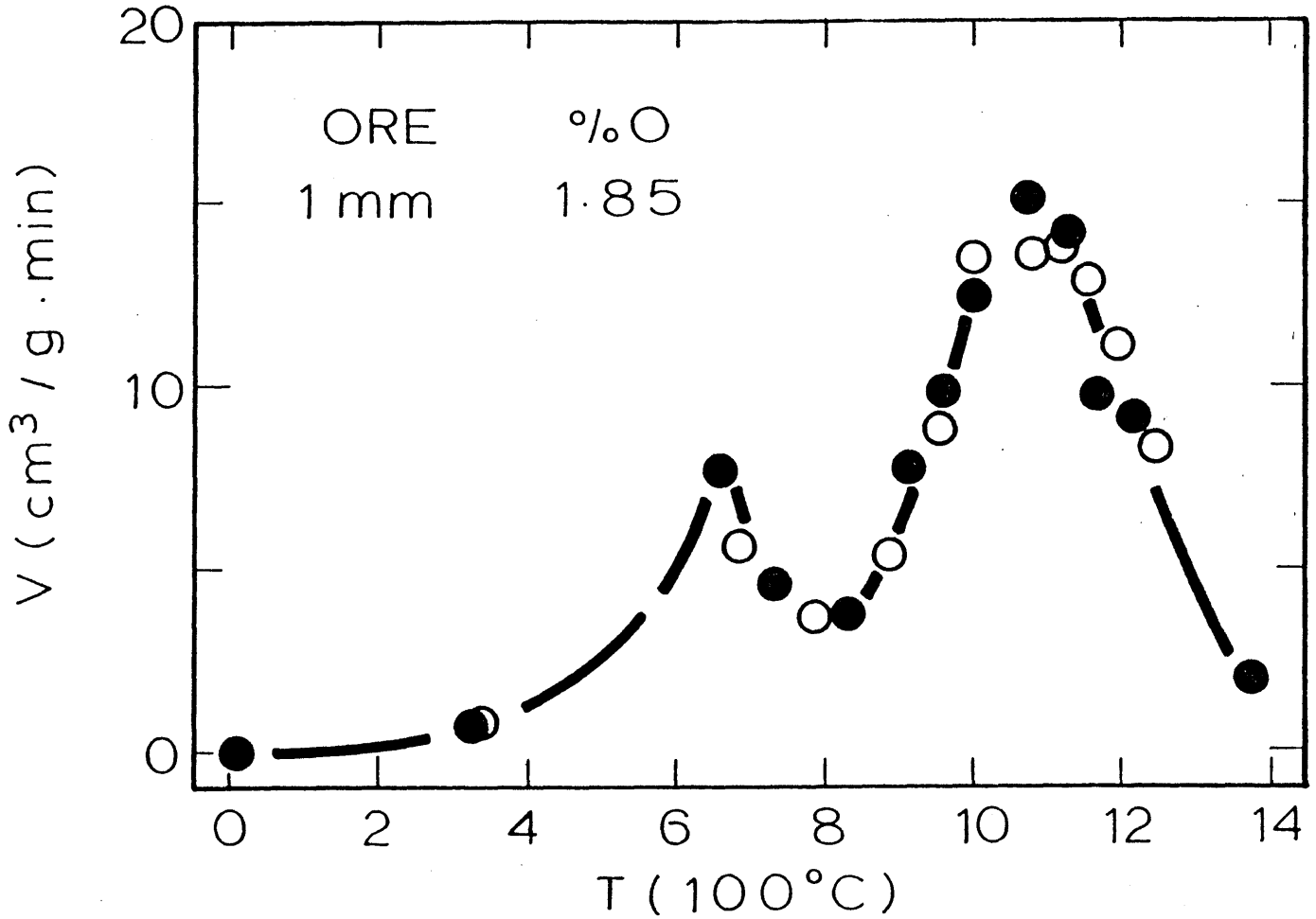


Fig. 4-6 Gas Evolution from Midrex Lump Ore. Temp. Rate, 250°C/min. Particle Size, 1 mm.

Plots are made of the rate of evolution of gas from type B pellets and lump ore materials in Figures 4-5 and 4-6. As is seen, the evolution of gas starts at about 600°C, reaches a maximum at about 700°C, decreases to a minimum at about 800°C, rises to a peak at around 1000°C, and falls off above that. A similar pattern has been obtained during the bomb extraction of DRI samples of various compositions (see Figures 4-11 to 4-13).

The shorter peak in gas evolution curve corresponds with the reduction of magnetite to wustite during which a gas mixture of about 50 percent CO will be produced. The carbide constituent of DRI also starts into solution around the same temperature (see IV.B). The larger peak is associated with the final reduction of wustite to pure iron. Above 1400°C, the rate of evolution of gas tends to zero. A detailed description of gas evolution from DRI is given in Chapter VI.

The total volume of gas was obtained by calculating the area under the gas evolution rate diagrams of DRI samples:

$$V_t = \int_0^t \dot{V} \, dt \qquad (4.1)$$

where $V_t$ is the total volume of the gas evolved from DRI until time t and $\dot{V}$ is the rate of evolution of gas at that time. The Trapezoidal Integration method was used for calculation of the area under the curve.

A plot is made of the total volume of the gases evolved versus temperature for type B pellets and lump ore materials in Figure 4-7. The helium extraction curves for these materials are reproduced in the same diagram. It is seen that the volumes of the gases evolved during

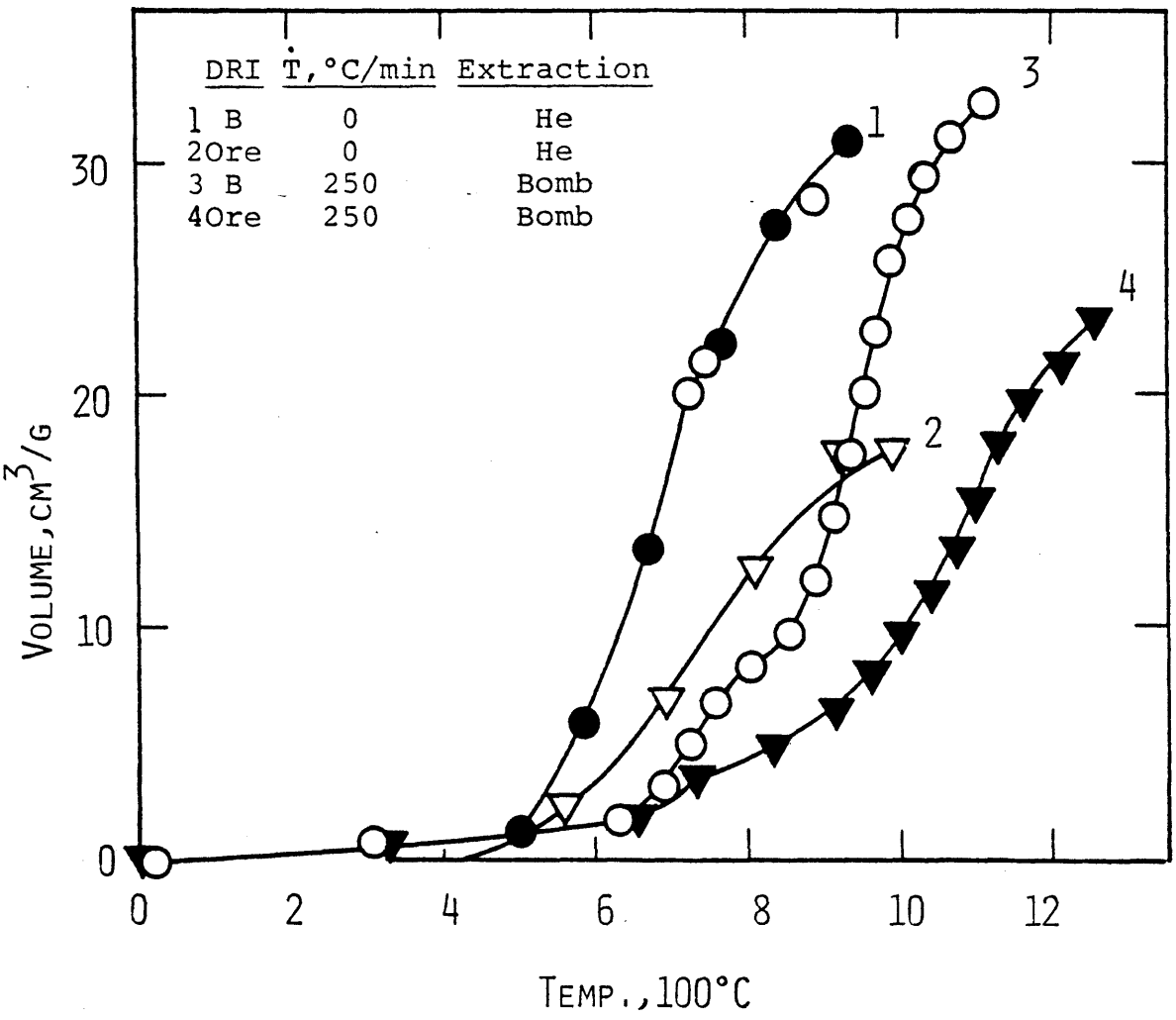


Fig. 4-7 Gas Evolution from Type B Pellets (1,3) and Midrex Lump Ore (2,4). Particle Size, 1 mm.

bomb extraction of the samples are less than those evolved during helium extraction.

Effects of chemical composition, size and the rate of rise of temperature on evolution of gas from DRI are described in subsequent sections.

1. Effect of DRI Composition

The total volumes of gases evolved during bomb extraction of DRI samples of different chemical compositions are plotted in Figures 4-8 and 4-9. The data points for curves which are reproduced are not shown. As is seen, the volumes are higher for DRI samples of higher oxygen contents. The carbon contents of the samples are almost sufficient for total reduction. The effect of the percentage of carbon can therefore be assumed insignificant.

In Figure 4-10, a plot is made of the total volumes of the gases evolved per gram of DRI materials and the balanced content of carbon that is necessary for release of these volumes against percent of metallization of DRI at different extraction temperatures. From this plot, it can be seen that the volume of the gases evolved is almost proportional to the oxygen content of DRI.

A comparison is made of the rate at which gases are evolved from D-R materials of type C with that of type H in Figure 4-11. It is seen that the 10 percent difference in oxygen content of the samples proportionately affects the rates of gas evolution. Because of the deficiency of carbon for total reduction of type H, however, the total volume of gases evolved from type H is less than that of type C at high temperatures.

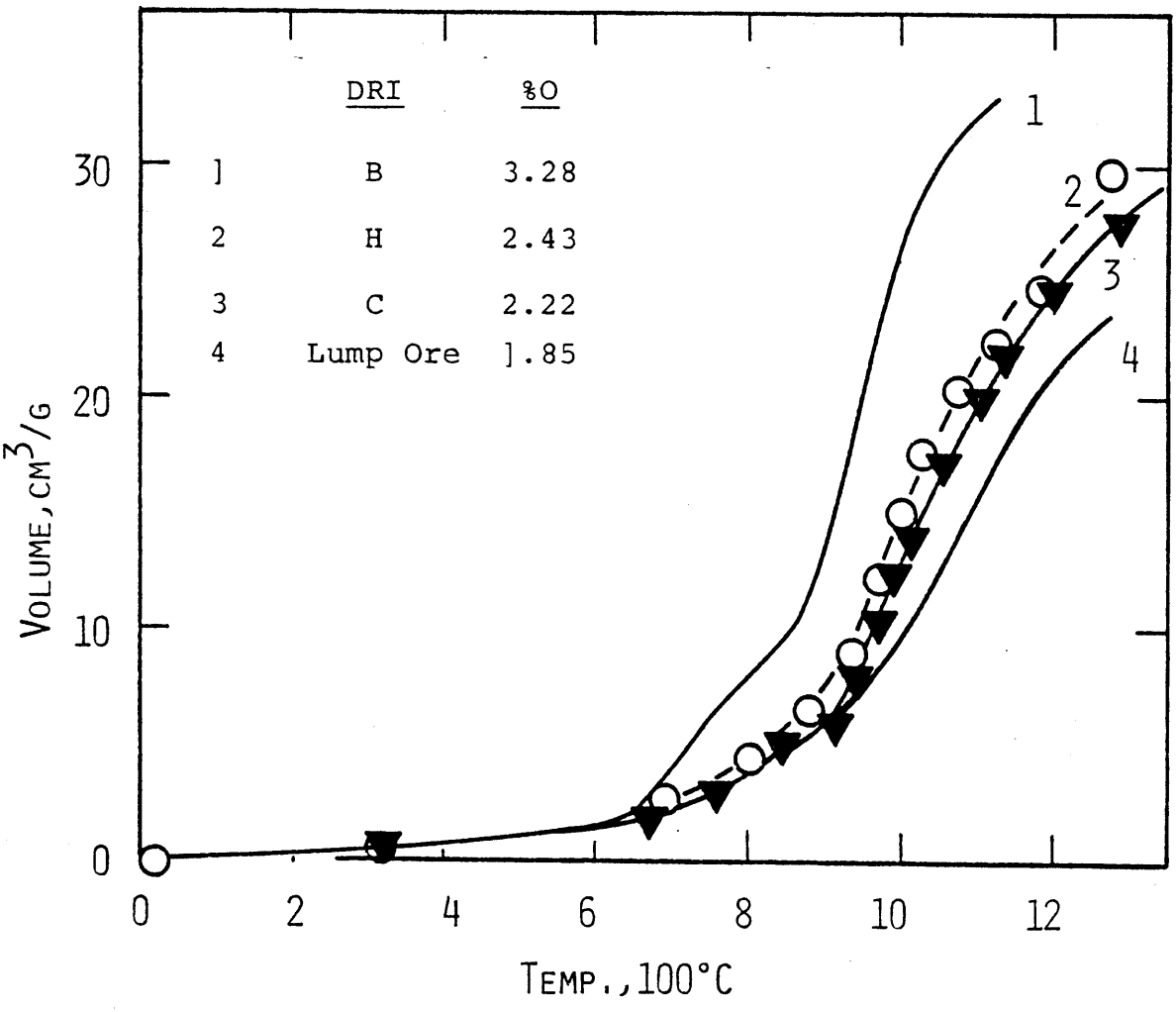


Fig. 4-8 Gas Evolution from DRI. Grain Size, 1 mm. Temp. Rate, 250°C/min.

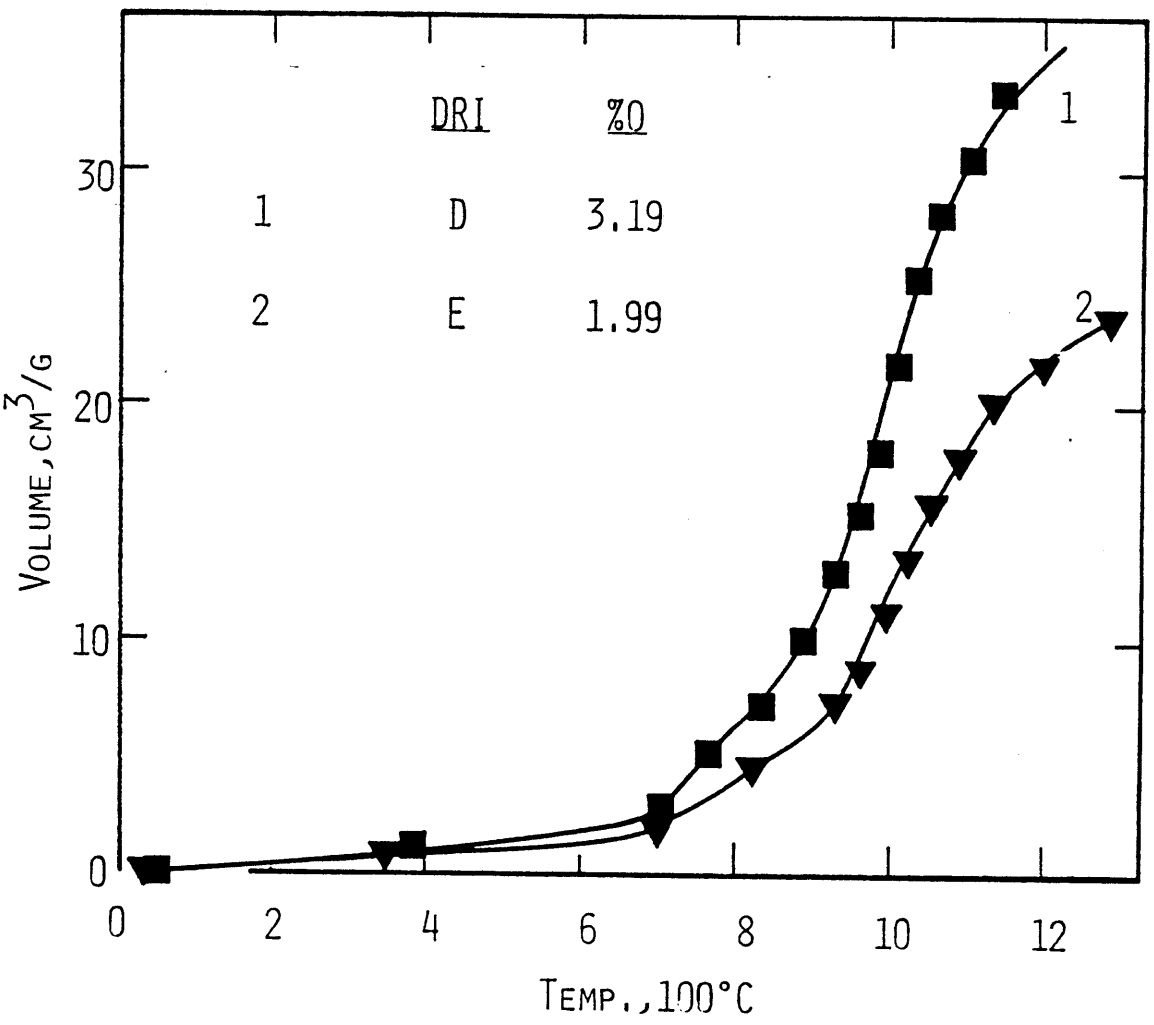


Fig. 4-9 Gas Evolution from DRI. Grain Size, 1 mm. Temp. Rate, 250°C/min.

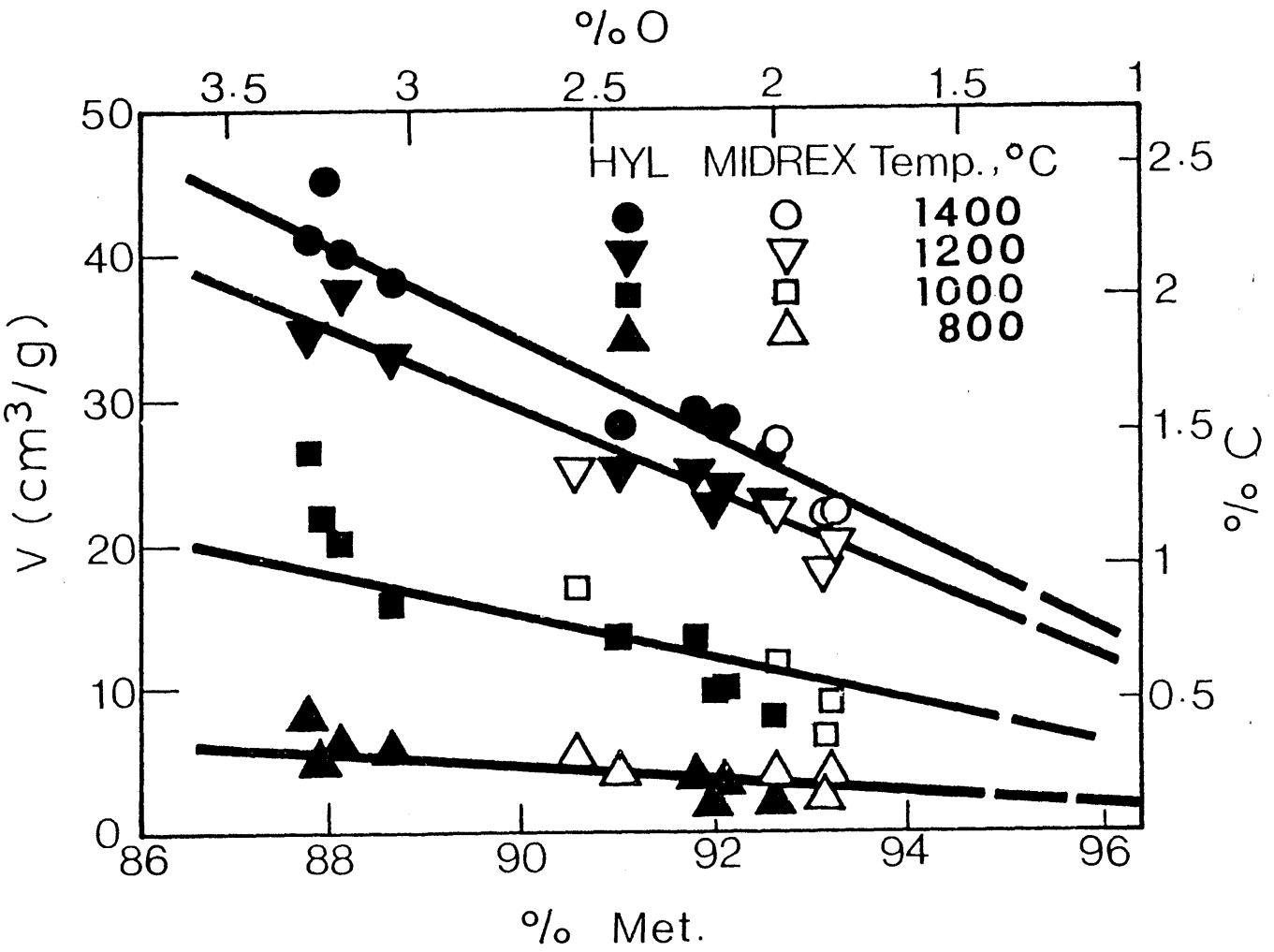


Fig. 4-10 Gas Evolution as a Function of Chemical Composition of D-R Materials. Temp. Rate, 250°C/min.

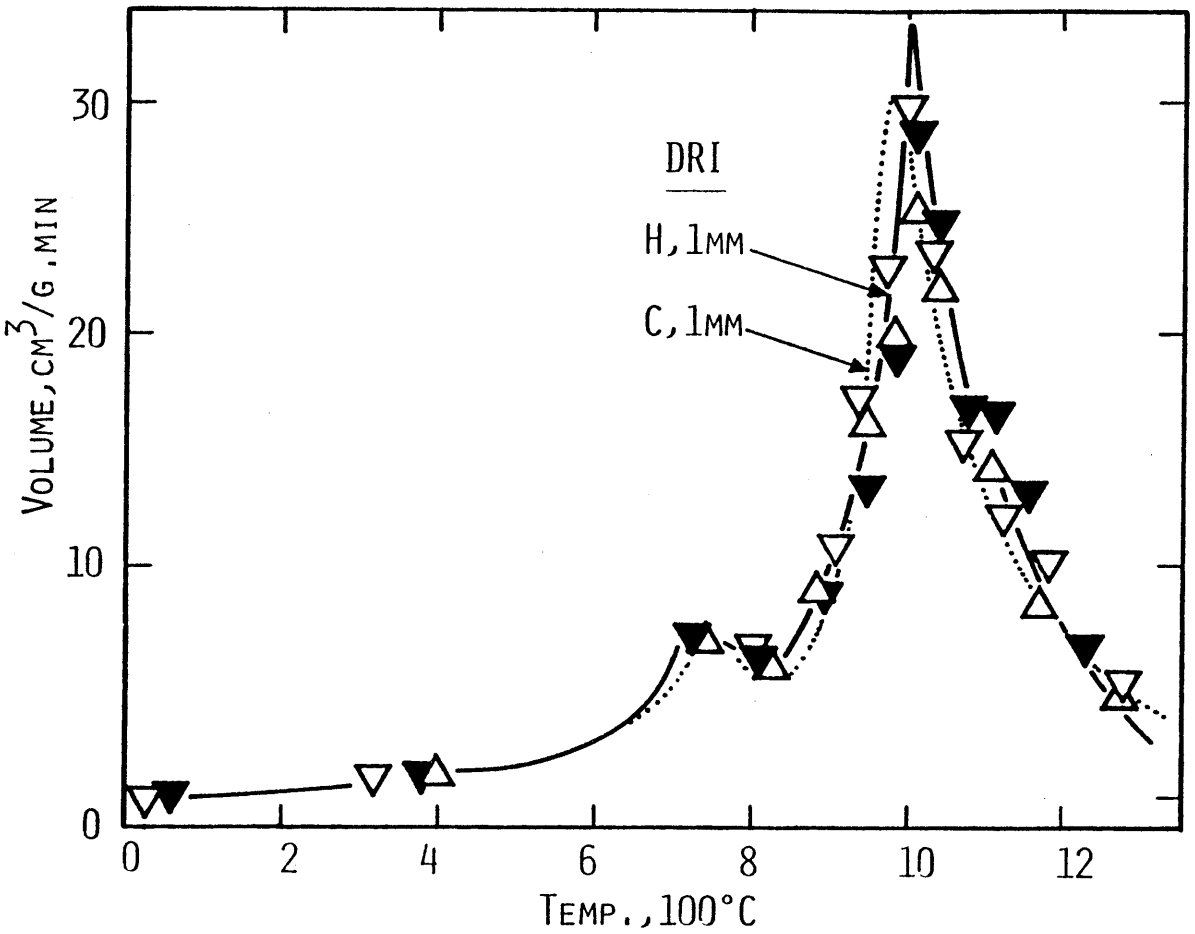


Fig. 4-11 Comparison of Gas Evolution from Type C and Partially Reduced Type H Pellets. Temp. Rate, 250°C/min. Particle Size, 1 mm.

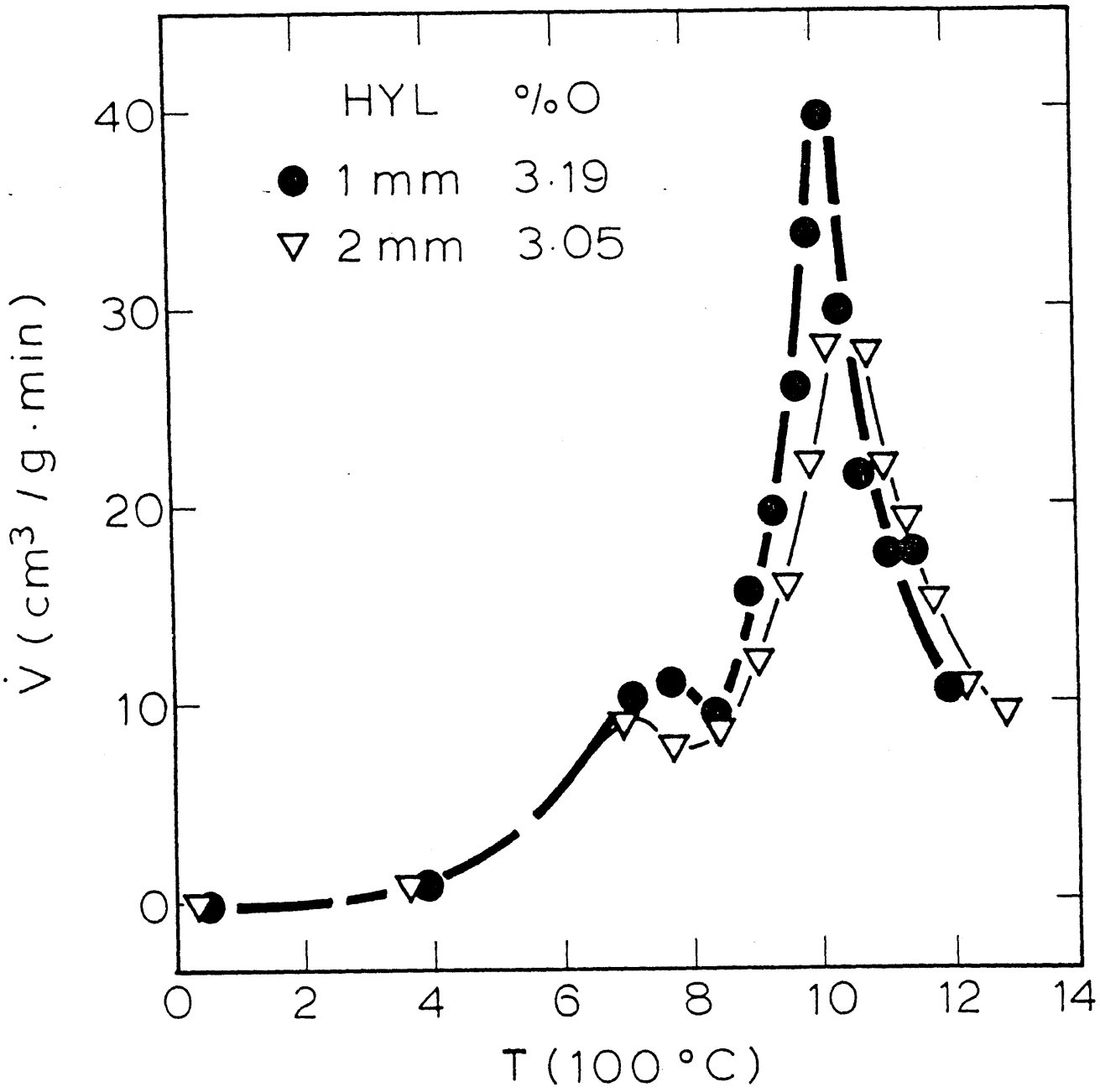


Fig. 4-12 Rate of Gas Evolution from Type D Pellets. Temp. Rate, 250°C/min. Particle Size, 1 and 2 mm.

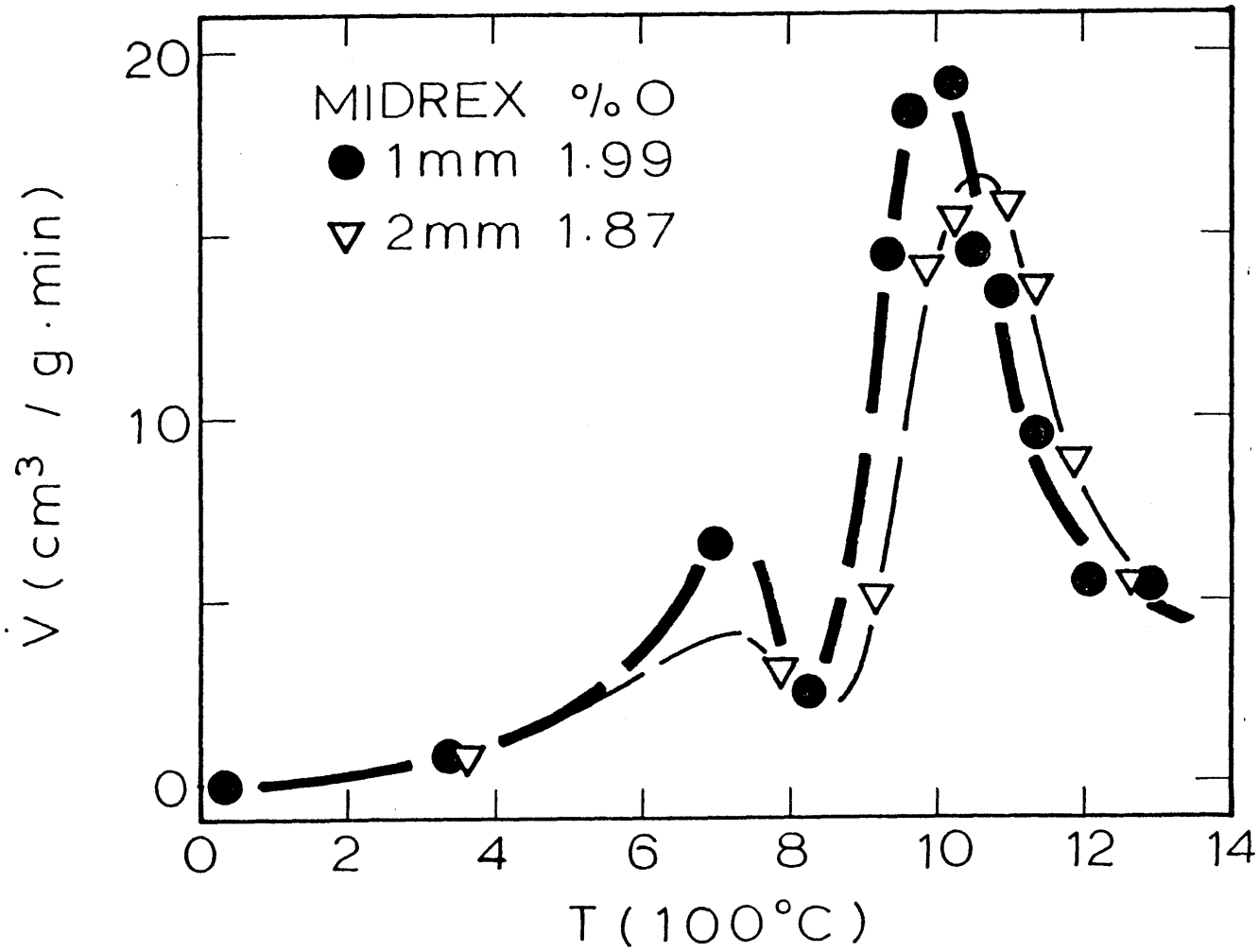


Fig. 4-13 Rate of Gas Evolution from Type E Pellets. Temp. Rate, 250°C/min. Particle Size, 1 and 2 mm.

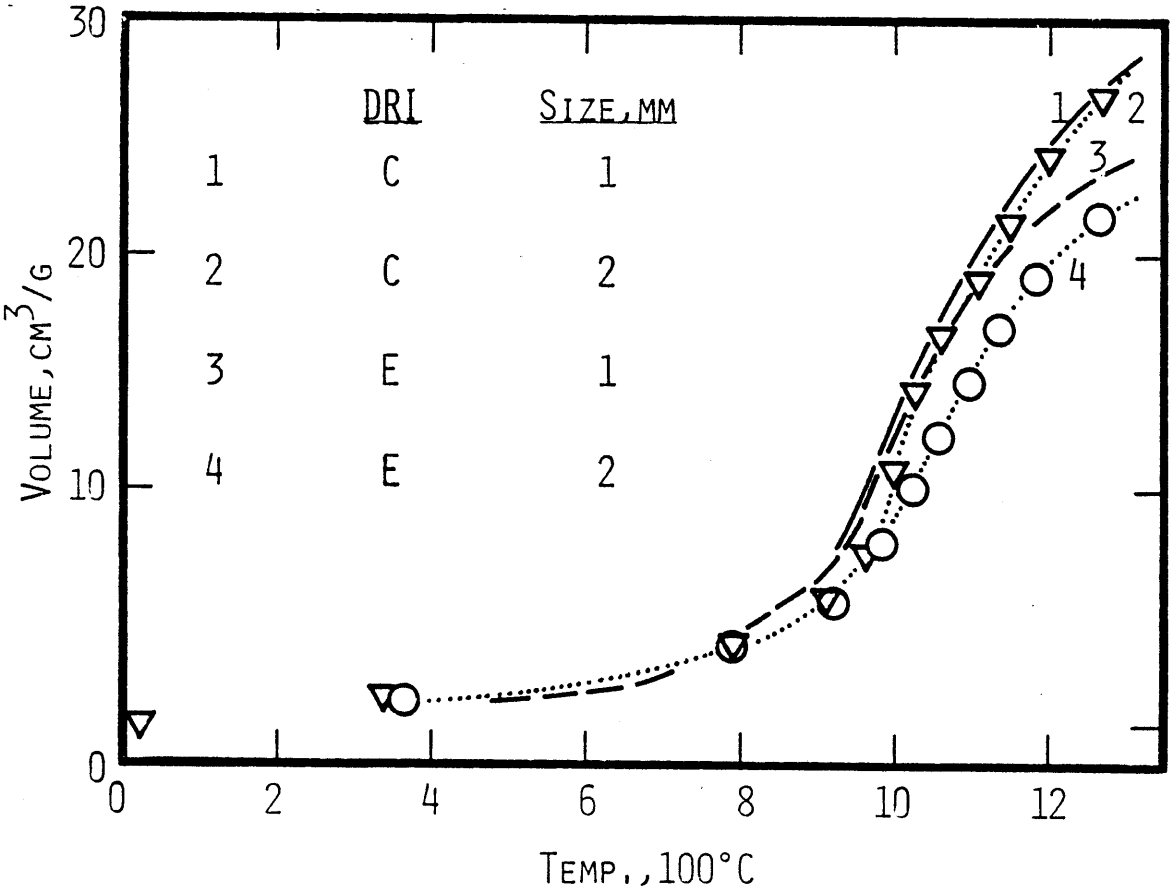


Fig. 4-14 Comparison of Gas Evolution During Bomb Extraction of D-R Materials of 1 and 2 mm Size.

2. Effect of Particle Size

Experimental results show that the effect of particle size on evolution of gas from DRI is not substantial. Comparisons are made of the rate of evolution of gas from D-R materials of 1 and 2 mm size in Figures 4-12, 4-13 and 6-2. The total volumes of the gases evolved are also compared in Figure 4-14. As is seen in these figures, the evolution of gas is slightly higher from samples of 1 mm grain size. The difference may be due to the difference in chemical composition of 1 and 2 mm crushed pellets.

It is seen from Figures 4-12, 4-13 and 6-2 that above about 1000°C the rate of evolution of gas from DRI shifts slightly to the higher temperatures as the particle size increases. This effect may be because of the variation of the thermal conductivity of DRI with grain size. A further explanation is given in Chapter VI.

3. Effect of Heating Rate

The effect of the rate of rise of temperature of DRI on evolution of gas from D-R materials is illustrated in Figures 4-15 and 4-16 where temperature rates ranging from 50 to 1000°C/min are employed. As is seen, the volume of the gases evolved is slightly influenced by the rate of rise of temperature of DRI. As this rate becomes greater, the total volume of the gases evolved increases below 1000°C but decreases above that temperature.

Comparisons are also made of the rate of evolution of gas from DRI materials heated under various temperature rates in Figures 4-17 and 4-18. It is seen that the rate of evolution of gas increases as the

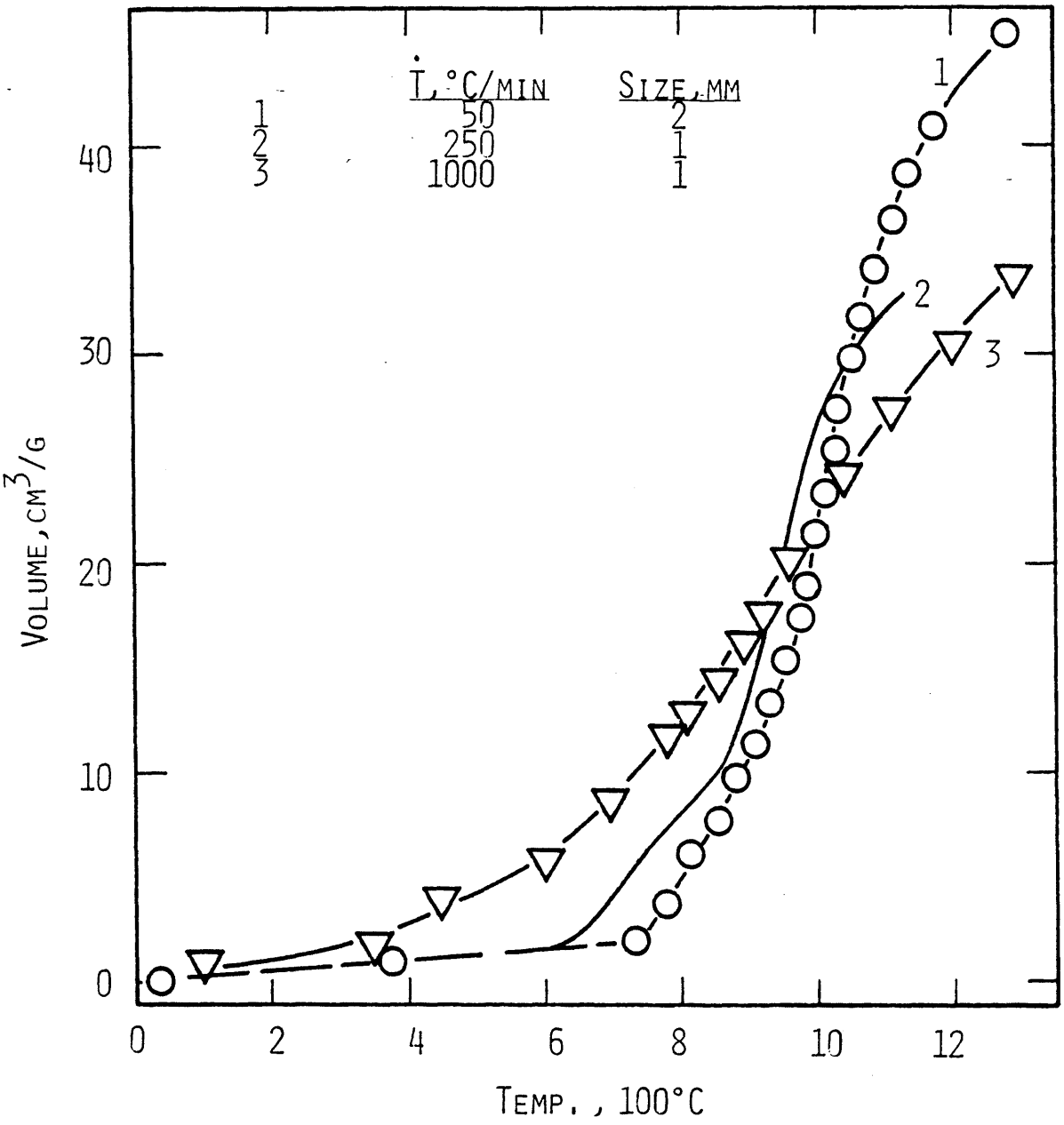


Fig. 4-15 Effect of Heating Rate on Gas Evolution from Type B Pellets. Particle Size, 1 and 2 mm.

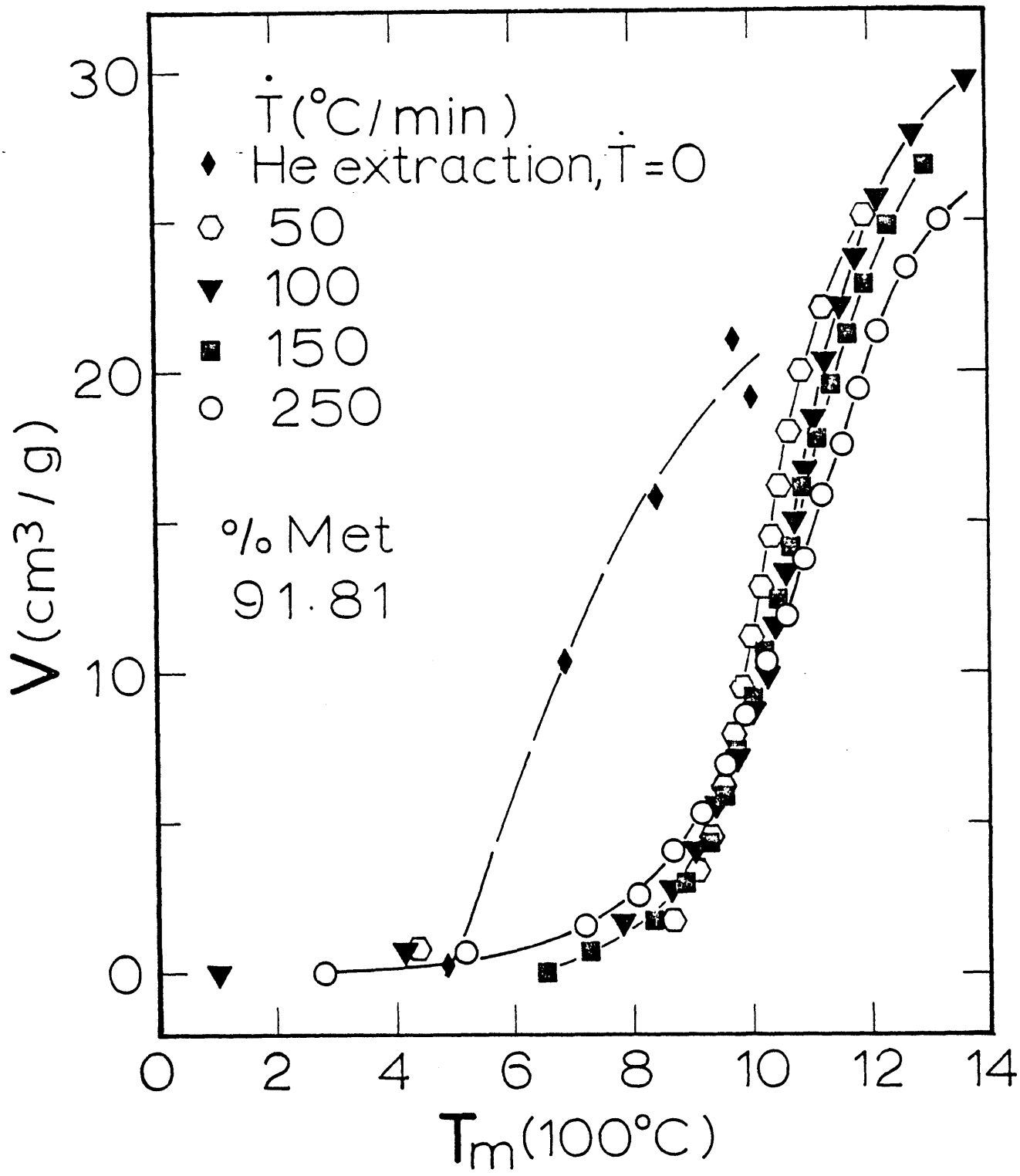


Fig. 4-16 Effect of Heating Rate on Gas Evolution from Type G Pellets. Particle Size, 2 mm.

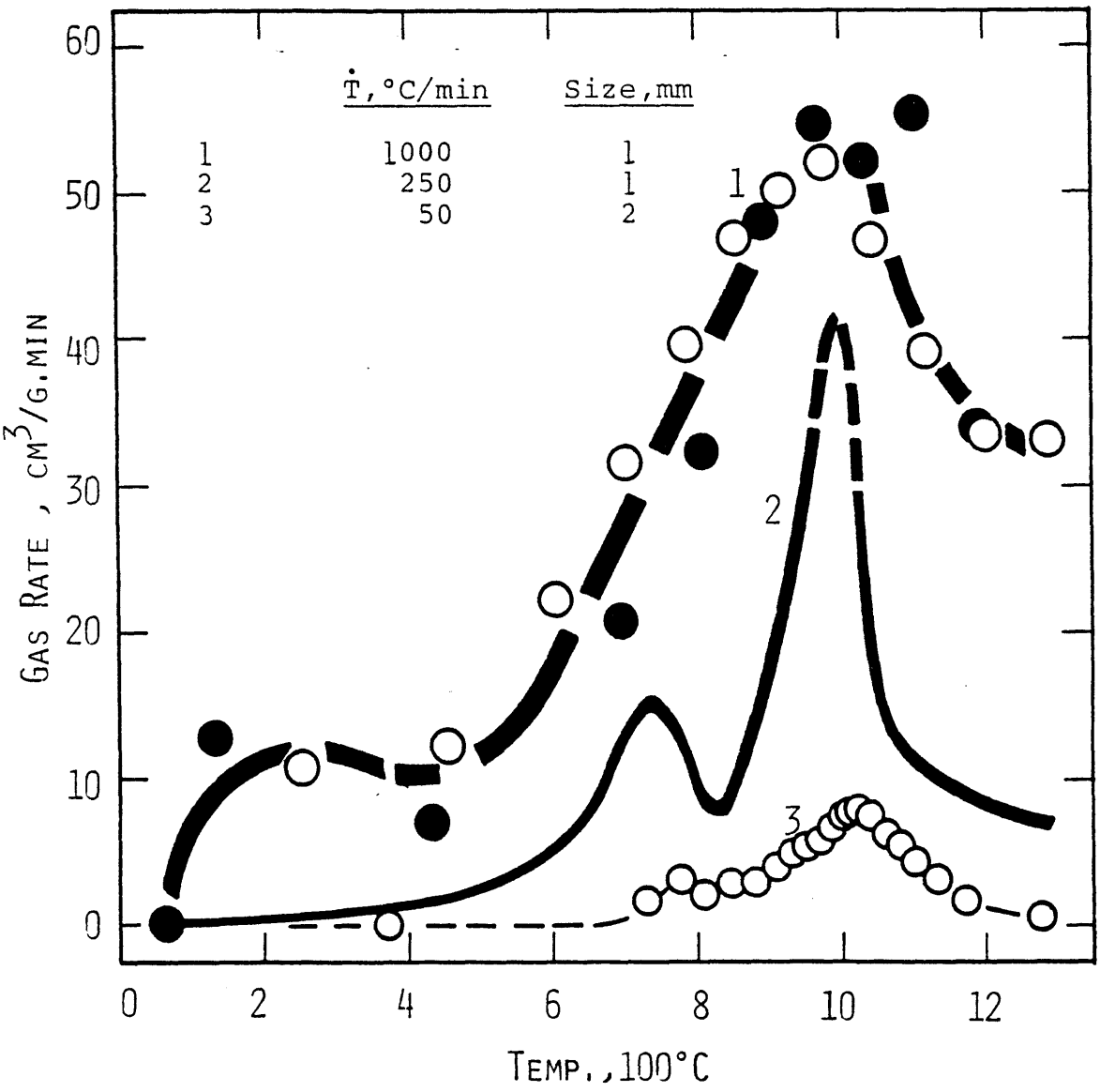


Fig. 4-17 Comparison of Gas Evolution from Type B Pellets at Different Heating Rates. Particle Size, 1 and 2 mm.

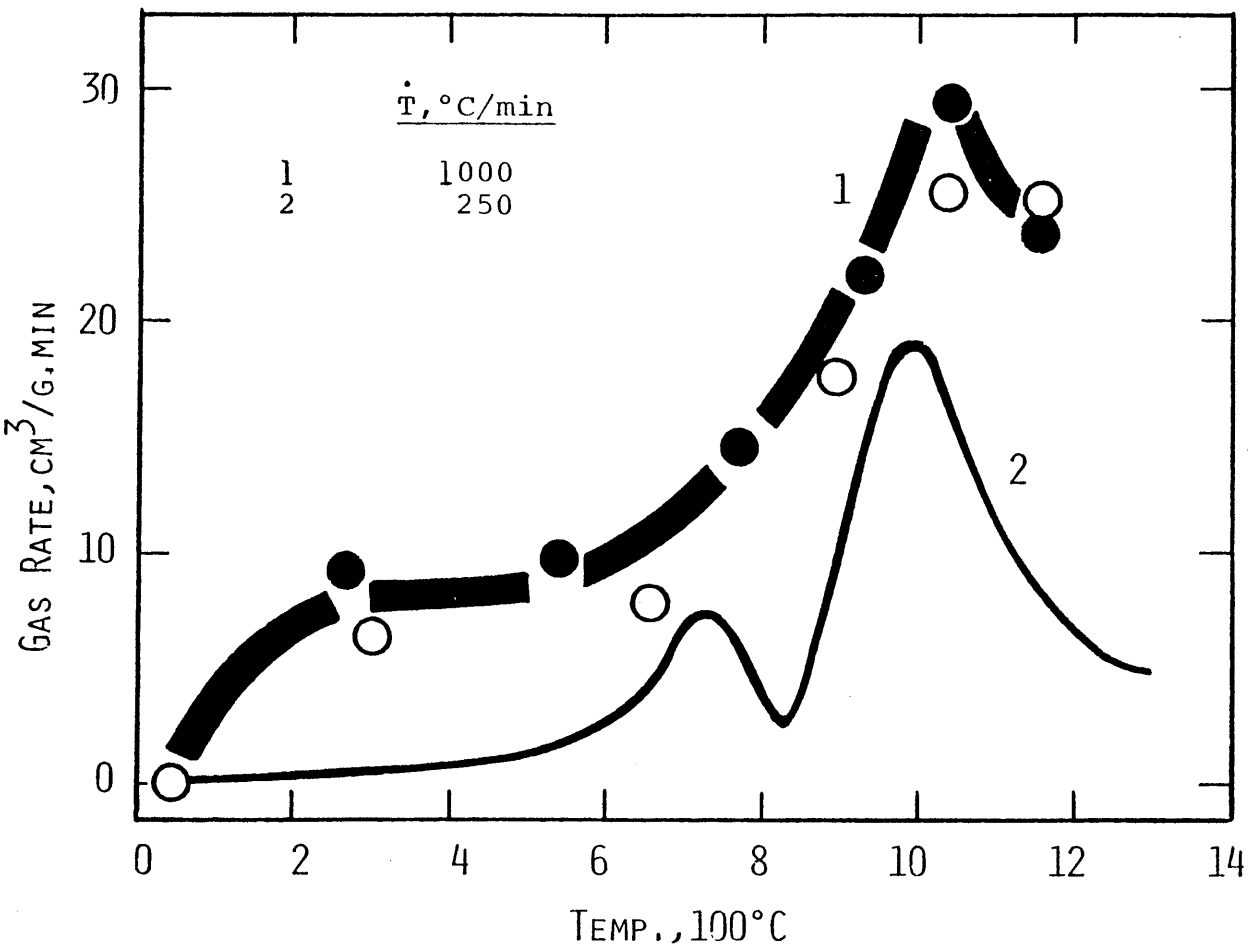


Fig. 4-18 Comparison of Gas Evolution from Type E Pellets at Different Heating Rates. Particle Size, 1 mm.

heating rate increases. For 1000°C/min, the evolution of gas occurs even at very low temperatures, but the smaller peak of the rate curves is eliminated.

b. Composition of Gas

The composition of gases evolved during bomb extraction of D-R materials was determined by analyzing the outlet gases from the bombs. These gases were principally CO with an undetectable ($\pm$ 0.1 $cm^3/g$) $H_2O$ content. The results are given in Table 4-9.

B. DRI Extraction Path

The temperatures at which DRI materials underwent a phase transformation were determined by differential thermal analysis of DRI. The rate of change of temperature during thermal analysis of DRI was about 10°C/min. Due to the higher thermal conductivity of DRI, the temperature of the sample was greater than that of the reference (powdered alumina). The difference was plotted against the temperature of the sample. Because of variation of the chemical composition of DRI, the transformation temperatures obtained during heating of DRI samples were not the same as those measured during cooling.

The results of bomb extractions were utilized to determine the changes of chemical composition of DRI materials when heated. The carbon and oxygen contents of the samples were determined by subtracting the quantities that underwent reduction reactions from the initial values.

The changes of oxygen and carbon content of different D-R samples as their temperature is increased are traced on binary iron-oxygen and

Table 4-9 Composition of Gases Evolved from DRI.

| Temp. Range, °C | $\dot{T}$, °C/min | Pellet Type | Particle size, mm | $\%CO_2$ |
|---|---|---|---|---|
| 25-1285 | 250 | B | 1 | 6.36 |
| 25-1282 | 150 | D | 2 | 6.01 |
| 25-1315 | 250 | D | 1 | 6.19 |
| 25-1323 | 250 | D | 2 | 5.98 |
| 1207-1299 | 250 | F | 1 | 2.67 |
| 943-1358 | 250 | G | 2 | 7.86 |
| 25 - 1219 | 250 | E | 1 | 2.09 |
| 25 - 1268 | 250 | E | 1 | 1.78 |

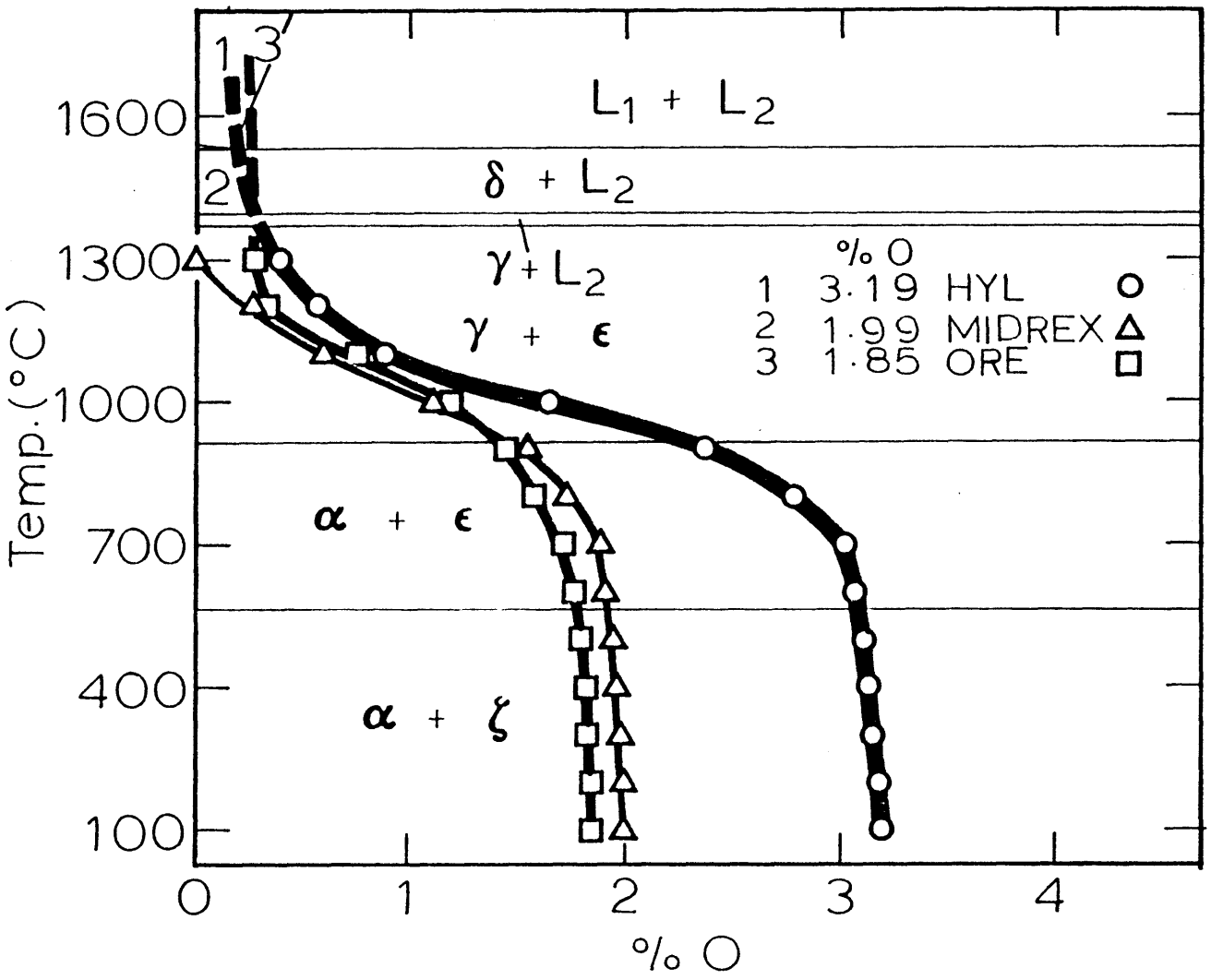


Fig. 4-19 Equilibrium Iron-Oxygen Binary System[77] and Change of Oxygen Content of 1: Type D, 2: Type E and 3: Lump Ore Materials when Heated in Extraction Bomb. Temp. Rate, 250°C/min.

iron-carbon phase diagrams shown in Figures 4-19 and 4-20. As is seen from the latter, at the eutectoid temperature, Ta, a portion of the carbon content of DRI dissolves into the iron, resulting in the formation of an austenitic solid solution:

$$Fe_3C_{(s)} = 3\ Fe_{(\gamma)} + \underline{C}_{(\%)} \qquad \Delta H = -220.0 \text{ cal/mole}$$

This transformation is exothermic and results in a change in the temperature difference between the reference and DRI. Above Ta, the percentage of austenite increases according to the lever rule. At b, the sample is entirely composed of austenite grains if equilibrium prevails. Above $T_b$, the oxidation of carbon continues and the percentage of the free iron increases. Above $T_c$, the FCC austenitic iron either transforms to BCC delta-iron or begins to melt into a high-carbon liquid iron phase. It can be seen that the melting temperature of DRI decreases if the percentage of carbon remaining in the sample increases.

A comparison is made of the transformation temperatures determined from the equilibrium diagram (Figure 4-20) and those measured by differential thermal analysis of D-R samples in Table 4-10. It is seen that the results are fairly consistent. The chemical composition and temperature associated with the phase changes of DRI materials are utilized to calculate the heat capacity and thermal conductivity of D-R particles when heated in steelmaking slags in Chapter V and Appendices E and F.

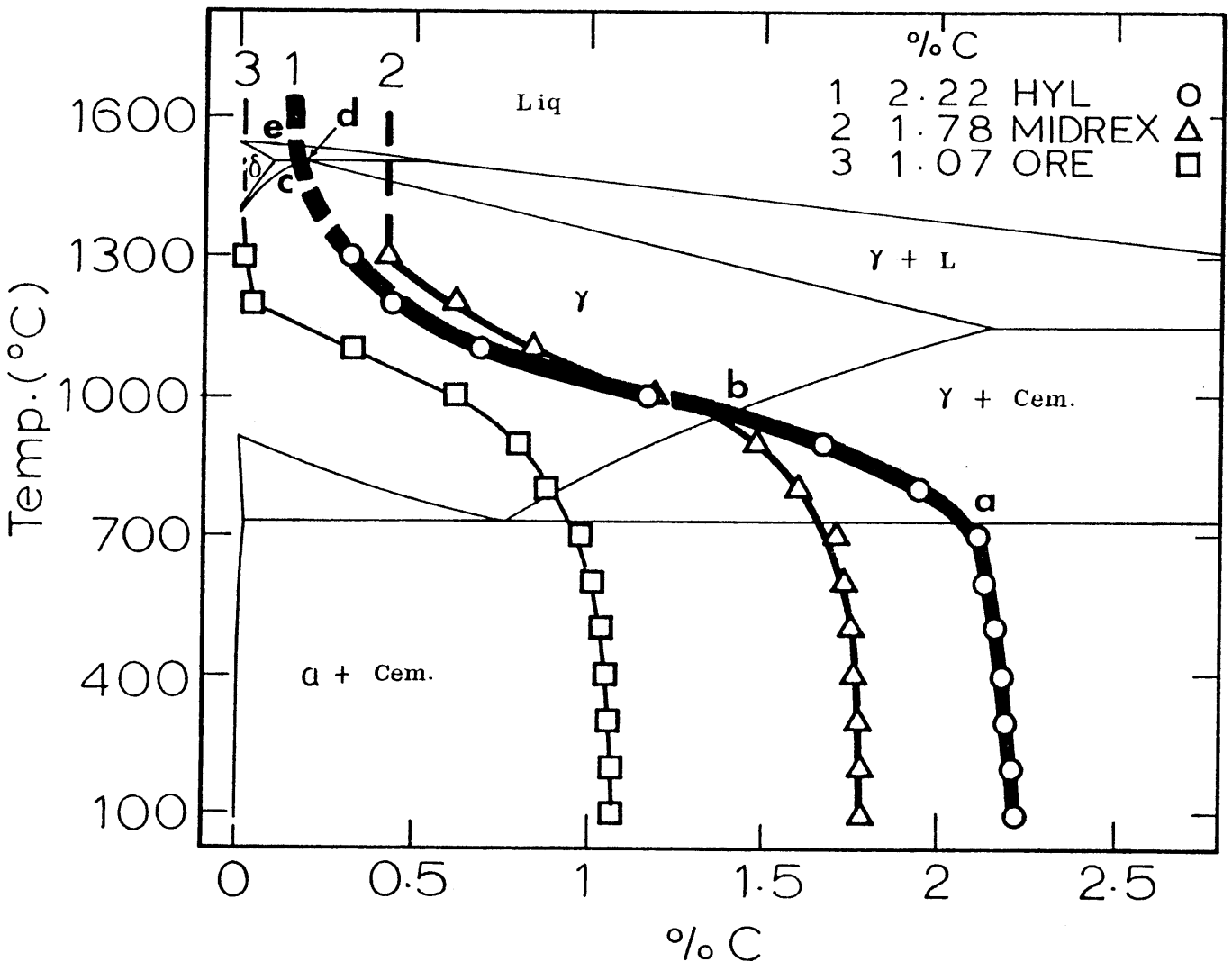


Fig. 4-20 Equilibrium Fe-$Fe_3C$ System[77] and Change of Carbon Content of 1: Type D, 2: Type E and 3: Lump Ore Materials when Heated in Extraction Bomb. Temp. Rate, 250°C/min.

Table 4-10 Transformation Temperatures of Type D, Type E and Lump Ore Materials Determined by DTA and from Heating Paths Shown in Fig. 4-20.

| Trans. Temps. (°C) | D-R Material | | | | | |
|---|---|---|---|---|---|---|
| | HYL | | MIDREX | | Ore | |
| | DTA | Eq. | DTA | Eq. | DTA | Eq. |
| a | 720 | 727 | 729 | 727 | 723 | 727 |
| b | 960 | 957 | - | 943 | 777 | 787 |
| c | - | 1494 | 1449 | 1457 | 1403 | 1398 |
| d | - | 1500 | 1488 | 1500 | - | - |
| e | - | 1526 | 1516 | 1510 | 1524 | 1535 |

C. Slag-Particle Heat Exchange

Typical results of heat transfer studies are given in this section. Detailed descriptions of the experimental data are given in Chapter VI.

1. Neutral Particle

The measured temperature of 3 cm diameter stationary nickel spheres immersed in hot liquid slags A and B is plotted in Figures 4-21 and 4-22. The effect of evolution of gas from the sphere into the slag on the rise of temperature of the particle is also shown. The rate of evolution of gas at the temperature of the bulk liquid slag and at atmospheric pressure ranges from 0 to 12 ℓ/min. It is seen that the effect of gas evolution on the rise of temperature at the center of the spheres is very small below a center temperature of about 700°C. Above 700°C, however, the rate of heating of the sphere increases with the gas evolution.

Comparisons are also made of the rise of the center temperature of 3 cm sintered iron spheres submerged into liquid slag B for different rates of evolution of gas in Figure 4-23. As is seen, the change of the heating rate of the sintered particles due to gas evolution is similar to that of the nickel spheres.

Growth of the shell of slag that solidifies on the surface of the immersed particles affects the rate of heating of the particle. The slag shell functions as a barrier, slowing the transport of heat to the surface of the sphere. The solidification and melting of this shell is influenced dramatically by the evolution of gas, as illustrated in Figure 4-24. Variation in the thickness of the shell (shown by vertical

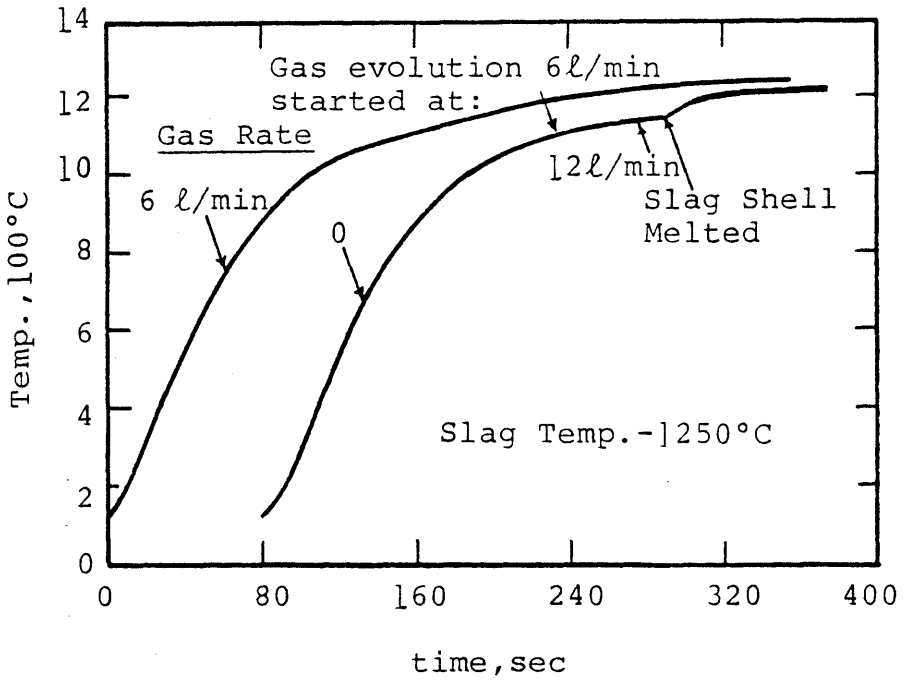


Fig. 4-21 Effect of Gas Evolution on Rise of Temp. of 3 cm Dia. Ni Sphere Heated in Slag A. Slag Temp., 1250°C. Curve for 0 flow rate displaced 80 sec. to right.

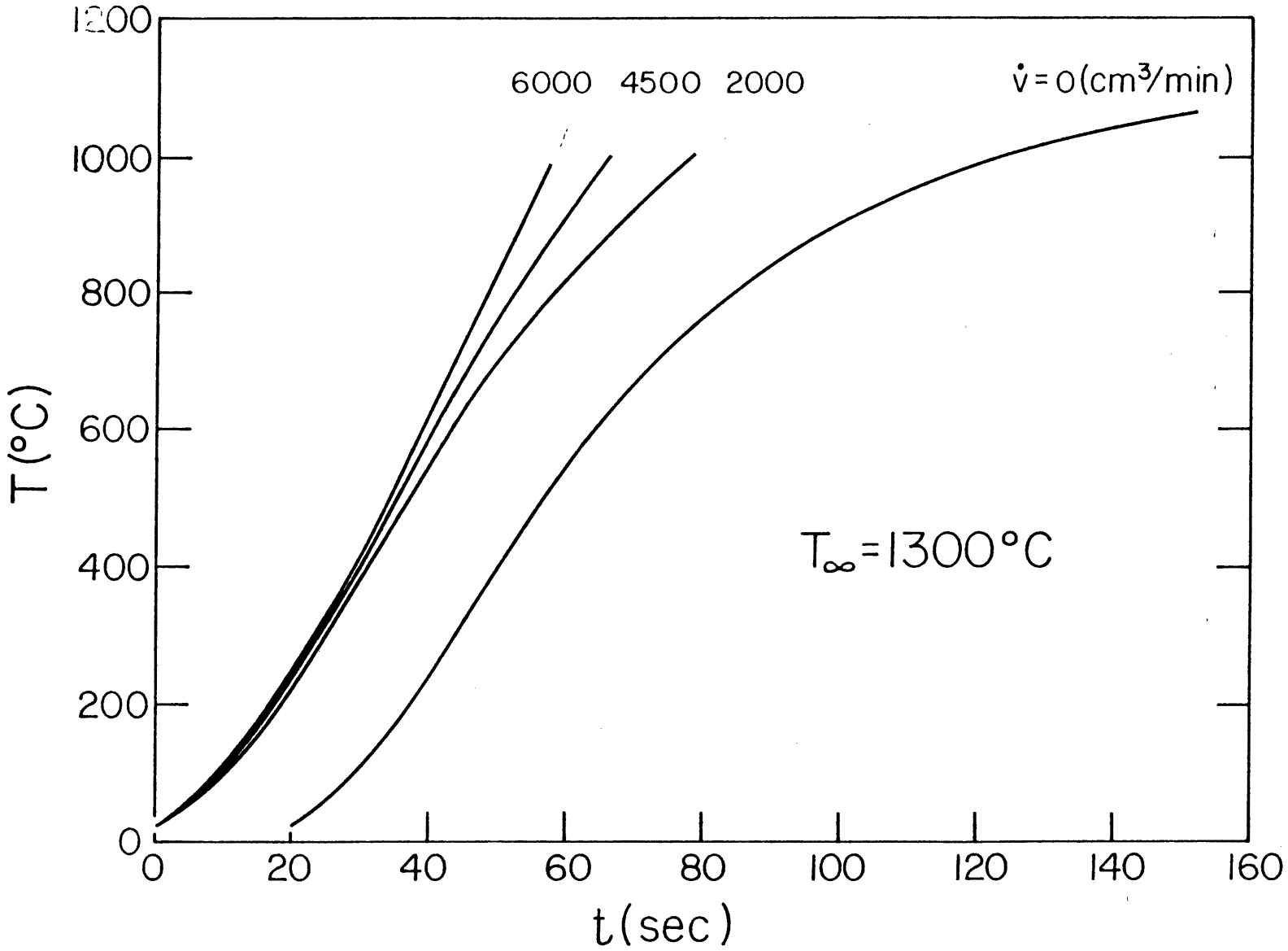


Fig. 4-22 Effect of Forced Bubbling on Rise of Temp. of 3 cm Dia. Ni Sphere Heated in Slag B. Slag Temp., 1300°C. Curve for 0 flow rate displaced 20 sec to right.

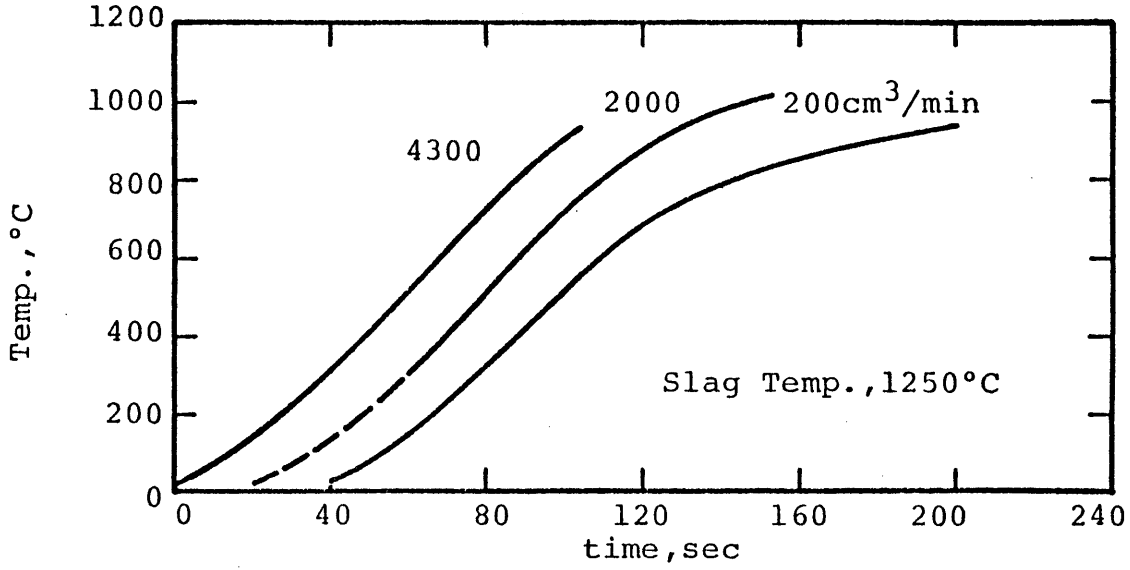


Fig. 4-23 Effect of Forced Bubbling on Rise of Temp. of 3 cm Dia. Sintered Iron Spheres Heated in Slag B. Slag Temp. 1250°C. Curves for 200 and 2000 $cm^3$/min. displaced 40 and 20 sec to right.

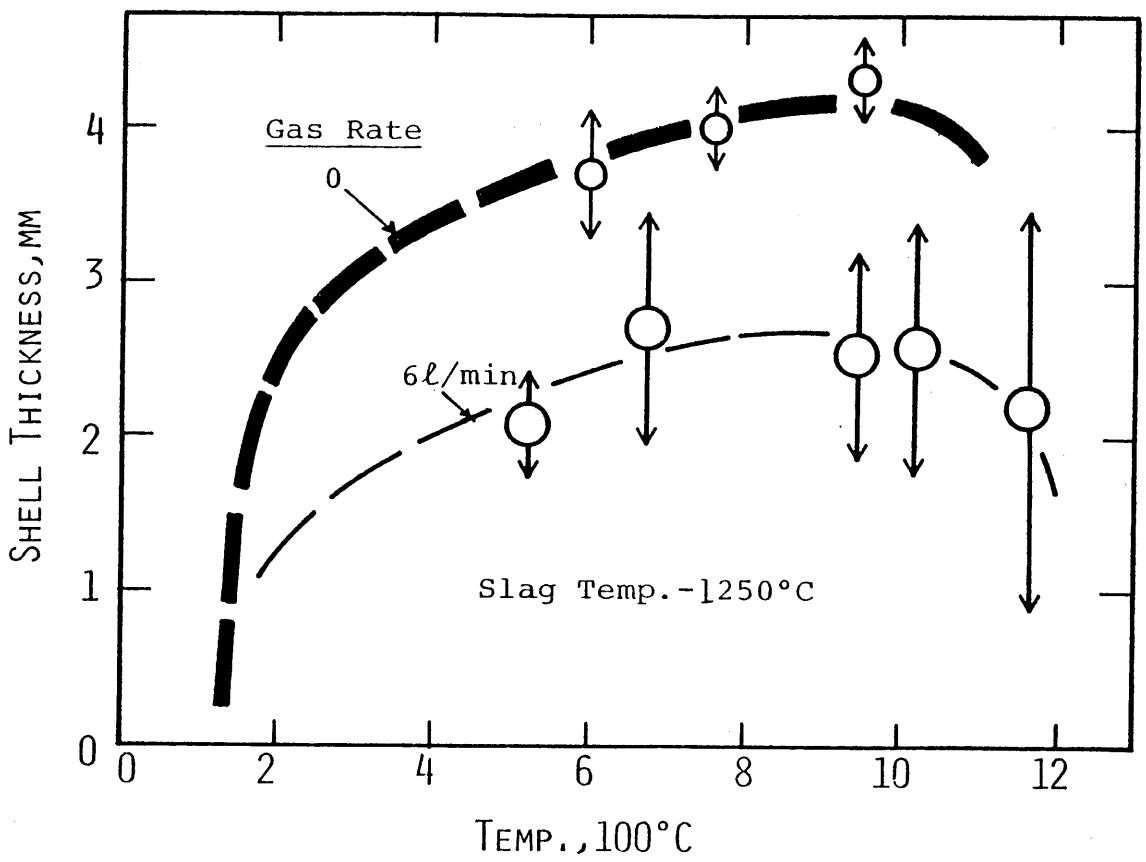


Fig. 4-24 Effect of Gas Evoluion on Thickness of Slag Shell Frozen on 3 cm Ni Sphere Heated in Slag A. Slag Temp., 1250°C.

arrows) is greater when evolution of gas is introduced.

The thickness of the shell of slag also depends on the temperature of the bulk slag, the temperature of the sphere before immersion and the thermo-physical properties of the slag and the particle. Effects of the temperature of the bulk liquid slag and the rate of evolution of gas on the thickness of the solid shell of slag when the measured temperature of the sphere is 600°C are illustrated in Figure 4-25. The effect of the changes of properties of materials on the growth of the shell and the heating of the particles are discussed in Chapter VI.

2. DRI Pellet

The rise in temperature of the center of various DRI pellets when immersed in a hot bath of liquid slag is illustrated in Figures 4-26 and 4-27. The specifications of the pellets and the conditions of the liquid slag are summarized in Table 4-11. The first letter of the symbols used to designate the pellets indicate the type of commercial material utilized (cf. Tables 4-1 and 4-2).

Because of variation of the properties of pellets when they are reduced, the effects of various parameters on the rate of heating of the pellets in slag should be considered in an analysis of the results. Such effects are discussed in Chapter VII. From the data given in Figures 4-26 and 4-27, it can be seen that, below about 700°C, the rate of rise of temperature at the center of a reduced pellet without gas evolution is greater than that of a nonreduced pellet with gas evolution. Above that temperature, the nonreduced pellet is heated more rapidly. The central temperature is, however, greater when the pellet is totally

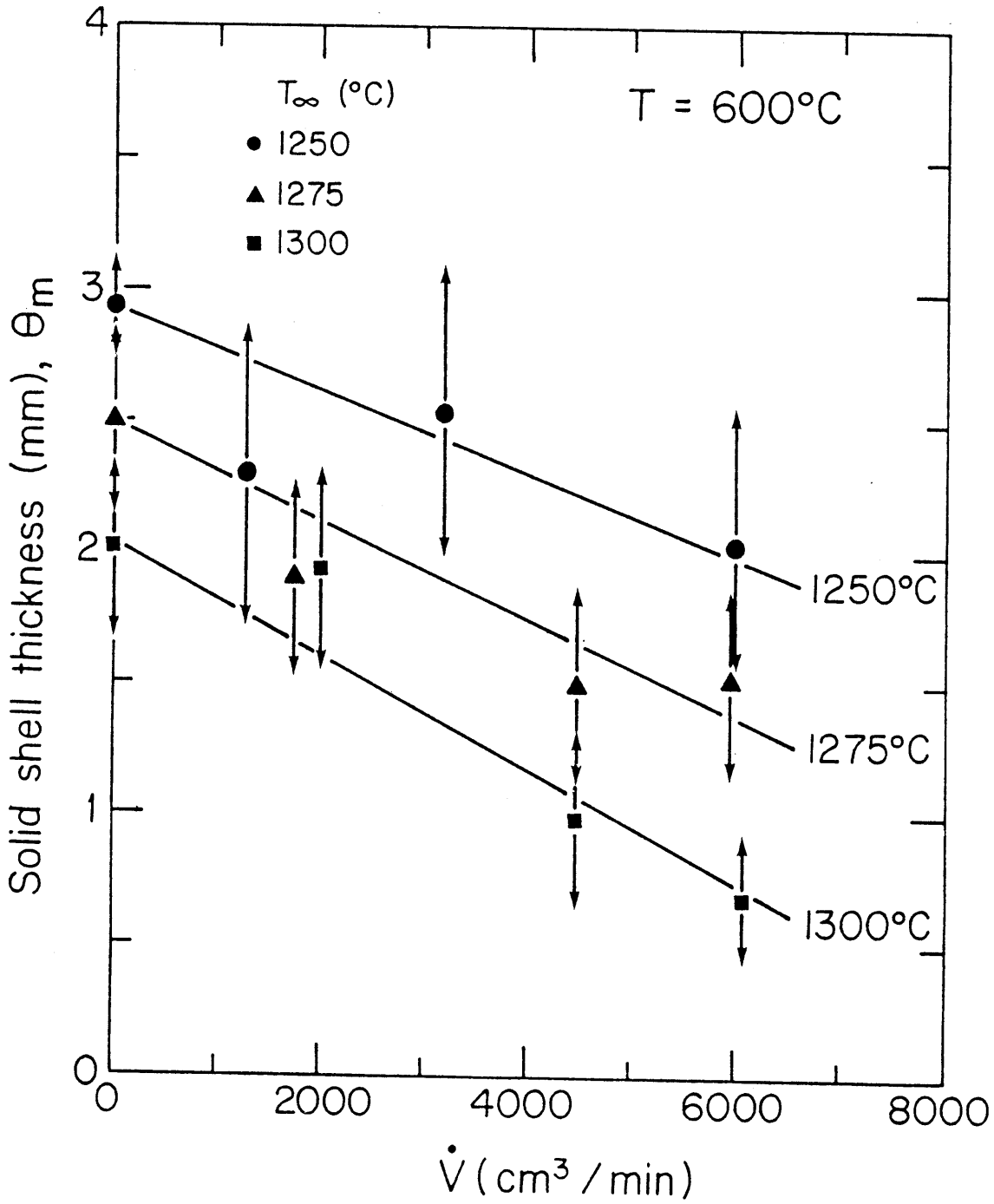


Fig. 4-25 Effects of Gas Evolution and Slag Temp. on Thickness of Slag Shell Frozen on 3 cm Ni Sphere. Temp. at Center of Particle, 600°C.

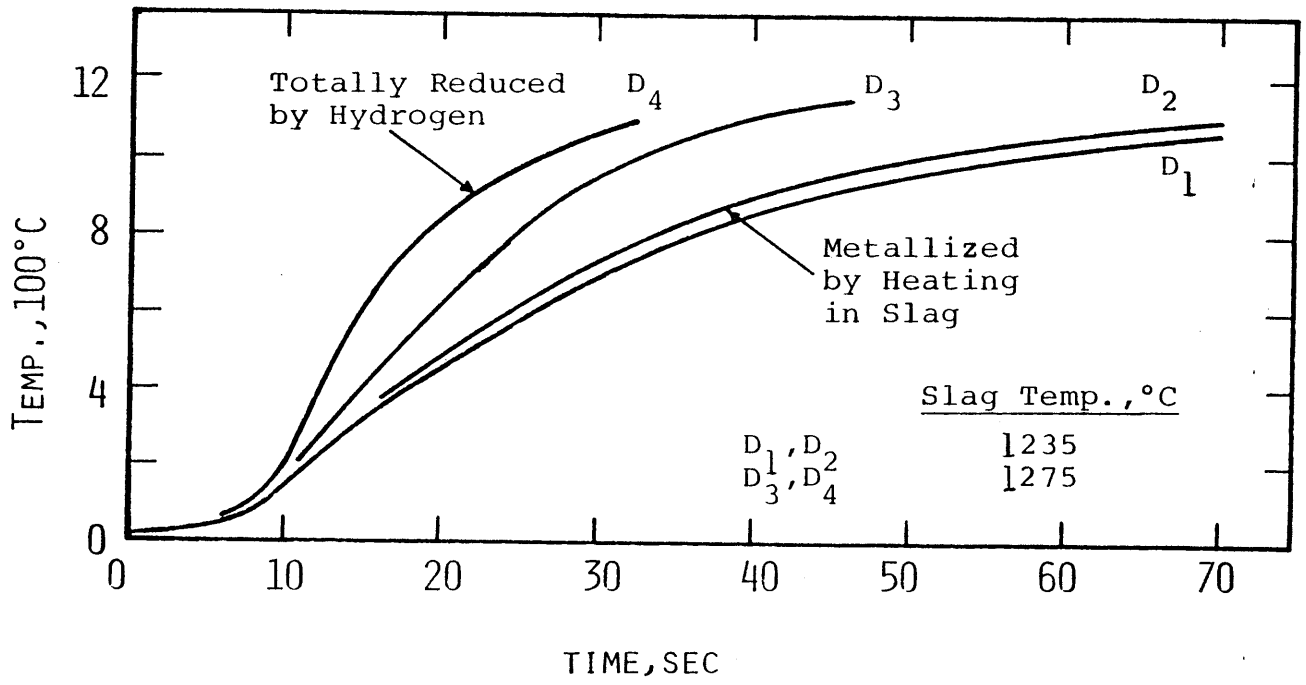


Fig. 4-26 Measured Temp. of Center of HYL Pellets (Type D) Heated in Slag A (cf. Table 4-11).

Table 4-11 Specifications of DRI Pellets Heated in Slag A (cf. Figures 4-26 and 4-27).

| | H Y L | | | | M I D R E X | | |
|---|---|---|---|---|---|---|---|
| Pellet | D1 | D2 | D3 | D4 | E1 | E2 | E3 |
| Diameter, cm | 1.62 | 1.62 | 1.61 | 1.62 | 1.43 | 1.43 | 1.43 |
| Weight, g | 5.14 | 4.86 | 5.05 | 5.63 | 3.65 | 3.58 | 3.52 |
| Dia. of Thermo-couple well, cm | 0.3 | 0.3 | 0.3 | 0.3 | 0.3 | 0.3 | 0.3 |
| Slag temp., °C | 1235 | 1235 | 1275 | 1235 | 1235 | 1235 | 1235 |
| Gas evolution | yes | nil* | yes | nil# | yes | yesX | nil# |

*Reduced by heating in slag.

#Totally reduced by $H_2$.

XAlthough the pellet was previously reduced by heating in slag, there was a considerable amount of gas being evolved during this experiment. The pellet had perhaps oxidized when cooled in the air after the first test.

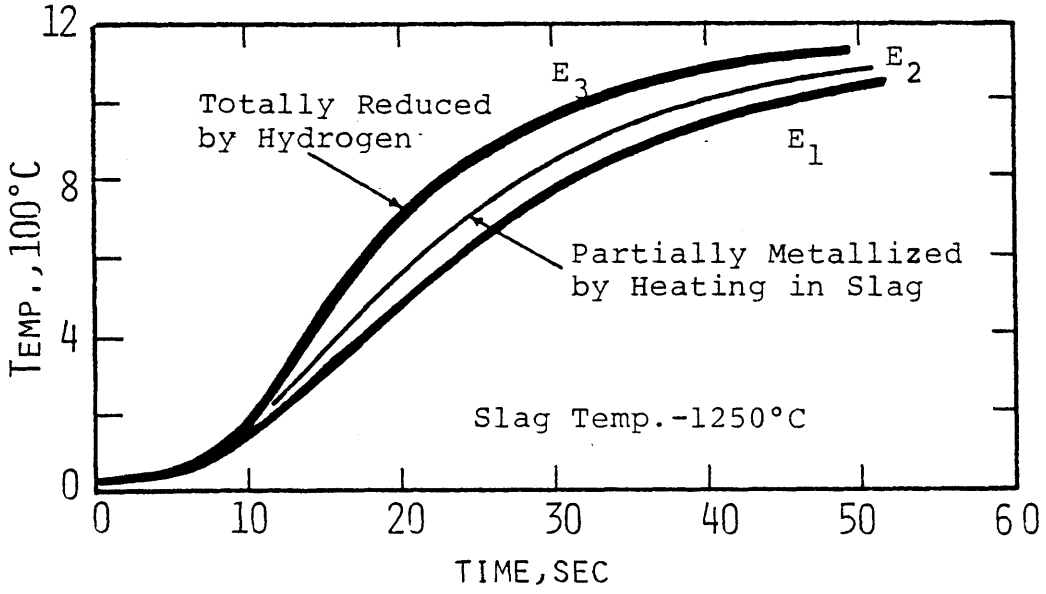


Fig. 4-27 Measured Temp. of Center of Midrex Pellets (Type E) Heated in Slag A (cf. Table 4-11).

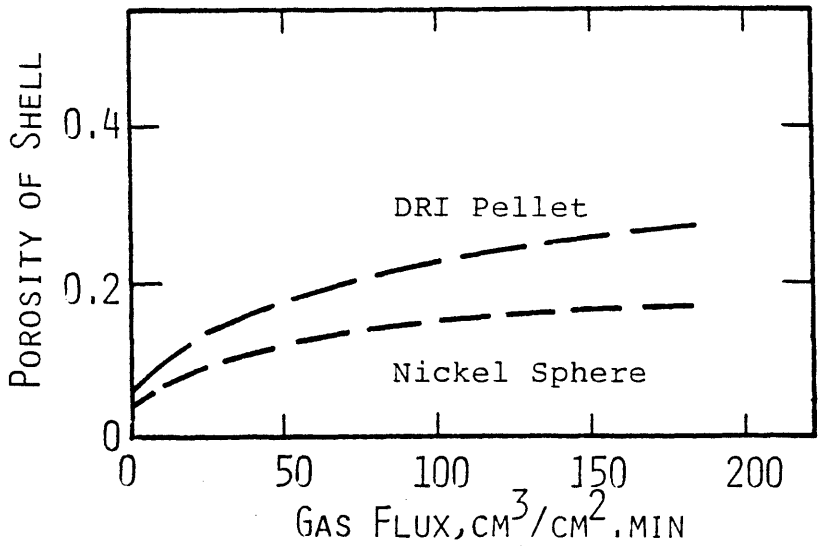


Fig. 4-28 Porosity of Solid Shell of Slag.

metallized.

3. Nature of Slag Shell

The thermal properties of the slag shell vary with various parameters such as porosity, diameter of the pores, direction of solidification, microscopic structure and the temperature of the shell. The porosity of the shell is influenced by gas evolution, as shown in Figure 4-28. The diameter of the pores varies from 10 micron to 2 mm. The distribution of pores of various sizes becomes less uniform as the rate of gas evolution increases. As is seen from the figure, the porosity of the shell of slag which forms on the surface of a DRI pellet is greater than that which solidifies on the surface of a nickel particle. The difference is due to the larger surface area of DRI pellets which is influenced by gas evolution as compared to that of nickel spheres. Variations of the thermal conductivity of the slag due to the change of the porosity of the shell are described in Appendix D.

The microscopic structure of the slag shell consists of three regions, as shown in Figure 4-29. Region I represents a sufficiently fast rate of cooling that has resulted in the formation of an amorphous structure. Region II indicates a slower rate of cooling that has allowed the growth of a coarse lamellar structure. Region III represents the solid-liquid interface (mushy zone) that has been chilled to tiny dendrites when the specimen has been withdrawn from the slag bath. Observation of the polished sections of solid slag shells under the microscope indicates that this region is usually sheared off. However, it cannot be determined from these observations whether shear occurs

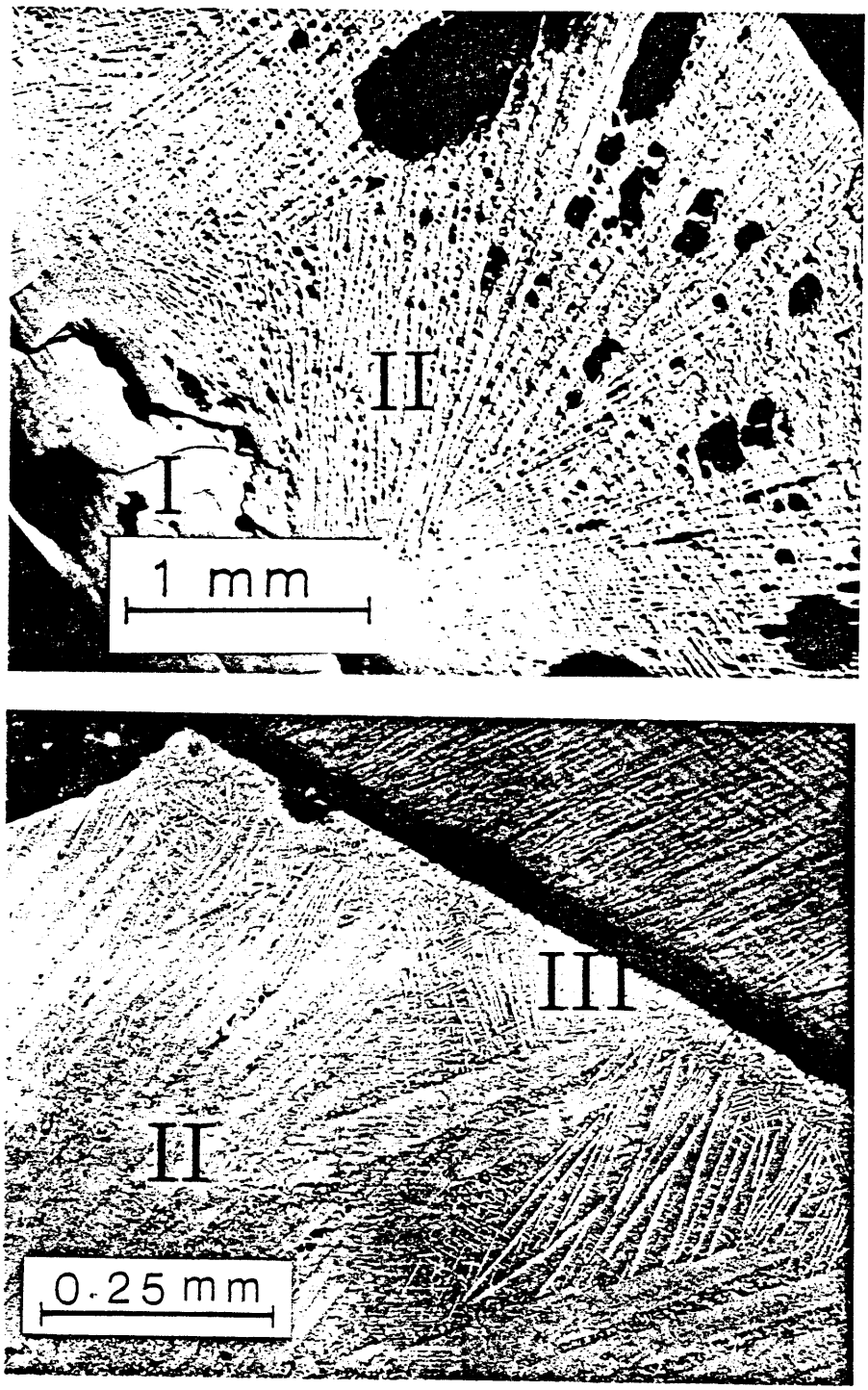


Fig. 4-29 Microstructure of Crust of Solid Slag B Frozen on 3 cm Dia. Ni Sphere.

when the particle is immersed or when it is withdrawn.

As is discussed in Chapter VI, the best fit of data has been obtained with a 100 percent shear of the mushy interface due to the free or forced convection of liquid slag around the particle. The effects of the microstructure and the direction of solidification on the thermal properties of the slag shell are described in reference 58. The effects of shear of the solid-liquid interface on heating of the particles are also discussed in reference 59.

# CHAPTER V

## MODEL SIMULATION

A mathematical model is developed to describe the behavior of DRI pellets submerged in liquid electric furnace slag. Nauman and Elliott[58,57] have previously developed a model for heating an inert spherical object immersed in a liquid slag by translating Fourier's law of heat conduction and the dominant boundary conditions to finite difference equations and solving them by a step-by-step numerical method (cf. see II.B).

The evolution of gas from D-R pellets during their heating and melting period results in variation of the properties of materials and the conditions of the slag bath and influences the behavior of the DRI-melting system. The experimental results described in Chapter IV show that the thickness of the solid shell of slag formed on the surface of a cold object decreases as a result of continued heating and because of the evolution of gas. Gas evolution changes the effective density of the frozen shell of slag as well as the liquid slag that surrounds the particle.

To construct a simple model that simulates the behavior of the DRI-slag melting system, the contribution of four major items should be considered: (a) evolution of gas from DRI, (b) change of properties of materials, (c) solidification and melting of slag, and (d) condition of the bath of liquid slag. The roles of these items are described in the rest of this chapter. A copy of the computer program that was developed is also given in Appendix J.

A. Gas Evolution

An immersed D-R pellet (assumed spherical) is divided into spherical shells with a finite thickness $\Delta r$ (Figure 5-1) to calculate the distribution of temperature and the evolution of gas from the pellet. The distribution of temperature in the pellet can be determined from solution of the heat conduction equation described in Section II.B. Knowing the temperature of an element, the volume of gas being evolved during heating of that element can be calculated. The total volume of the gas evolved from the pellet is then computed by summing the volumes of gases evolved from various elements of the pellet:

$$V = (V_1 \cdot W_1 + \ldots V_i \cdot W_i + \ldots V_n \cdot W_n)/W \qquad (5.1)$$

where V is the total volume of gas evolved from unit weight of the pellet, $V_i$ is the volume of gas formed per unit weight of element i, $W_i$ is the weight of element i, and W is the total weight of the pellet. Assuming the density of the particle is constant along its radius and substituting for the weight terms in Eq. (5.1), the following equation is obtained:

$$V = (V_1 \cdot v_1 + \ldots V_i \cdot v_i + \ldots V_n \cdot v_n)/v \qquad (5.2)$$

where $v_i$ is the volume of element i and v is the total volume of the pellet. The volume of gas evolved from element i during the time interval $2\Delta t = t_{j+1} - t_{j-1}$ is evaluated from Eq. (5.3):

$$V_i = G_i (T_{i,j+1} - T_{i,j-1}) \qquad (5.3)$$

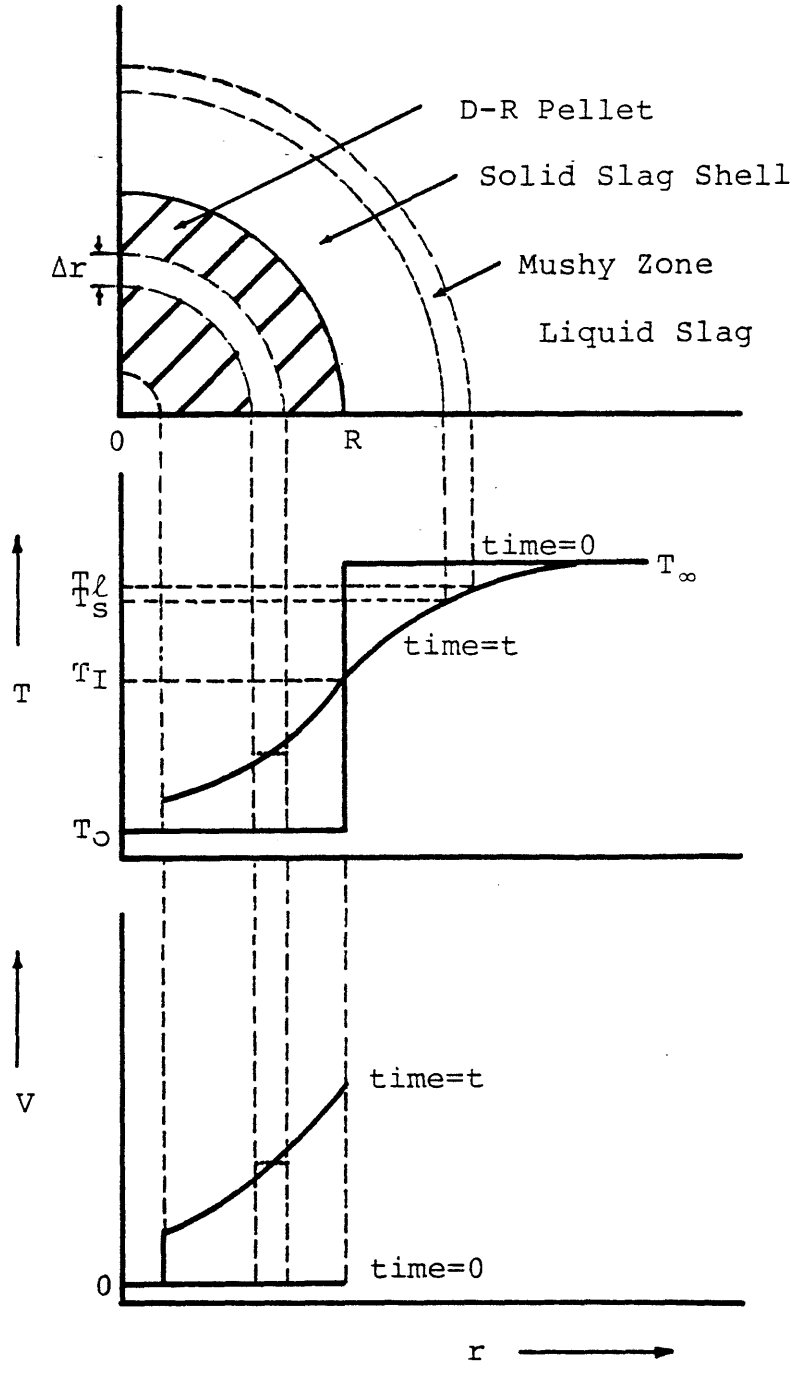


Fig. 5-1 Distribution of Temp. and Gas Volume for a D-R Pellet Immersed in Liquid Slag.

where $T_i$ is the temperature of element i and $G_i$ is "specific gas volume" for element i and is defined as the total volume of gas released per gram of DRI for a temperature increment of 1°K at temperature $T_i$.

The quantity, $G_i$, can be determined from the results of the bomb extractions. For simplicity, the temperature axis of the gas evolution curve (see Figure 5-2) is divided into 100°C intervals, then the mean derivative of gas volume is calculated for these intervals:

$$G_i = (V_{i+1/2} - V_{i-1/2})/(T_{i+1/2} - T_{i-1/2}) \qquad (5.4)$$

The results of the gas evolution experiments conducted at various heating rates show that the total volume of the gas evolved is not appreciably influenced by the rate of heating of DRI (see Section IV. A.2.a.3). The gas evolution patterns obtained for a rate of rise of temperature of 250°C/min are therefore used to calculate the specific gas volume $G_i$.

Since the volumes of the gases that evolve are almost proportional to the degree of metallization of DRI (Figure 4-10) when there is enough carbon in the sample to reduce the oxides completely, the volumes of the gases evolved can be expressed in terms of the degree of metallization or the oxygen content of DRI. The gas evolution data for a reference sample can thus be utilized to calculate the volume of gases evolved from a DRI sample as follows:

$$V_T = V_T^{\circ} \quad (\%Met^{\circ}/\%Met) \qquad (5.5)$$

where $V_T$ is the total volume of gas evolved from a DRI sample at

temperature T, $V_T^\circ$ is that of the reference, %Met° is the degree of metallization of the reference and %Met is that of the sample. Equation (5.5) can also be expressed in terms of the oxide content of DRI:

$$V_T = V_T^\circ \ (\text{"FeO"}/\text{"FeO"}^\circ) \qquad (5.6)$$

This equation was inserted in the model to compute the gas evolution from a DRI sample. The results were tested against those obtained by utilizing the gas evolution patterns of different DRI samples as reference as well as those obtained by heating a pellet in slag (see Section VI.B.3).

The rate of evolution of gas is equal to the time derivative of the total volume of gas evolved from the pellet:

$$\dot{V}_j = (V_{j+1} - V_{j-1})/2\Delta t \qquad (5.7)$$

where $V_j$ is the total volume of gas evolved from the pellet from the time zero to the time $j.\Delta t$.

The influence of gas evolution on the transmission of heat from liquid slag to an immersed particle can be attributed to the following possible transport mechanisms: (a) partial shielding of the moving solid-liquid slag interface by departing gas bubbles, (b) replacement of cold solid and liquid layer in contact with the moving interface by "pumping" associated with bubbles departure,[78] and (c) circulation of the liquid slag due to the evolution of the rising gas bubbles.

The shielding of the particle by the evolved gas bubbles may result in a decrease or an increase in the rate of heating of the particle depending on temperature and thermal properties of the materials involved.

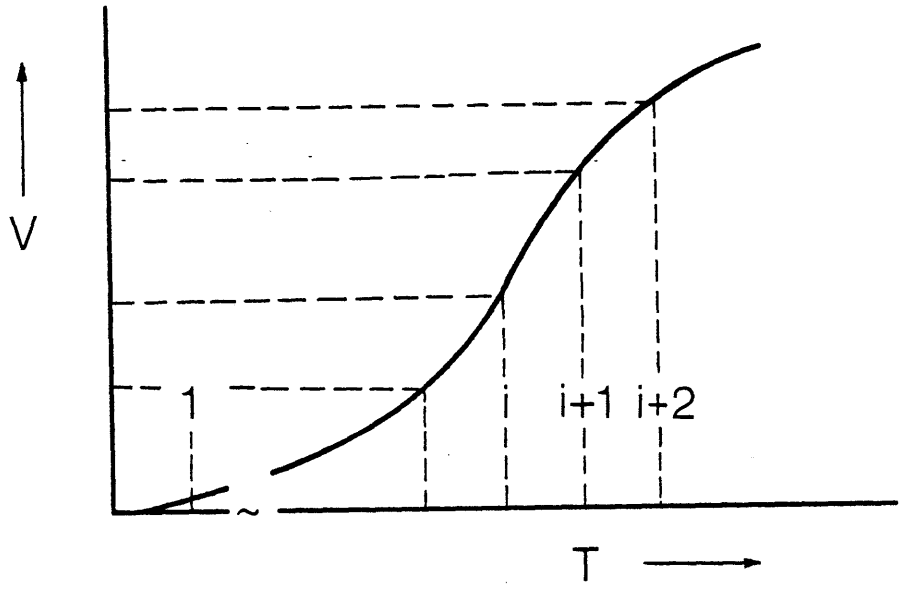


Fig. 5-2 Gas Evolution from DRI.

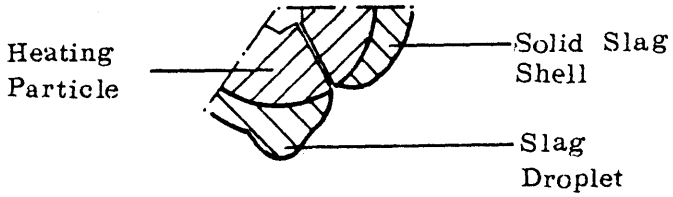


Fig. 5-3 Solidified Slag Shell Around an Active Gas Port on Ni Sphere.

The effect of this factor will be discussed in Section VI.B.2. The replacement of the layer of cold slag from the solid-liquid slag interface results in a decrease in the thickness of the solid slag shell. The effects of this factor and the circulation of the liquid slag due to the rising of gas bubbles will be described in Sections V.C and V.D.

B. Properties of Materials

A precise knowledge of the properties of the solid and liquid slag and of the metallic particles immersed in the slag is necessary to develop the mathematical model for melting of the pellets.

1. Properties of Slag

A detailed discussion of the thermo-physical properties is given in Appendix D. Thermo-physical properties of the slags utilized in heat transfer studies are summarized in Table 5-1. The Grashof and Rayleigh numbers of slags are calculated for bulk temperature of 1250°C and a constant particle radius of 1.8 cm including the thickness of the shell of slag. The chemical composition of the slags are given in Table 3-4.

2. Properties of Specimen

The physical properties of the specimens used in heat transfer studies are summarized in Table 5-2. The overall specific heat of DRI is calculated in Appendix F based on the contribution of the following items:

a. specific heat of the constituents as given in the thermodynamical tables,

b. enthalpy of the reduction reactions occurring during heating of DRI,

c. heat of the phase transformation of DRI materials:

Table 5-1 Properties of Slags.[58,59]

| Property | Slag A | | Slag B | | Slag C | |
|---|---|---|---|---|---|---|
| | Sol. | Liq. | Sol. | Liq. | Sol. | Liq. |
| Melting range, °C | 1140 | 1215 | 1125 | 1220 | 1230 | 1310 |
| Heat of fusion,* cal/g. | 80.7 | - | 102.0 | - | 130.0 | - |
| Thermal expansivity, $cm^3/cm^3$. °C | - | 0.00014 | - | 0.00014 | - | 0.00014 |
| Conductivity, cal/cm. sec.°C | 0.0059 | 0.0052 | 0.0043 | 0.0046 | 0.0028 | 0.0032 |
| Density, $g/cm^3$ | 3.7 | 3.6 | 3.8 | 3.5 | 2.9 | 2.9 |
| Specific Heat, cal/g. °C | 0.25 | 0.28 | 0.25 | 0.28 | 0.24 | 0.28 |
| Diffusivity, $cm^2/sec.$ | 0.0064 | 0.0052 | 0.0045 | 0.0047 | 0.0040 | 0.0040 |
| Viscosity, poise | - | 2 | - | 2 | - | 5 |
| Kinematic viscosity, $cm^2/sec.$ | - | 0.56 | - | 0.57 | - | 1.72 |
| Prandtl number | - | 108 | - | 122 | - | 431 |
| Grashof number | - | 286 | - | 307 | - | 5 |
| Rayleigh number | - | $3.1 \times 10^4$ | - | $3.7 \times 10^4$ | - | $2.3 \times 10^3$ |

*Based on heats of fusion of components (cf. Table 3-4).

Table 5-2 Physical Properties of Specimens Used for Heat Transfer Studies.

| Specimen | Nickel Sphere | | DRI Pellet E | DRI Pellet D |
|---|---|---|---|---|
| Diameter, cm | 1.84 | 3.00 | 1.60 | 1.62 |
| Rad. of Thermocouple well, cm | 0.22 | 0.38 | 0.15 | 0.15 |
| Effective density, $g/cm^3$ | 8.29 | 8.00 | 2.60 | 2.33 |
| Porosity, fraction | 0.02 | 0.10 | 0.55 | 0.55 |
| Radial distance of bead from center of particle, cm | 0.35 | 0.72 | 0.08 | 0.08 |
| Mass, g | 25.5 | 106.4 | 5.8 | 5.2 |

$$Fe_3C_{(s)} = 3Fe_{(\gamma)} + \underline{C}\ (\%) \quad \Delta H = -1.23\ (\text{cal. } g_{Fe_3C}^{-1}) \qquad (5.8)$$

The effective thermal conductivity and heat of fusion of DRI and the constants used for calculation of the flow of heat transmitted to the thermocouple bead embedded inside the specimens are computed in Appendix E. A summary of the thermal properties of materials that are utilized in simulation of the computer model is given in Table 5-3.

C. Solid Shell of Slag

Because of transfer of heat from liquid slag to the cold immersed particle, a shell of slag freezes initially at the periphery of the particle and will remelt later. The thickness of the slag shell is a function of many variables such as time, temperature of the slag, initial temperature of the particle, properties of the slag and of the specimen, and motion of the slag relative to the specimen.

The thickness of the shell varies on the surface of the particle from place to place, becoming thicker as the distance from an active bubbling site increases, as represented in Figure 5-3.

Similar results are obtained for the shell of slag frozen on the surface of DRI pellets. For moderate rates of gas evolution (1000 $cm^3$/min for a 2-cm diameter pellet) a number of active bubbling sites form on the surface of the solid shell which permit the evolution of gas from the pellet into the liquid slag. For higher rates of gas evolution (3000 $cm^3$/min for a 2-cm diameter pellet), the shell of slag is highly porous and allows the evolution of gas from all over the surface. A comparison is made of the shells of slag solidified on the surface of a totally metallized pellet, a 95 percent, and an 87 percent metallized

Table 5-3 Thermal Properties of Materials

| Property | Relationship | Temp., °K |
|---|---|---|
| Specific heat of nickel,[83] cal/g. °K | $0.13-8.01\ E-6T - 2.27\ E3T^{-2}$ | $T<903$ |
| | $0.12 + 1.70\ E-5T - 3.80\ E3T^{-2}$ | $T\geq 903$ |
| Conductivity of nickel,[82] cal/sec. cm.°K | 0.25/0.22/0.19/0.17/0.16/0.16/0.16/0.17 | T = 100 i |
| | 0.17/0.18/0.18/0.19/0.20/0.20/0.20 | i = 2,3,...,17 |
| Heat of fusion of Ni[77], cal/g | 71.70 | M.P., 1726 |
| Specific | $C_M + 1.29\ G(T)$ | $T<T_a$ |
| Heat of | $C_M + 1.35\ G(T)+CT$ | $T_a\leq T\leq T_a+8$ |
| DRI | $C_M + 1.47\ G(T)$ | $T_a+8<T<T_b$ |
| Materials,* cal/g. °K | $C_M + 1.35\ G(T)$ | $T\geq T_b$ |
| Conductivity of Iron[82] | 0.2/0.18/0.17/0.15/0.13/0.12/0.10/0.09 | T = 100 i |
| | 0.07/0.07/0.07/0.07/0.07/0.08/0.08/0.10 | i = 2,3,...,17 |
| "FeO" | 0.0144 | - |
| $Fe_3C$ | 0.0170 | - |
| $Al_2O_3$ | 0.0190 | - |
| $SiO_2$ | 0.0069 | - |
| Cal/sec. cm.°K | | |
| Heat of fusion of DRI,[77] cal/g | $66\ W_{Fe} + 255\ W_{Al_2O_3} + 34W_{SiO_2}$ | 1773 |

*cf. Appendix F.

pellet in Figure 5-4. For the totally metallized pellet, the shell of slag is continuous and dense. For the 95% metallized pellet, there are several bubbling sites on the surface of the slag. For the 87% metallized pellet, the slag shell is very thin due to the vigorous disturbance introduced in the slag by gas bubbles.

The variation of the thickness of the shell of solid slag is computed in the model based on the difference of the heat which is transferred from the liquid into the surface of the solid particle and that which is conducted from the surface of particle to the cold core. Since the difference between the temperature of the bulk slag and the liquid-solid interface is constant, the flow of heat to the surface of solid particle is basically controlled by the condition of the bath which is quantified by the Nusselt number of the bath. The flow of heat transferred from the interface to the cold core is however determined from the temperature gradient in and the thermal conductivity of the solid shell which is influenced by the porosity and the pore diameter of the shell. The thermal conductivity of the shell is calculated from Equation (D.7) and the information given in Figure 4-28. Since the evolution of gas affects the porosity of the shell, it will indirectly influence the thermal conductivity and the rate of growth of the solid shell. These effects are inserted into the structure of the model and will be discussed further in Chapter VI.

D. Condition of Bath

The condition for transfer of heat from the liquid slag can be expressed in terms of an overall Nusselt number which is a dimensionless

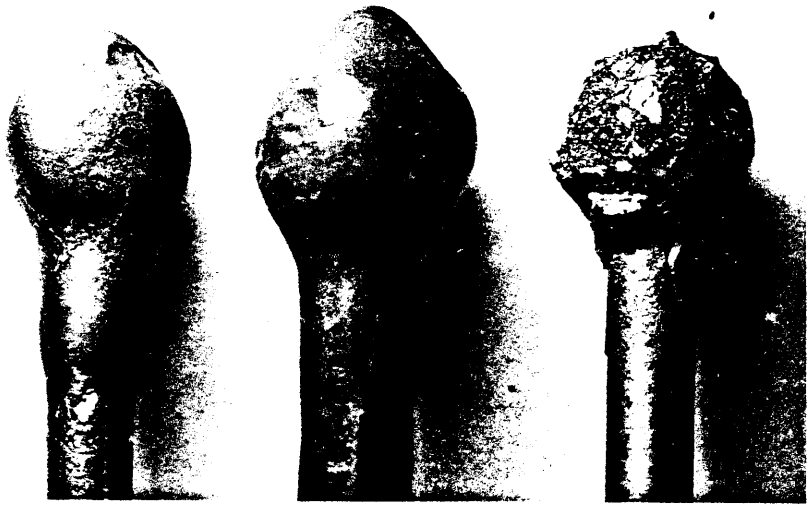


Fig. 5-4 Shell of Slag Frozen on Surface of DRI Pellets: (a) Totally Metallized, (b) 95 Percent Metallized, (c) 87 Percent Metallized.

version of heat transfer coefficient. For a system in which the conditions of a moving solid-liquid interface prevail, the overall Nusselt number is defined as follows:

$$Nu \equiv 2h(R+\theta)/(\alpha\rho C_p)_\ell \qquad (5.9)$$

where h is the heat transfer coefficient, R is the radius of the specimen, $\theta$ is the thickness of the shell of solid slag, and $\alpha$,$\rho$ and $C_p$ are thermal diffusicity, density and specific heat of the liquid slag. The transmission of heat from hot liquid slag to the specimen is by conduction, free convection and forced convection as will be described in the subsequent sections.

Since the densities of slags do not change appreciably during solidification, the movements of the solid-liquid interface do not appear to affect the motion of the fluid around the particle significantly. The movements of the interface may, however, influence the coefficient of transfer of heat by changing the thickness of the thermal boundary layer of the slag. The Nusselt number in such a case will increase during the period that the shell grows and will decrease when the shell melts.

A simple calculation shows that the thickness of the thermal boundary layer is about 3 times greater than the thickness of the solid shell of slag when steady state transfer conditions prevail (Appendix G). The effects of the movements of the solid-liquid interface on the flow of heat to the particle were, for simplicity, neglected throughout the mathematical calculations.

1. Conduction

The Nusslt number for a stationary sphere submerged in a motionless body of liquid can be calculated from the solution of the conduction equation in spherical coordinates.[85] This solution is valid for short times when the velocities generated in the liquid because of development of nonuniform temperature profiles are small.

A simple manipulation of the conduction equation yields the following solution for the distribution of temperature outside a sphere of constant surface temperature, $T_i$ (Appendix H):

$$\frac{T-T_\infty}{T_i-T_\infty} = \frac{R+\theta}{r} \operatorname{erfc} \frac{r-R-\theta}{\sqrt{\pi\alpha t}} \tag{5.10}$$

where $T_\infty$ is temperature of the bulk liquid, R is radius of the specimen, $\theta$ is thickness of the frozen shell, T is temperature at time t after immersion and at radial distance r>R from center of the sphere, $\alpha$ is thermal diffusivity of the liquid and erfc is the complementary error function defined in reference 85. The coefficient of transfer of heat determined from the above equation leads to the following correlation (see Appendix H):

$$Nu_t = 2 + 2(R+\theta)/\sqrt{\pi\alpha t} \tag{5.11}$$

As is seen from Equation (5.11), the heat transfer coefficient is initially infinite. This is because of the sudden change of temperature at the surface of the sphere when immersed. But it decreases to a minimum of 2 after a long time has elapsed.

2. Natural Convection

If the temperature of the bath is substantially different from that of the surface of the particle, the effect of natural convection should also be included in computation of the Nusselt number. In contrast to the relatively rapid heating of the particle by conduction, the contribution of natural convection is not considerable during the initial transient period, when the Nusselt number for natural convection rises from zero to a maximum of about 4 (see Table 5-4).

Hellums and Churchill[86] have studied the transient natural convection of a fluid initially at rest on an isothermal vertical plate and inside a horizontal cylinder. Their results show that the time necessary for these systems to reach steady state is less than 3 seconds. This time is shorter than that of initial transient forced convection produced by sudden submersion of the particle (see V.D.3) and the time that must elapse until the contribution of conduction described by Equations (5.11) falls to that of natural convection. Since conduction and forced convection mechanisms are therefore initially dominant in the system (see also Section V.D.3) the effects of transient natural convection can be neglected.

The contributions of long term conduction and steady state free convection on transfer of heat to the particle are given in the following empirical expression:[87]

$$Nu = 2 + 0.1\ Gr^{1/4} \cdot Pr^{1/3} \qquad (5.12)$$

when the quantity of the combination $Gr^{1/4} \cdot Pr^{1/3}$ is no more than 200.

Table 5-4 Average Nusselt Number for Natural Convection in Liquid Slag Calculated from Eq. (5.12).[87]

| No. | Particle Type | Particle Rad., cm | Ave. Shell Thick., cm | Slag Type | Slag Temp., °C | Nu |
|---|---|---|---|---|---|---|
| 1 | Ni | 0.92 | 0.25 | A | 1250 | 3.43 |
| 2 | Ni | 1.50 | 0.3 | A | 1250 | 3.97 |
| 3 | Ni | 1.50 | 0.27 | B | 1250 | 4.07 |
| 4 | Ni | 1.50 | 0.23 | B | 1275 | 4.13 |
| 5 | E | 0.80 | (0.10) | B | 1250 | 3.18 |
| 6 | E | 0.80 | - | C | 1600 | 3.30 |
| 7 | D | 0.81 | (0.10) | B | 1250 | 3.19 |
| 8 | D | 0.81 | - | C | 1600 | 3.31 |

The average Nusselt numbers calculated from the above relationship for particles and slags of various types and conditions are given in Table 5-4. These quantities were utilized to compute the heating rate of neutral spheres and DRI pellets when submerged into a hot bath of slag.

3. Forced Convection

Transient forced convection may be generated when the particle is plunged into the liquid slag. Since the actual liquid velocities that may be produced by the plunged particle are not defined, the available correlations cannot be conveniently utilized to predict the contribution of forced convection to transfer of heat to the particle during the corresponding transient period. Because of the relatively large Prandtl number of the slags (and from the experimental results) this period does not appear to be long (cf. Section VI.B for the best fit of the data).

The evolution of gas from an immersed particle may also generate forced convection in the bath and increase the Nusslt number of the system. Mikic and Rohsenow[78] have studied the transfer of heat from a hot surface to the cold liquid of a nucleate pool boiling system. The physical model they have used consists of the removal of a part of the natural convection layer by each departing bubble when the areas of influence of the bubbles do not overlap.[91] Using the transient solution of the heat conduction equation for calculation of the flow of heat to the layer of liquid in contact with the surface, they have been able to compute the rate of transfer of heat due to the evolution of gas bubbles from the surface into the pool.

Employing a similar physical model to that which Mikic et al.[78]

have used and assuming the area of influence of gas bubbles is equal to their equatorial surface area, the local Nusselt number for transfer of heat to the immersed particles when gas evolution occurs into the slag bath may be computed as follows:

$$Nu_b = (\pi f \rho C_p/k)^{1/2} D_b^2 n (R+\theta) \qquad (5.13)$$

where f is bubbling frequency, $\rho$, $C_p$ and k are properties of the liquid slag, $D_b$ is the diameter of gas bubbles when evolved from the particle, and n is the number of active bubbling sites per unit area of the particle. If N is the total number of active gas holes in the particle an average Nusselt number may be computed as follows:

$$\overline{Nu_b} = (f \rho C_p / \pi k)^{1/2} D_b^2 N/4(R+\theta) \qquad (5.14)$$

A plot is made of $\overline{Nu_b}$ for particles with 2 active gas ports in Figure 5-5. It is to be noted that the areas of influence of gas bubbles do not overlap when the rate of evolution of gas from nickel spheres is less than 4000 $cm^3$/min. port.

The evolution of gas may also result in generation of stirring in the liquid slag. The direction of motion is however opposite to that which is produced by natural convection. The produced stirring may therefore increase or decrease the rate of heating of the immersed sphere.

As is discussed in the next chapter, the Nusselt numbers determined by comparing the experimental results with the mathematical calculations are smaller than those which were calculated in this section. The overall Nusselt numbers for slags of various conditions which were utilized in

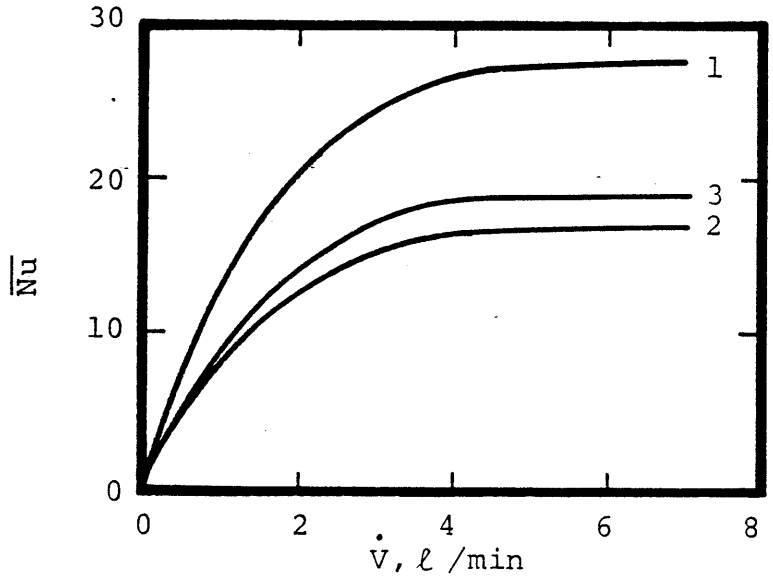


Fig. 5-5 Local Bubbling Nusselt Number for Particles and Slags Specified in Lines 1, 2 and 3 of Table 5-4.

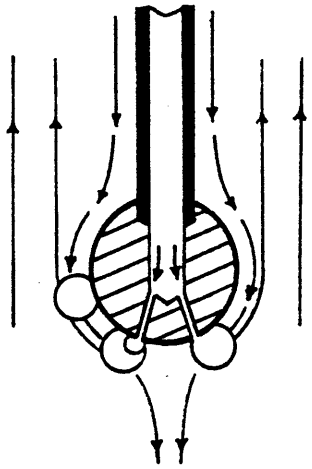

Fig. 5-6 Natural and Forced Bubbling Convection in Liquid Slag.

model calculations are summarized in Figure 6-9.

# CHAPTER VI

# DISCUSSION

The experimental results summarized in Chapter IV are discussed in this chapter. The information on the formation and evolution of gas from DRI is first analyzed through the thermodynamics of carbon-oxygen reactions. Then the data on the transfer of heat to the metallic particles immersed in hot slags are discussed through comparisons made with the results of the simulation model described in Chapter V.

## A. Evolution Results

A brief discussion of the constant and variable temperature extractions is given in this section.

### 1. Constant Temperature

Removal of oxygen from DRI when heated in a capsule of helium is accomplished by carbon or carbon monoxide. The carbon present in DRI may be in form of $Fe_3C$, free graphite or dissolved in the iron. For HYL and Midrex materials, $Fe_3C$ is reportedly the major constituent. The reduction reactions are thus as follows:

$$Fe_xO_y + y\ Fe_3C = (x+3y)Fe + y\ CO \qquad (6.1)$$

$$Fe_xO_y + y\ CO = xFe + yCO_2 \qquad (6.2)$$

$$CO_2 + Fe_3C = 3Fe + 2CO \qquad (6.3)$$

A combination of reaction (6.2) with reaction (6.3) also leads to the reduction of DRI with cementite, as is illustrated by reaction (6.1). Reaction (6.3) is endothermic ($\Delta H$ = 35,240 cal/mole $CO_2$[77]) and is

favored by high temperatures, as is shown in Figure 6-1. The amount of water vapor collected during the helium extraction tests was very small and probably entered the capsule as moisture with DRI or with DRI container.

The equilibrium partial pressure of CO in iron-oxygen system at total pressure of 1 atm is shown in Figure 6-1. Because of dissociation of carbon monoxide according to reaction (6.3) iron oxide cannot in theory be completely reduced below about 700°C. The broken lines in Figure 6-1 represent the metastable reduction reactions occurring in the Fe-O-C system. Also as is seen, when temperature rises, the equilibrium $CO/CO_2$ ratio for production of iron increases.

The partial pressure of CO that is in equilibrium with $CO_2$ and carbon changes from about zero to one when temperature rises from 500 to 800°C, as shown in Figure 6-1. Comparing with the data given in Tables 4-3 to 4-8, it is seen that these changes are consistent with results of the helium extraction tests. Also, as is seen from the equilibrium Fe-O-C diagram, above 700°C and with CO partial pressures of more than about 0.7, DRI can completely reduce to free iron. The results of helium extractions show that the effect of temperature on removal of oxygen from DRI samples decreases as temperature rises above 700°C.

Below 650°C, magnetite is stable. Between 650 and 700°C, wustite is expected to appear according to the following reactions:

$$Fe_3O_4 + Fe_3C = 3Fe + 3"FeO" + CO \qquad (6.4)$$

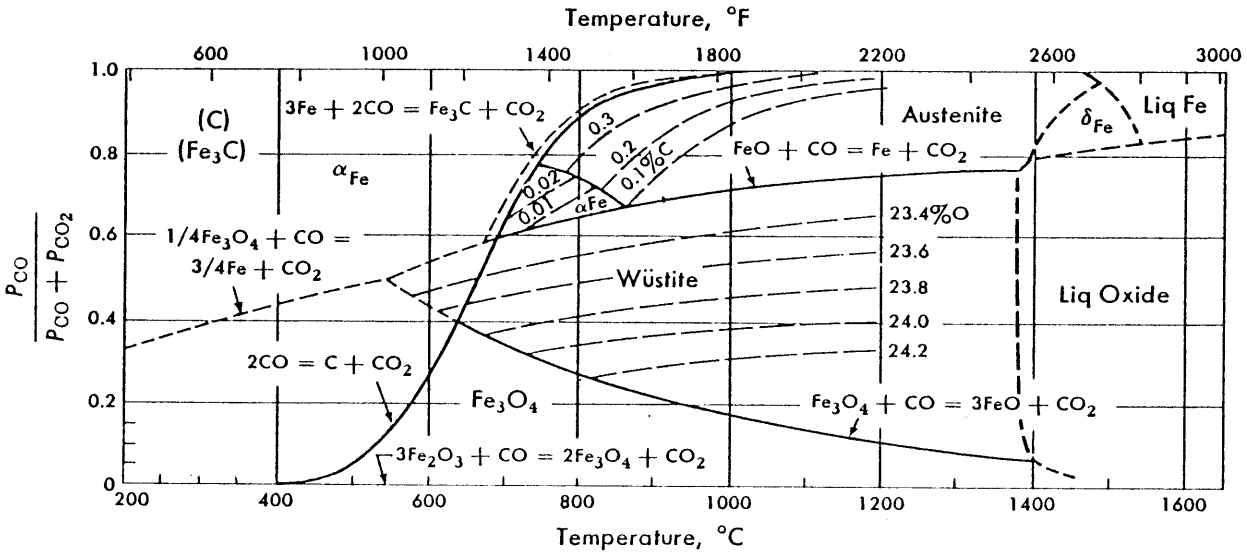


Fig. 6-1 Equilibrium Fe-O-C System at 1 atm (after Elliott, et al.[77]).

$$2Fe_3O_4 + Fe_3C = 3Fe + 6"FeO" + CO_2 \qquad (6.5)$$

The equilibrium partial pressure of CO is 0.4 at 650°C. For Equations (6.4) and (6.5) the total volume of gas can be calculated as a function of the oxygen content of DRI:

$$V_E = 2.19 \ \% \ O \qquad (6.6)$$

where $V_E$ is in $cm^3/g$ and %O is weight percent of oxygen. A comparison is made of the volumes of gas ($CO + CO_2$) calculated from Equation (6.6) and the values measured during helium extraction of DRI samples in Table 6-1. For samples of higher oxygen contents, the measured volumes of evolved gases are slightly higher than the equilibrium gas volumes. The difference may be due to the reduction of small quantities of $Fe_2O_3$ to $Fe_3O_4$ at low temperatures.

2. Variable Temperature

Reactions (6.4) and (6.5) can similarly occur during bomb extraction of DRI. The formation of "FeO" starts at 650°C and will proceed at higher temperatures until the complete conversion of magnetite to wustite is achieved. This is due to the continuous increase of the temperature of DRI. Assuming 50 percent of the exhaust to be CO (cf. Figure 6-1), the total volume of the evolved gas can be computed from the following equation:

$$V_B = 2.3 \ \% \ O \qquad (6.7)$$

The total gas volumes calculated for various DRI samples are given in Table 6-2. The temperatures of the samples up to which these volumes

Table 6-1 Volume of Gas Evolved from DRI at 650°C.

| Sample | %O | $V_{CO} + V_{CO_2}$, $cm^3/g$ | |
|---|---|---|---|
| | | He Extraction | Equilibrium |
| B | 3.26 | 10.6 | 7.1 |
| D | 3.12 | 10.8 | 6.8 |
| C | 2.18 | 5.0 | 4.8 |
| G | 2.01 | 4.5 | 4.4 |
| E | 1.92 | 4.2 | 4.2 |
| Lump Ore | 1.85 | 4.0 | 4.0 |

Table 6-2 Calculated Gas Volumes and Corresponding Bomb Temperatures.

| Sample | $V_B$, $cm^3/g$ | Temp., °C |
|---|---|---|
| B | 7.7 | 800 |
| D | 7.3 | 841 |
| C | 5.1 | 791 |
| G | 4.7 | 850 |
| E | 4.5 | 821 |
| Lump Ore | 4.3 | 806 |

have been evolved are determined from the experimental results and are illustrated in the same table.

The results shown in Table 6-2 indicate that the conversion of magnetite to wustite ends at about 850°C. Above 700°C, the reduction of wustite to pure iron is thermodynamically possible:

$$\text{"FeO"} + Fe_3C = 4Fe + CO \qquad (6.8)$$

$$2\text{"FeO"} + Fe_3C = 5\ Fe + CO_2 \qquad (6.9)$$

The tendency for reactions (6.4) and (6.5) to proceed is however higher than that of reaction (6.8) at high temperatures due to the larger free energy changes. At about 750°C the rate of evolution of gas from DRI materials undergoing bomb extraction reaches a maximum. Above 750°C, although the conversion of $Fe_3O_4$ is favored by high temperatures, the rate of gas evolution decreases due to the decrease in the magnetite content of DRI. A minimum in the gas evolution curves is observed at about 850°C. This corresponds with the temperature at which $Fe_3O_4$/"FeO" conversion becomes complete, as shown in Figures 6-2 and 6-3 (cf. Table 6-2).

The reduction of wustite to pure iron is also favored by high temperatures. At about 1000°C, a peak is observed in the rate of evolution of gas. At higher temperatures, although the reduction reactions are thermodynamically possible, the diffusion of reactants controls the rate of reduction of the sample. This rate decreases with increasing progress of reactions and removal of the last traces of oxygen or carbon from DRI. It can be seen from the equilibrium

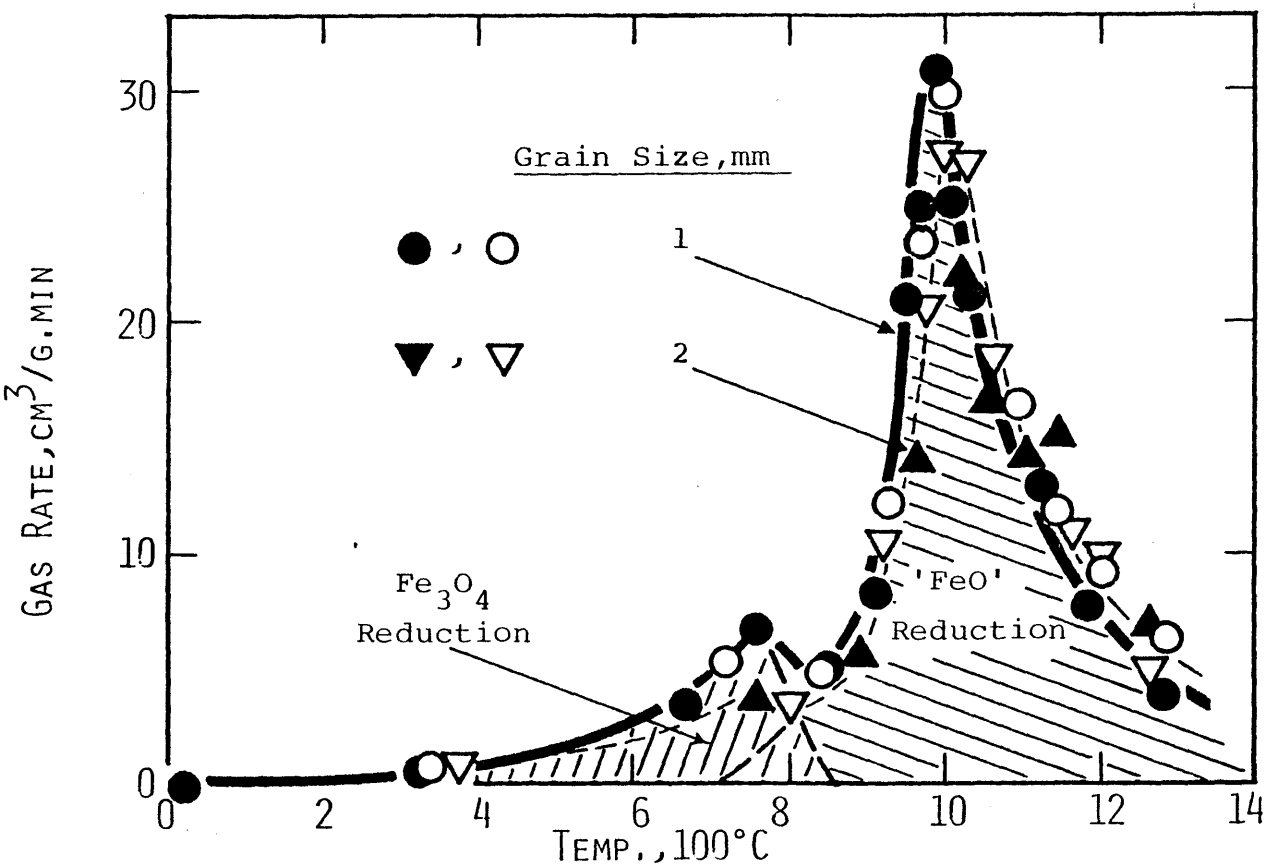


Fig. 6-2 Gas Evolution from Type C Pellets. Temp. Rate, 250°C/min. Particle Size, 1 and 2 mm.

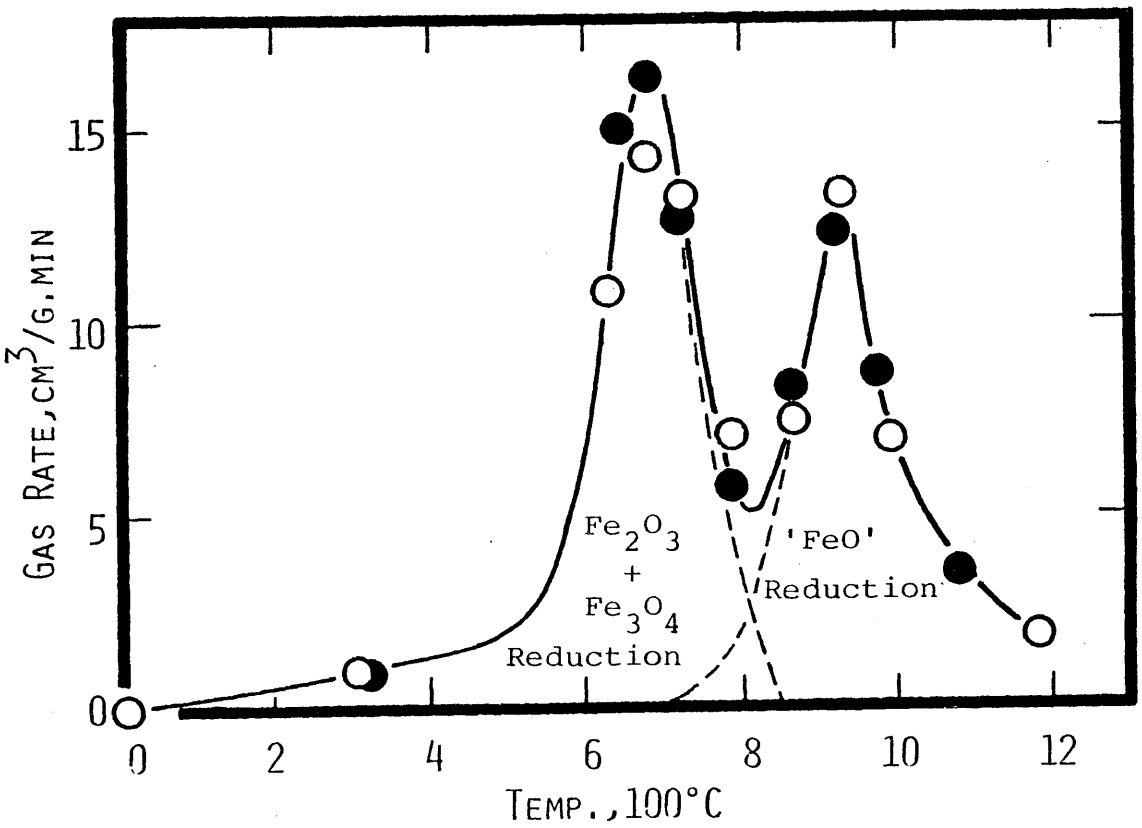


Fig. 6-3 Gas Evolution from Type F Pellets. Temp. Rate, 250°C/min. Particle Size, 1 mm.

diagram that above 1000°C, the gas evolved is almost pure CO.

a. Effect of Grain Size

The overall thermal conductivity of crushed DRI when charged into an extraction bomb was calculated from Equation (D.7). The fraction of the pores produced between the grains was determined from the difference between the overall density of the crushed charge and the density of DRI. The thermal conductivity of the pores was computed from Equation (D.11). The diameter of the pores was assumed equal to that of the grains. The thermal conductivity of DRI grains was calculated from Equation (E.1). The results for 1 and 2 mm crushed materials of type D are plotted in Figure 6-4. It can be seen that the overall thermal conductivity for 2 mm size grains is higher than that of 1 mm grains. This difference may be responsible for the slight shift of the gas exgraction curves to the higher temperatures described in Section IV.A.2.a.2.

The effects of the change of the overall thermal conductivity of the charge of an extraction bomb on the temperature profile and the rate of extraction of gas are shown schematically in Figure 6-5. The temperature profile $\gamma$ corresponds to a high conductivity or a low heating rate. The temperature of the charge in this case is the same as that of the thermocouple bead. The associated gas evolution curve is also shown in Figure 6-5. The temperature profile $\gamma$ can be replaced by $\beta$, if the thermal conductivity associated with $\gamma$ decreases to that of $\beta$. The gas evolution curve, however, can be the same, if the rate of extraction of gas is plotted against the mean temperature of the charge. Since the gas evolution curve is plotted against the temperature

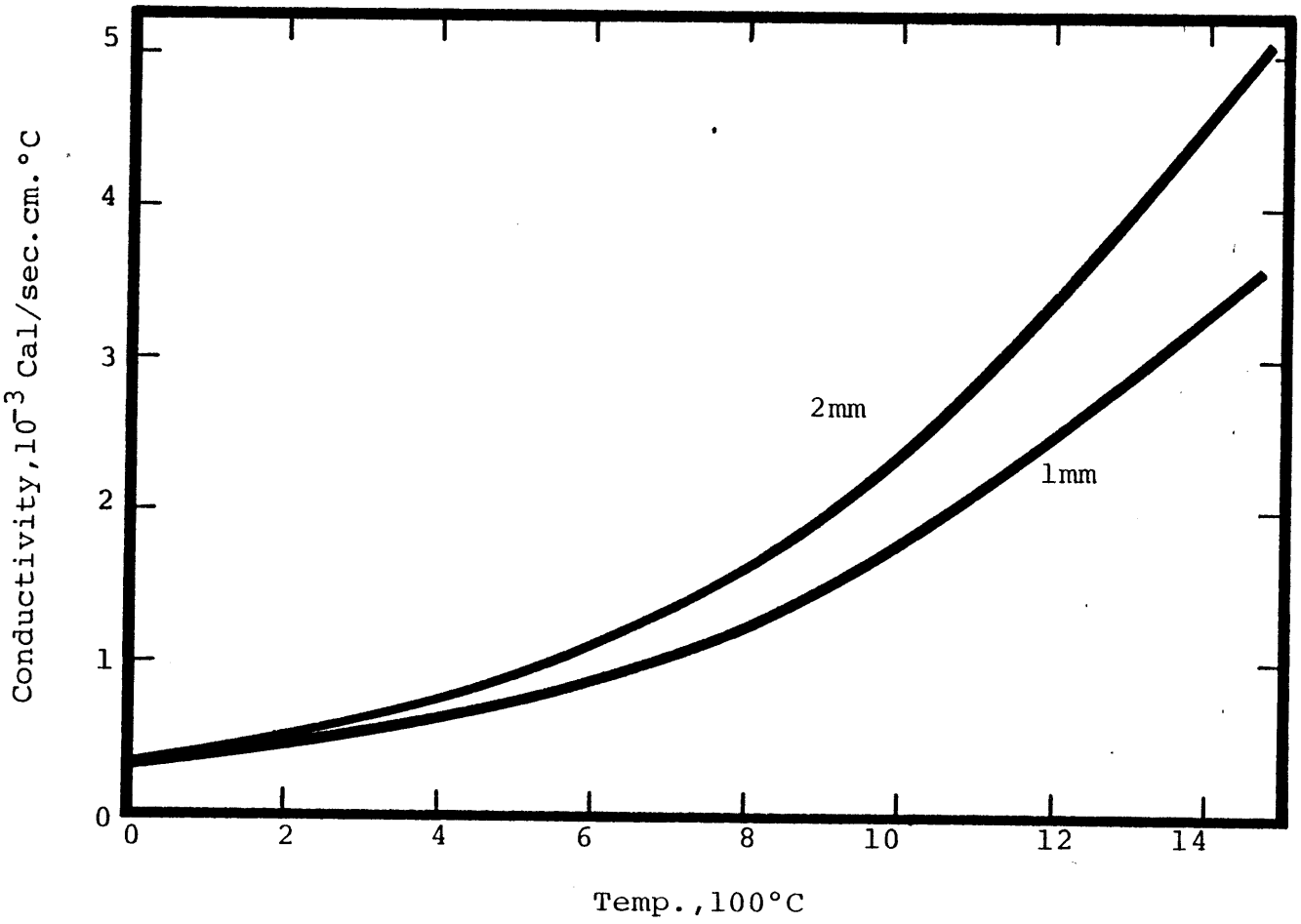


Fig. 6-4 Estimated Overall Thermal Conductivity of Type D Pellets of 1 and 2 mm Size.

registered by the thermocouple which is less than the mean temperature of the charge, it is shifted to the lower temperatures. If the temperature profile becomes less uniform (curve $\alpha$), the gas evolution curve will shift to the lower temperatures even further.

b. Effect of Heating Rate

A slow heating rate favors a more uniform temperature distribution which results in a decrease in the total volume of the gas evolved below the temperature associated with the larger gas evolution peak (1000°C) and an increase in the volume of the gas evolved above that temperature (Figures 4-15 and 14-16). A less uniform temperature profile results in shifting of the gas evolution rate curve to the lower temperatures, as shown in Figure 6-5. Changing the rate of rise of temperature of the sample also affects the rate of reduction of DRI. At very high heating rates the diffusion of reactants through DRI grains may contol the rate of formation of gas and shift the gas evolution rate pattern to that at higher temperatures. A combination of these effects results in a slight shift of the larger gas evolution peak to the right for temperature rate of 1000°C/min in Figures 4-17 and 4-18.

B. Heat Transfer Results

The experimental results of the heat transfer studies are discussed through comparison with the mathematical calculations for heating both inert and DRI particles in hot liquid slags with and without local gas bubbling.

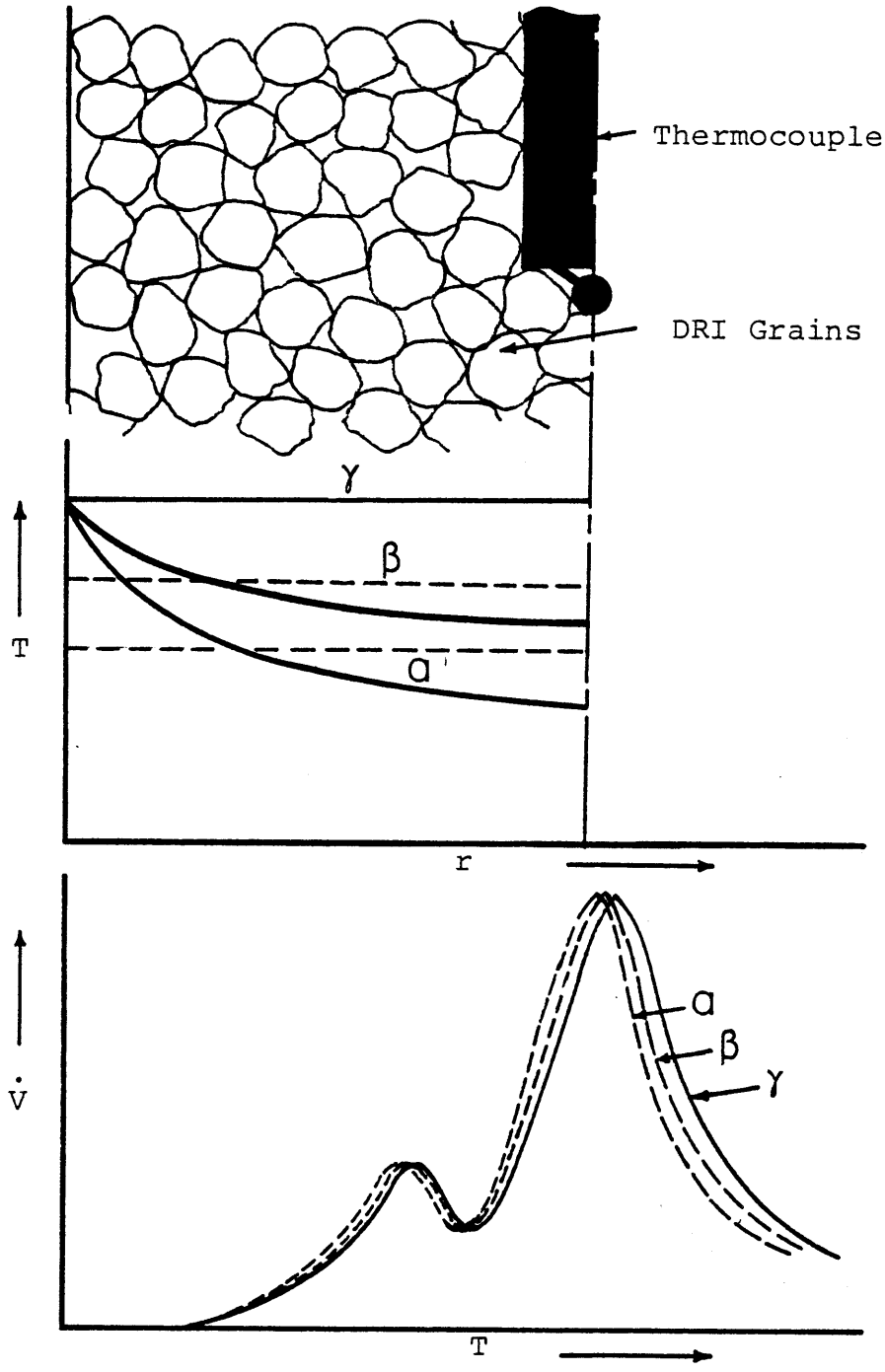


Fig. 6-5 Temperature Profile and Gas Evolution for DRI of Different Thermal Conductivities Increasing from $\alpha$ to $\gamma$.

1. Inert Specimen

The growth of the shell of solid slag and the rise of temperature at the center of 1.8 cm diameter nickel sphere when immersed in a bath of hot slag are illustrated in Figures 6-6 and 6-7. The rates of evolution of gas from the specimens are specified. The thickness of the shells of slag and the central temperatures of the specimens determined from the mathematical model described in Chapter V are also plotted in the same diagrams.

Without gas evolution, as is seen, the growth of the shell of slag and the rise of the temperature at the center of the specimen determined experimentally and mathematically both are consistent. The Nusselt numbers employed for these calculations are given in Figure 6-9 in which the contributions of conduction--Equation (5.11)--and initial transient forced convection are included. The latter is assumed to last for 5 seconds during which the corresponding Nusselt number drops linearly from 175 to 0. Since the information available on natural convection--Equation (5.12)--leads to smaller Nusselt numbers, it may be concluded that the short-term conduction is the dominant mechanism for transfer of heat to the particle.

2. Effect of Local Bubbling

An example of the effects of evolution of gas on solidification and melting of slag on a submerged sphere is demonstrated in Figure 6-6. As is seen, the evolution of gas from the specimen shifts the curve to the lower thicknesses. The shifted curve is however almost parallel to the curve for no gas evolution (cf. Figures 4-23, 6-11 and 6-12).

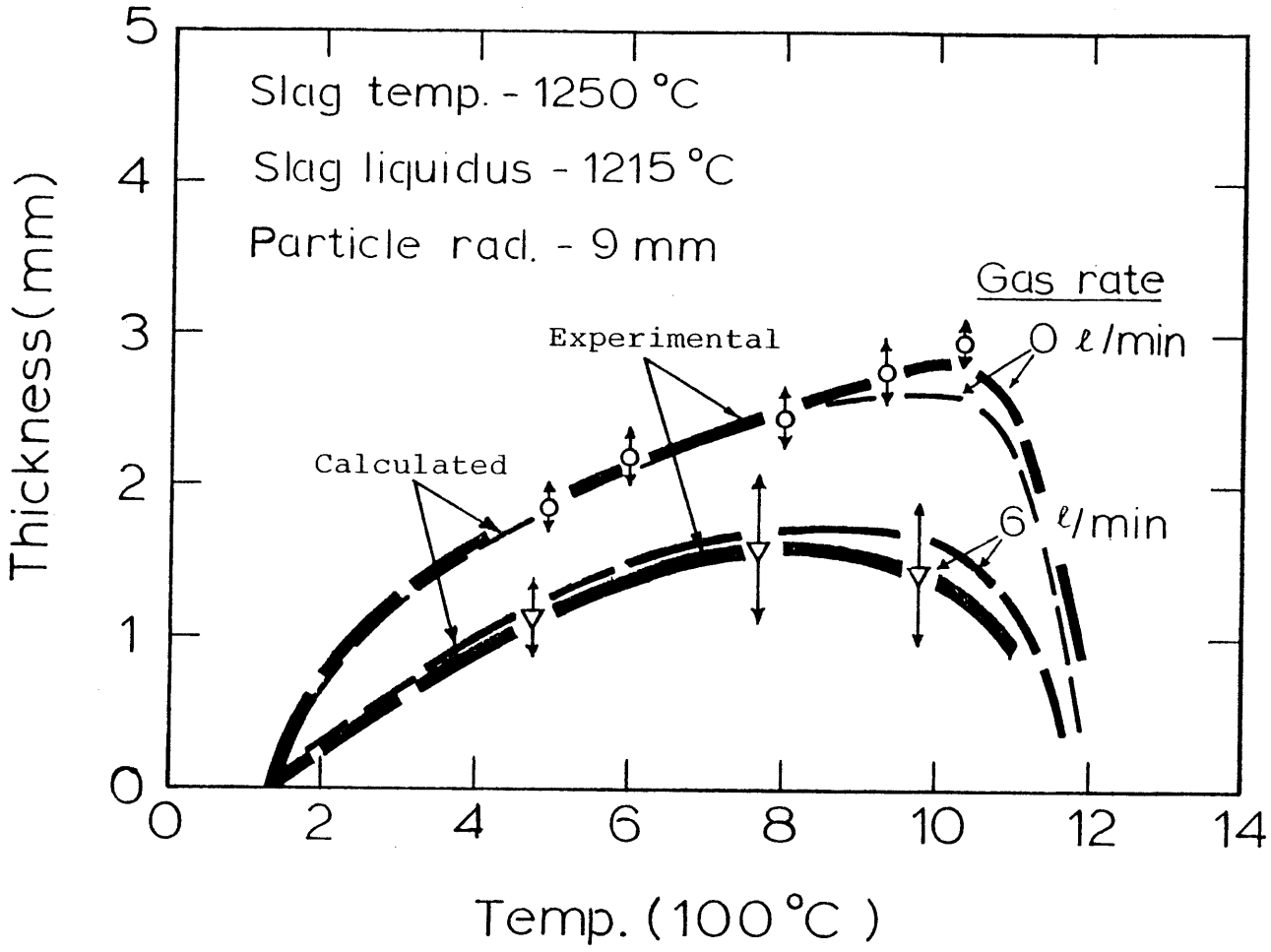


Fig. 6-6 Effect of Gas Evolution on Thickness of Solid Slag on 1.8 cm Dia. Ni Sphere Heated in Slag A. Slag Temp., 1250°C.

This finding indicates that, after the root of the shell freezes, the rate of transfer of heat to the solid-liquid slag interface is almost the same for experiments with and without gas bubbling. It may be concluded that the evolution of gas from the sphere basically affects the thickness of the solid shell at the initial transient period (assumed 5 seconds) during which the root of the shell may grow.

During this period, the evolution of gas accompanied with the plunging effects may generate an enormous amount of violence in the bath. The cold layer of solid slag immediately formed on the sphere can be removed by departing gas bubbles which sweep their way from the gas ports into the liquid (Figure 6-8). Since the particle and its steel tubing support are still cold, the temperature of the gases evolved from the sphere may be substantially less than that of the bulk liquid slag resulting in a low thermal conductivity of the departing gas bubbles which partially shield the exterior of the specimen (Figure 3-10).

The partial removal of the cold slag from around the sphere results in a decrease of the thickness of the shell of slag while the shielding of the particle with gas bubbles has a decreasing or an increasing effect on the rate of transfer of heat into the particle. The overall effect is an increase in the rate of heating of the specimen, as is seen from the calculated curves plotted in Figure 6-7.

The thermal conductivity of the liquid slag as influenced by the rising gas bubbles is estimated from Equation (D.7) and plotted in Figure 6-10. The temperature of the evolving gas is assumed to be the

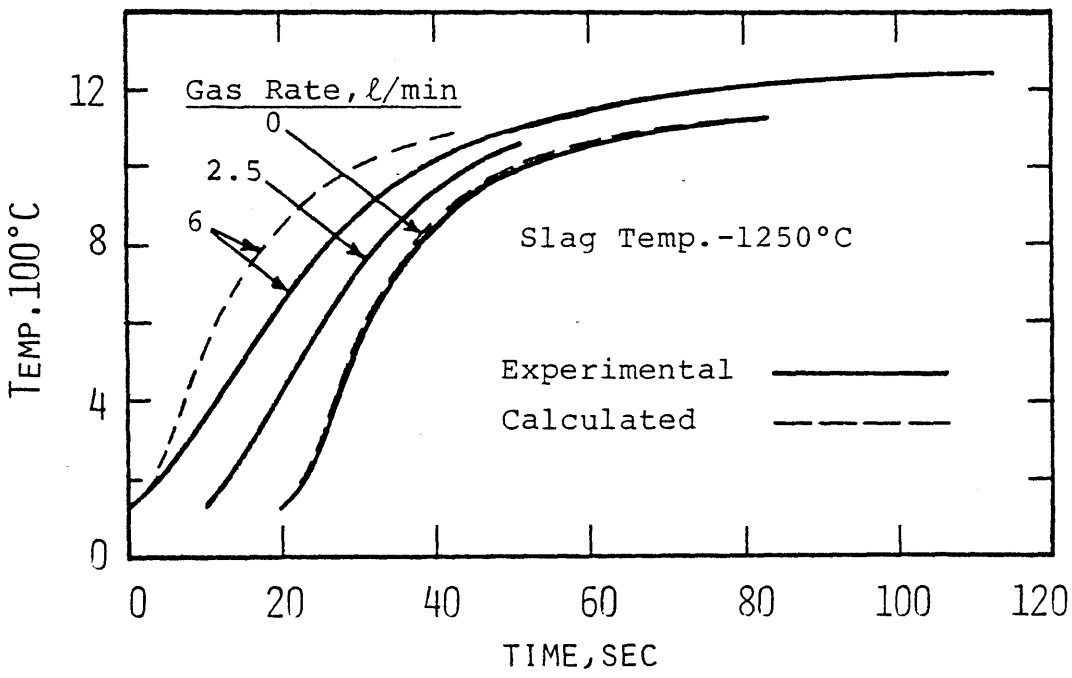


Fig. 6-7 Effect of Gas Evolution on Rise of Temp. of 1.6 cm Dia. Ni Sphere Heated in Slag A. Slag Temp., 1250°C. Curves for 0 and 2.5 ℓ/min are displaced 20 and 10 sec to right.

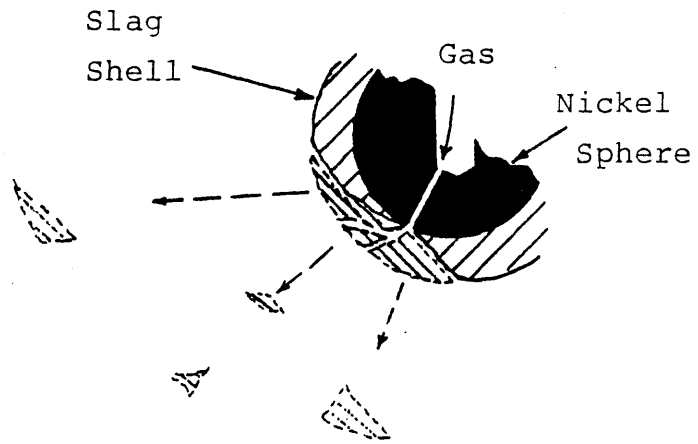


Fig. 6-8 Physical Model for Removal of Slag Shell by Evolving Gas.

same as the temperature of the wall of the thermocouple well. The gas bubbling data given in Table 3-7 were utilized for these calculations (see Appendix I for estimation of porosity of slag). The results show that below 600°C, the thermal conductivity of the liquid decreases with gas bubbling. Above that temperature, the thermal conductivity of the gas bubbles exceeds that of the liquid slag because of radiation effects and the overall thermal conductivity rises. For large nickel spheres (3 cm diameter) the fraction of the surface area that is shielded by gas bubbles is about 70 percent less than that of the small spheres. The rate of heating of the large spheres must therefore be less sensitive to the shielding effects of gas bubbles.

Although the temperatures at the center of the spheres measured after a long time, when the slope of the heating curves is very small, were found insensitive to sudden changes of the gas flow rate (Figure 4-21) and the heat capacity of the evolved gases is small as compared to the enthalpies absorbed by the sphere, the difference between the measured and calculated heating curves appears to be due to the cooling (or heating) effects of the gas stream on the temperature sensing device. The observed insensitivity might have been due to the heating of the gas stream when passing through the long and hot steel tube used to support the sphere and supply the evolving gas.

A simple calculation of the heat capacity of the evolved gas shows that the rate of transfer of heat to the surface of a small nickel sphere is more than 10 times greater than the total rate of absorption of heat by the stream of gas flowing at 6 ℓ/min (at slag temperature) to reach the temperature of the bulk (1250°C). For a large sphere under

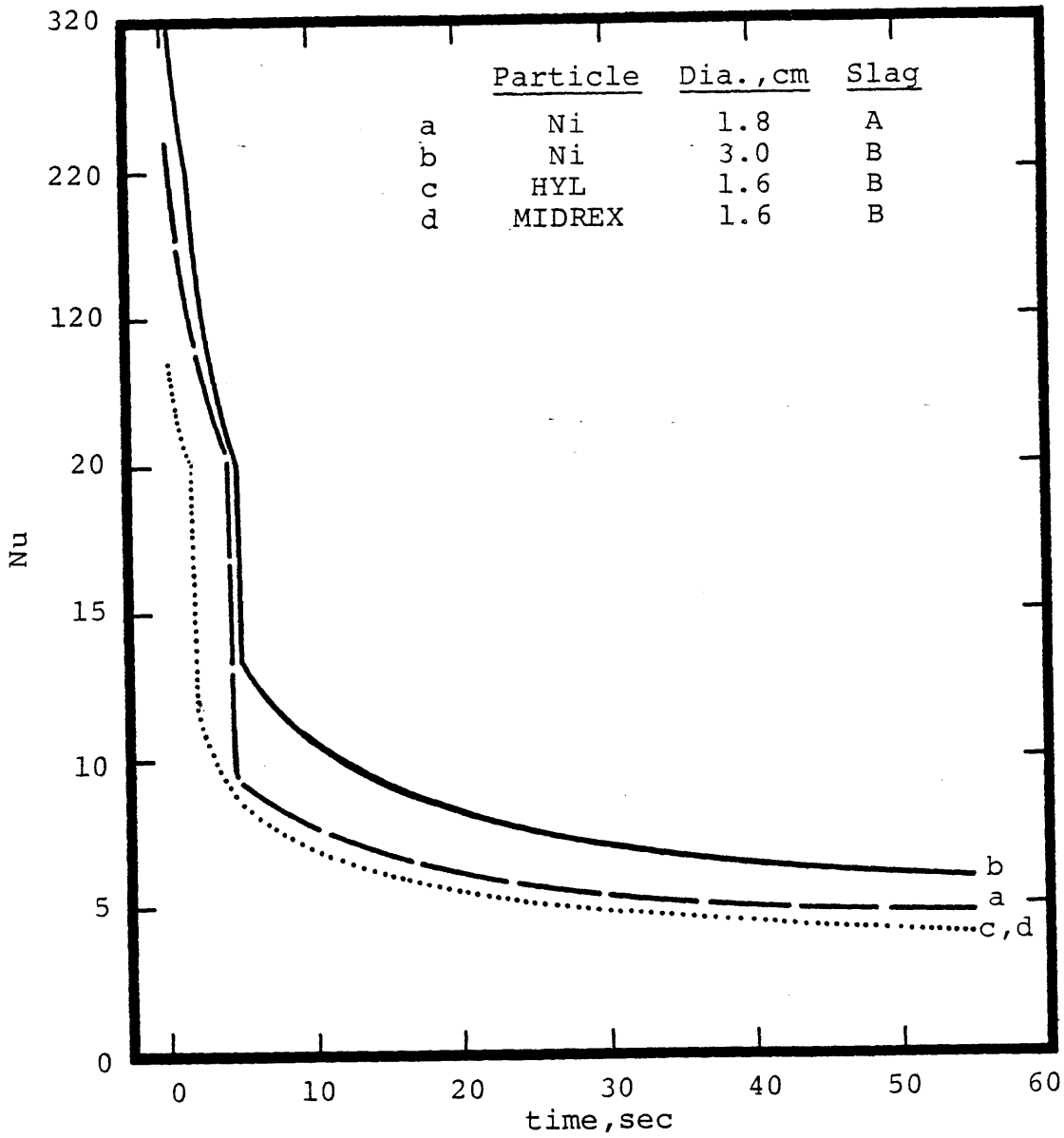


Fig. 6-9 Overall Nusselt Number for Heating Ni Spheres and DRI Pellets in Liquid Slags with or without Gas Evolution.

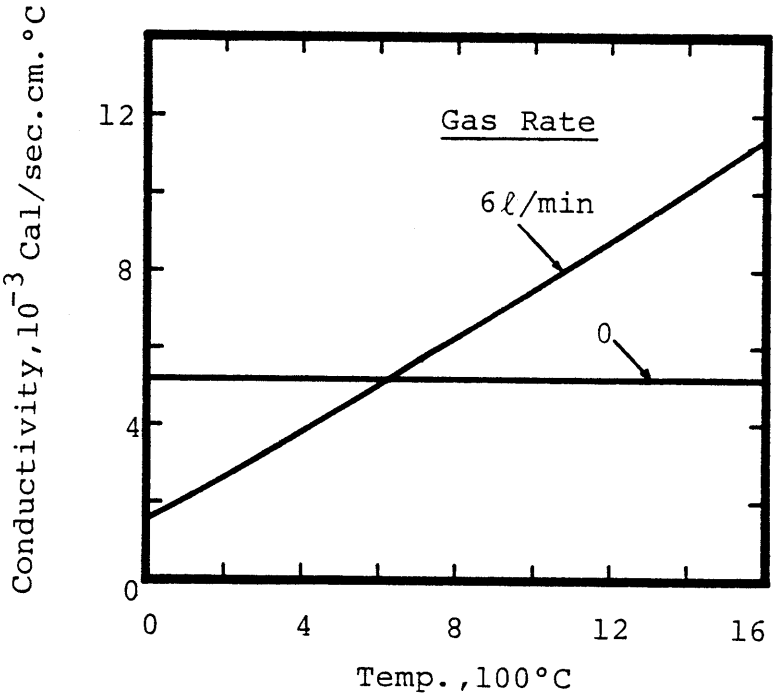


Fig 6-10 Estimated Thermal Conductivity of Liquid Slag Surrounding 1.8 cm Dia. Ni Sphere (cf. Table 3-5 and Appendix I).

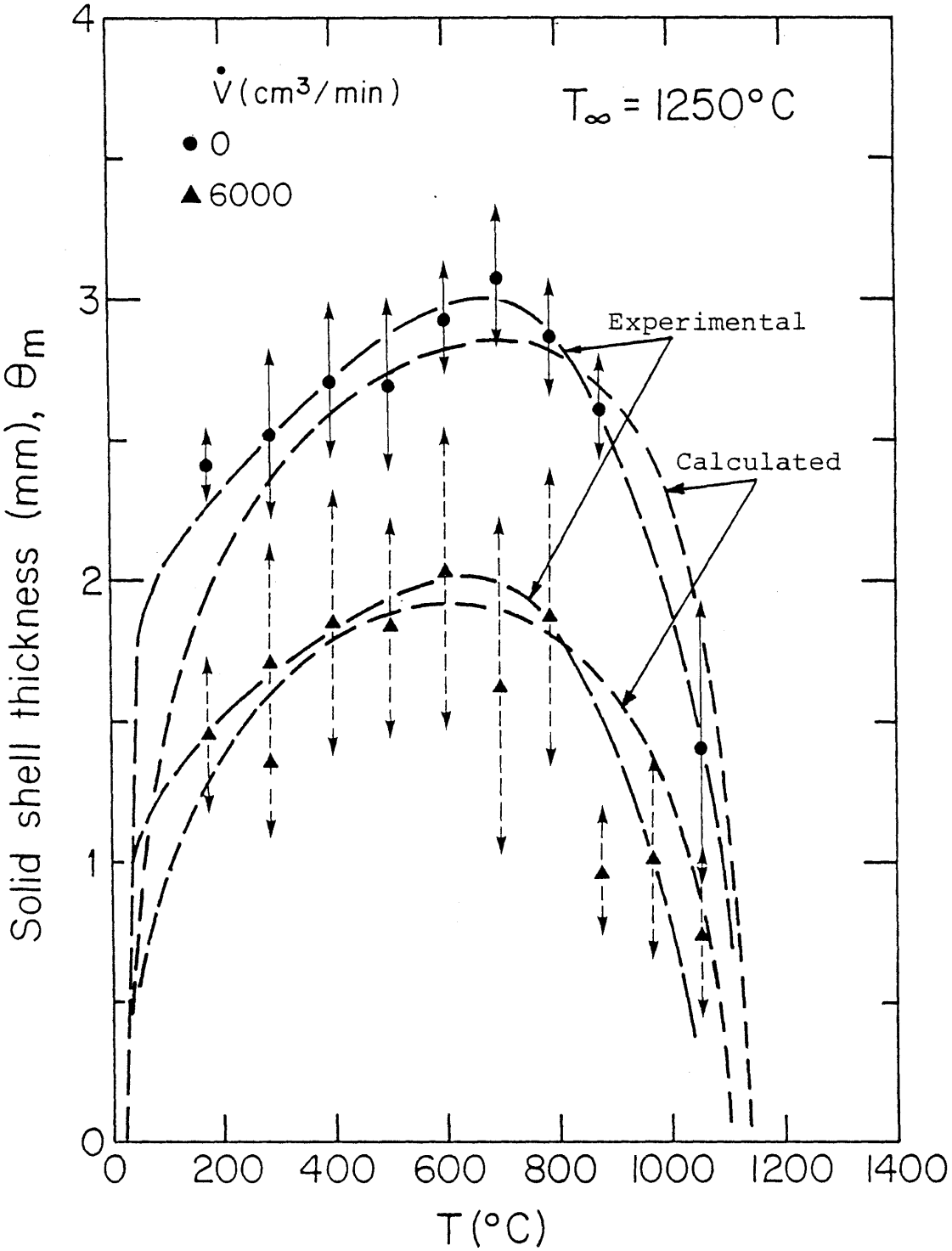


Fig. 6-11 Effect of Gas Evolution on Thickness of Slag Shell Frozen on 3 cm Dia. Ni Sphere Heated in Slag B. Slag Temp., 1250°C.

the same conditions, the rate of flow of heat to the particle is more than 30 times greater than that absorbed by the gas.

The growth of shells of slag on 3 cm nickel spheres immersed in liquid slag B at bulk temperatures of 1250 and 1275°C are compared with the calculated thicknesses in Figures 6-11 and 6-12. The Nusselt numbers utilized for calculations are illustrated in Figure 6-9. From the best fit of data, neither the contribution of the steady state natural convection--Equation (5.12)--is present nor that of the forced convection by gas bubbling, Equation (5.14). Using the same Nusselt quantities as were used for heat transfer calculations in absence of gas evolution leads to the best set of results. Hence, short-term conduction is the dominant heat transfer mechanism in this case too.

It was assumed that the removal of the shell of slag due to the evolution of gas occurs during the initial transient period. The change of the average thickness of the slag shell during this period was corrected by a factor inserted into the model which specified the fraction of solid slag that remained on the surface of the particle. For heating of a particle without gas evolution, this fraction is 1. The removal of the cold crust of slag from the surface of the particle can also be expressed in terms of a large initial Nusselt number which can function in the same way as the correction factor does.

The overall effect of the decrease of the thickness of the shell of slag due to the gas evolution is an increase in the rate of heating of the particle, as shown in Figures 6-13 and 6-14. This effect may result in a decrease in the melting time of the particles charged into

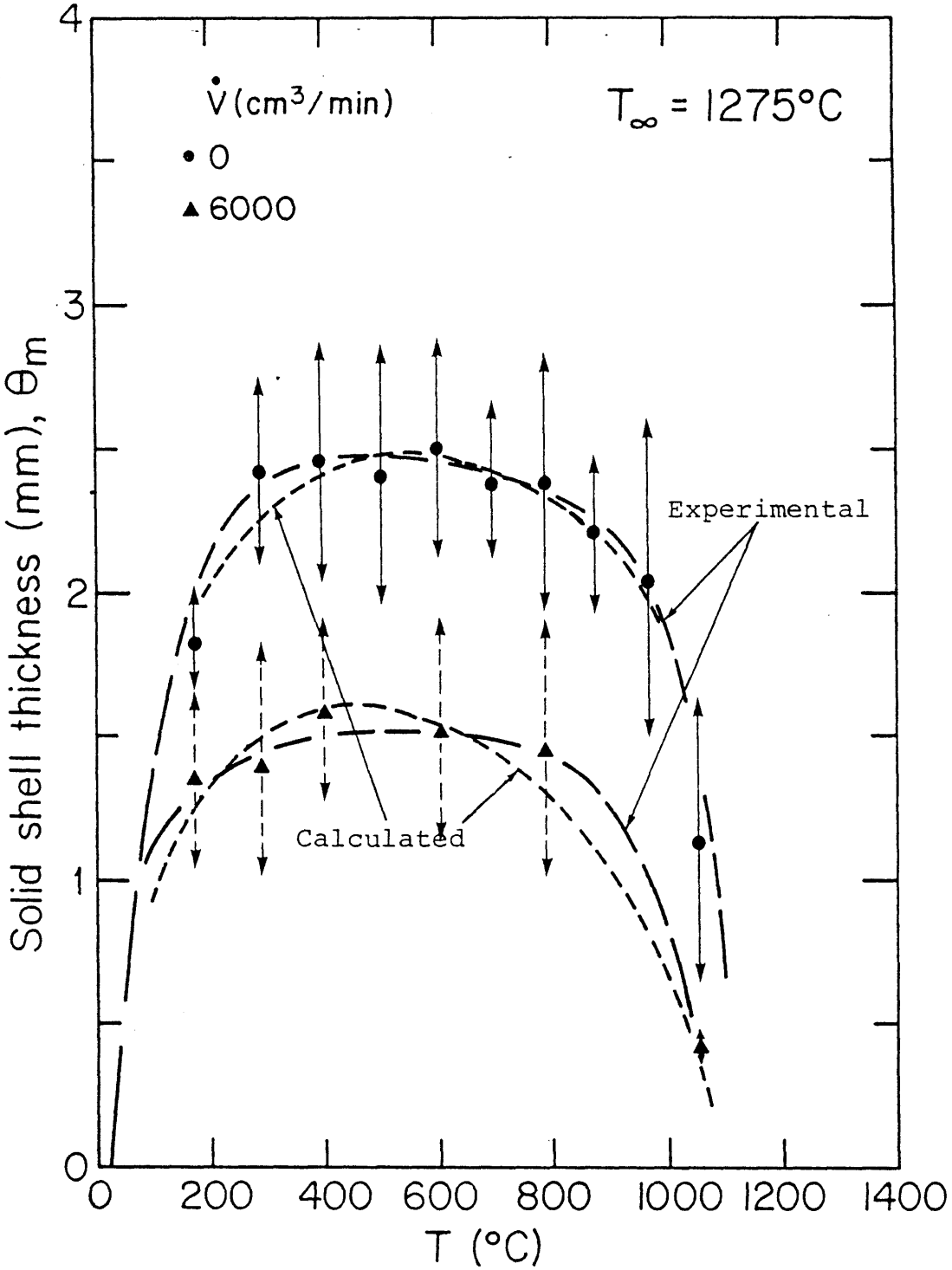


Fig. 6-12 Effect of Gas Evolution on Thickness of Slag Shell Frozen on 3 cm Dia. Ni Sphere Heated in Slag B. Slag Temp., 1275°C.

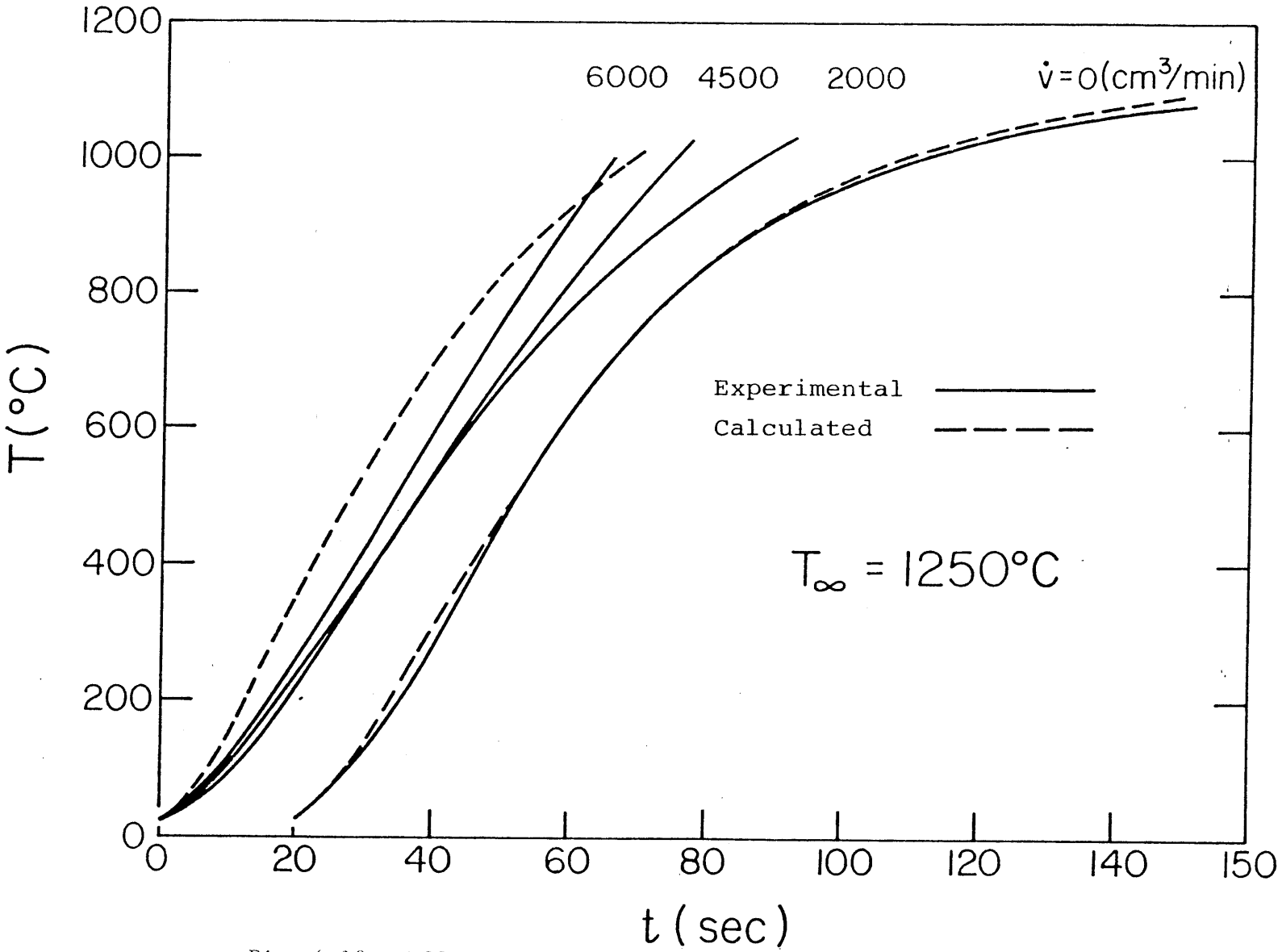


Fig. 6-13 Effect of Forced Bubbling on Rise of Center Temp. of 3 cm Dia. Ni Sphere Heated in Slag B. Slag Temp., 1250°C.

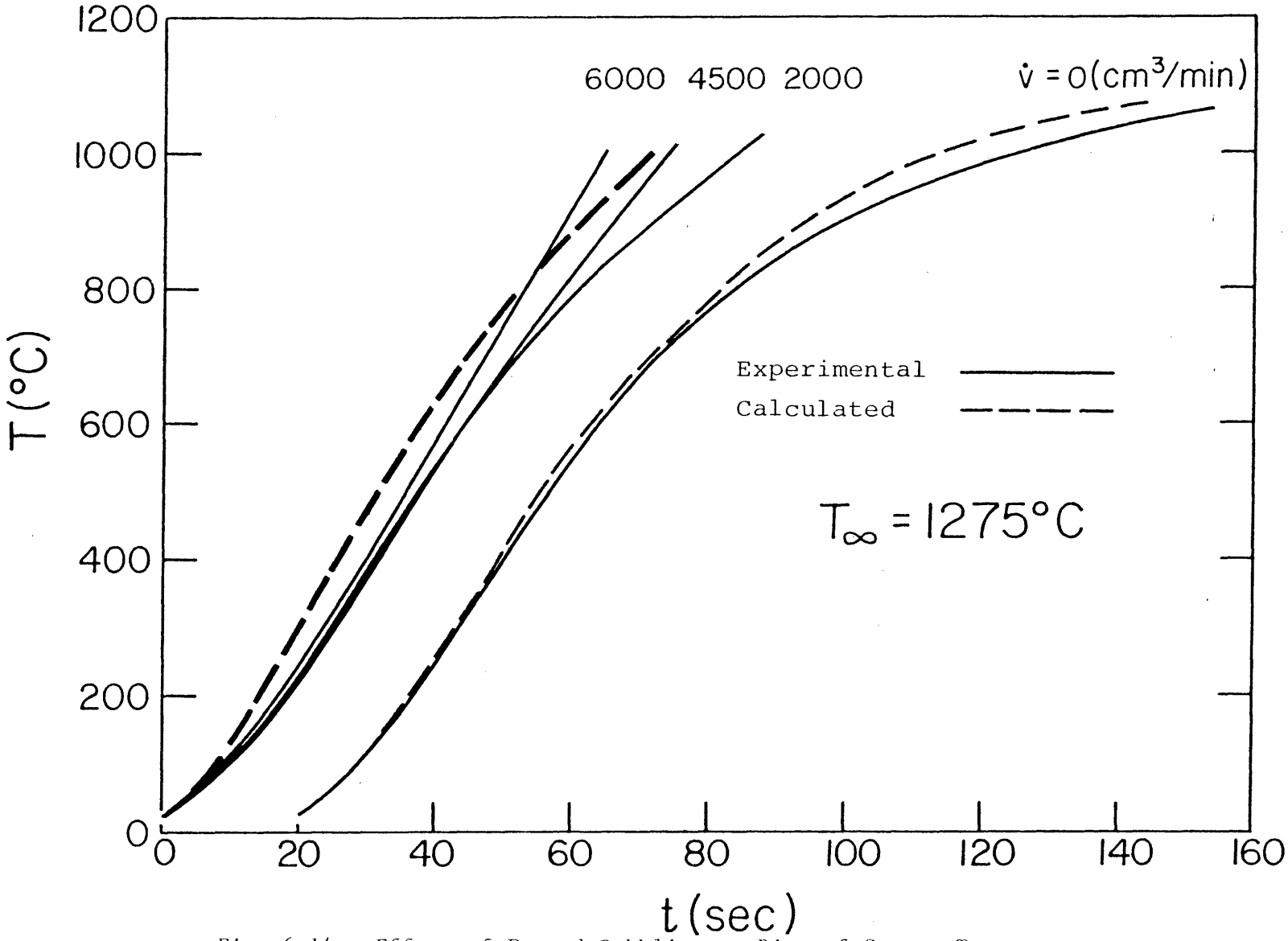


Fig. 6-14 Effect of Forced Bubbling on Rise of Center Temp. of 3 cm Dia. Ni Sphere Heated in Slag B. Slag Temp., 1275°C.

steelmaking slags, as will be discussed later.

3. Formation of Gas

The temperature at the center and the volume of the gases evolved from D-R pellets E and D described in Table 5-2 were calculated from the simulation model and compared with the experimental results, as illustrated in Figures 6-15 and 6-16. The mathematical calculations show a larger thermal lag than is registered by the thermocouple during the measurements. The rapid rise of the temperature of the thermocouple immediately after immersion of the pellet may be due to convective heat transfer from the flowing stream of hot gas that forms at the external layer of the pellet into the thermocouple bead.

When a cold DRI pellet is plunged into a hot bath of slag, the temperature of its surface rises rapidly while, because of the low thermal conductivity of the pellet, its core remains cold (Figure 6-15). A large volume of hot gas may thus form at the areas close to the periphery of the pellet which is sucked into the steel tube used to support the pellet (see Section III.D.2.c and Appendix B for experimental details). This gas can heat up the thermocouple bead as well as the cold core and result in the rapid rise of temperature that is measured by the thermocouple. When the difference between the temperature of the surface and the temperature at the center of the pellet becomes substantially small, the measured temperature approaches the calculated one.

The volumes of the gases evolved from pellets E and D are calculated and compared with the experimental results in Figure 6-16 using the gas evolution data for type E or D as reference (see Section

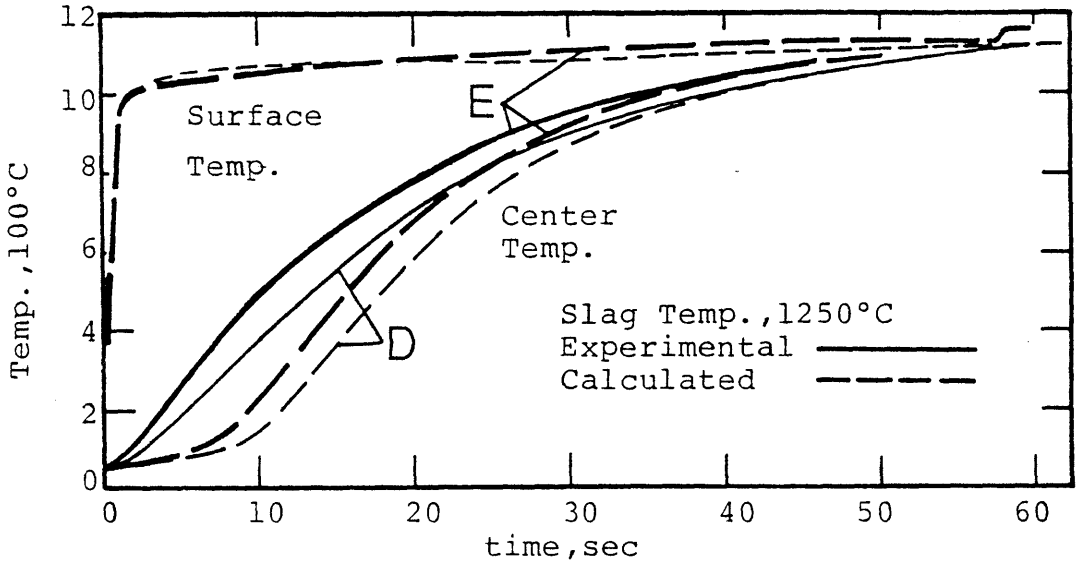


Fig. 6-15 Rise of Temp. of D-R Pellets E and D Immersed in Slag B (cf. Table 5-2).

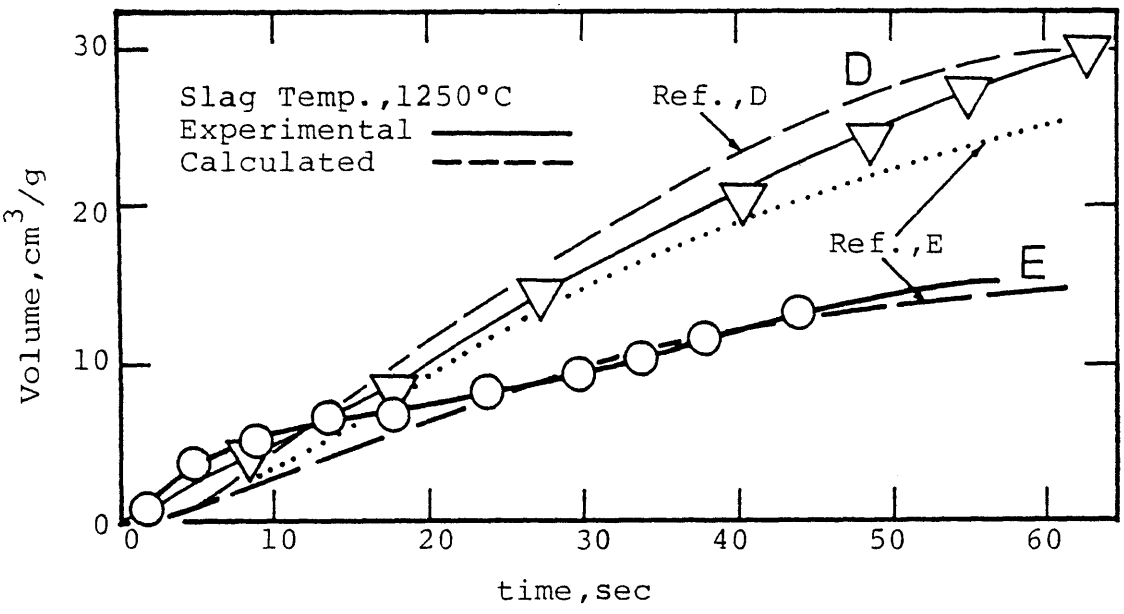


Fig. 6-16 Gas Evolution from DRI Pellets E and D when Heated in Slag B (cf. Table 5-2).

V.A). The slight difference between measured and calculated volumes of the evolved gases produced for a short period after immersion may be due to the convective heating of the cold core. The variation of the chemical compositions of the pellets from the mean compositions may also be responsible for further differences between the measured and calculated quantities. Yet,the results are satisfactorily consistent.

The growth of the shell of solid slag on the pellets obtained from model calculations is plotted in Figure 6-17. The initial growth of the solid shell on pellet E is faster than on D, but the maximum thickness of the shells is about the same. Pellet E is a highly metallized Midrex pellet (see Table 4-2), D is a low metallized HYL pellet (see Table 4-1). The density of E is greater than that of D, its porosity less (see Table 5-2). Hence the thermal conductivity of pellet E is greater than that of D. This results in a higher rate of absorption of heat by E and a thicker shell of frozen slag formed on its surface initially.

Since pellet D is less metallized than E, when the temperature is high enough that a substantial quantity of gas is evolved, its heat capacity will exceed from that of E (see Appendix F) resulting in a lower surface temperature (Figure 6-15) and a higher rate of transfer of heat to the surface. The difference in the heat absorped by the pellets is responsible for the slower remelting of the slag shell solidified on pellet D for times greater than 20 seconds after immersion.

After about 60 seconds the shell of solid slag formed on surface

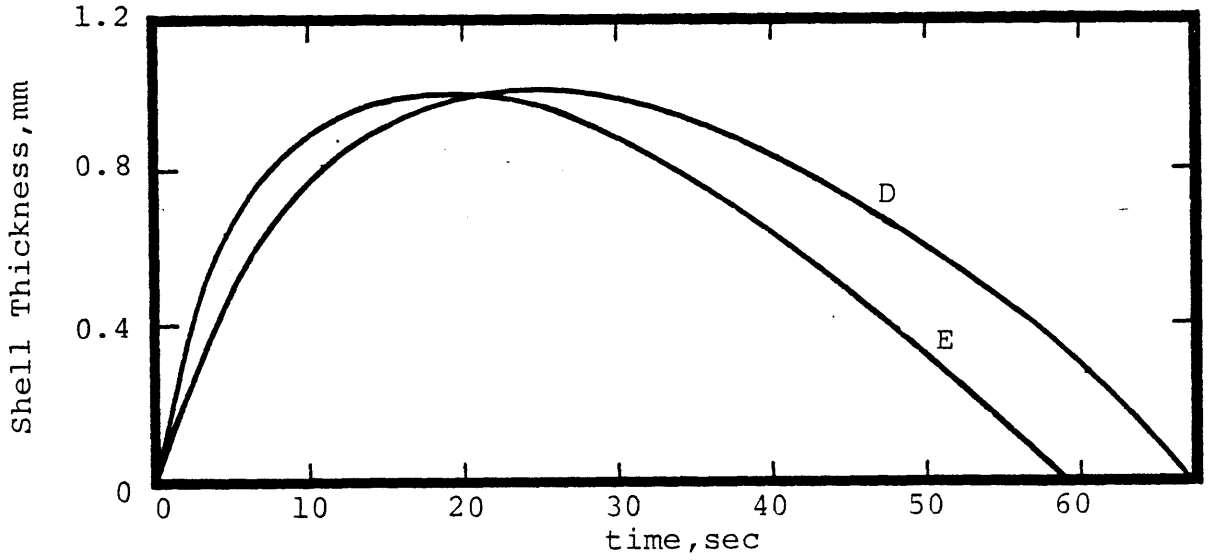


Fig. 6-17 Solid Shells of Slag on Surface of DRI Pellets E and D (cf. Table 5-2).

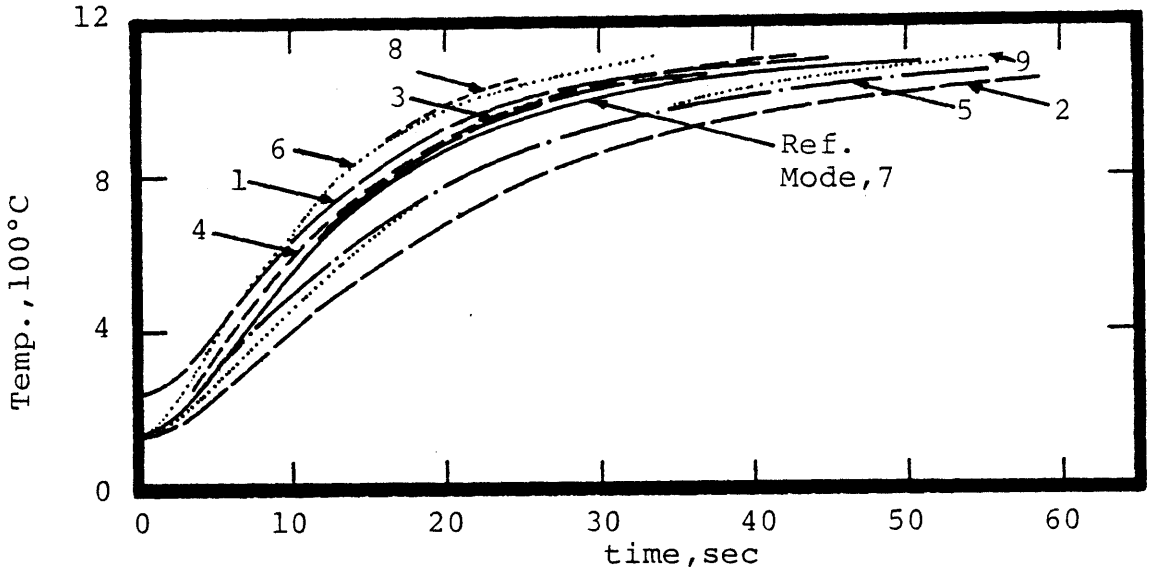


Fig. 6-18 Sensitivity of Temp. at Center of 1.8 cm Ni Sphere to Changes Specified in Table 6-3.

of pellet E is totally remelted (Figure 6-17). The total removal of the shell results in a rapid rise of the surface temperature of the pellet, as shown in Figure 6-15. Because of the relatively low thermal conductivity of the pellet, however, the response of the center temperature of the particle to this change is not illustrated in the figure.

4. Sensitivity Analysis

The effect of variation of the input parameters of the system on the heating curves and the thickness of the solid shell of slag were determined from the simulation model. The reference conditions and the changes of the parameters to which the results of the model are most sensitive are summarized in Table 6-3. The sensitivity of the results to the specified changes are compared in Figures 6-18 and 6-19. As is seen, 50°C increase in the temperature of the solid-liquid slag interface results in the greatest change of the solid slag shell thickness.

The model was found insensitive to the parameters summarized in Table 6-4 in which the average changes of the slag shell thickness and the center temperature are also given.

E. Conclusions

The conclusions to be drawn from the experimental and calculated results discussed in the previous sections may be summarized as follows:

1. Gas Evolution.

a. The reduction of magnetite to wustite between about 600 to 850°C and that of wustite to iron above 700°C result in the evolution of gas from DRI.

Table 6-3 Changes of Conditions of the System for Sensitivity Analysis.

| No. | Property | Quantity | |
|---|---|---|---|
| | | reference | current |
| 1 | Initial temp. of particle, °C | 130 | 230 |
| 2 | Interfacial resistance between particle and slag, surface fraction isolated | 0 | 0.5 |
| 3 | Heat of fusion of slag, cal/g | 80 | 120 |
| 4 | Conductivity of Liq. slag, cal/cm. sec. °C | 0.0052 | 0.0062 |
| 5 | Plunging transient period, sec. | 5 | 2.5 |
| 6 | Initial Nu number for plunging | 210 | 315 |
| 7 | Long-term Nusselt number | 3.43 | 6.86 |
| 8 | Temp. of bulk liq. slag, °C | 1250 | 1300 |
| 9 | Solidus temp. of slag, °C | 1140 | 1190 |

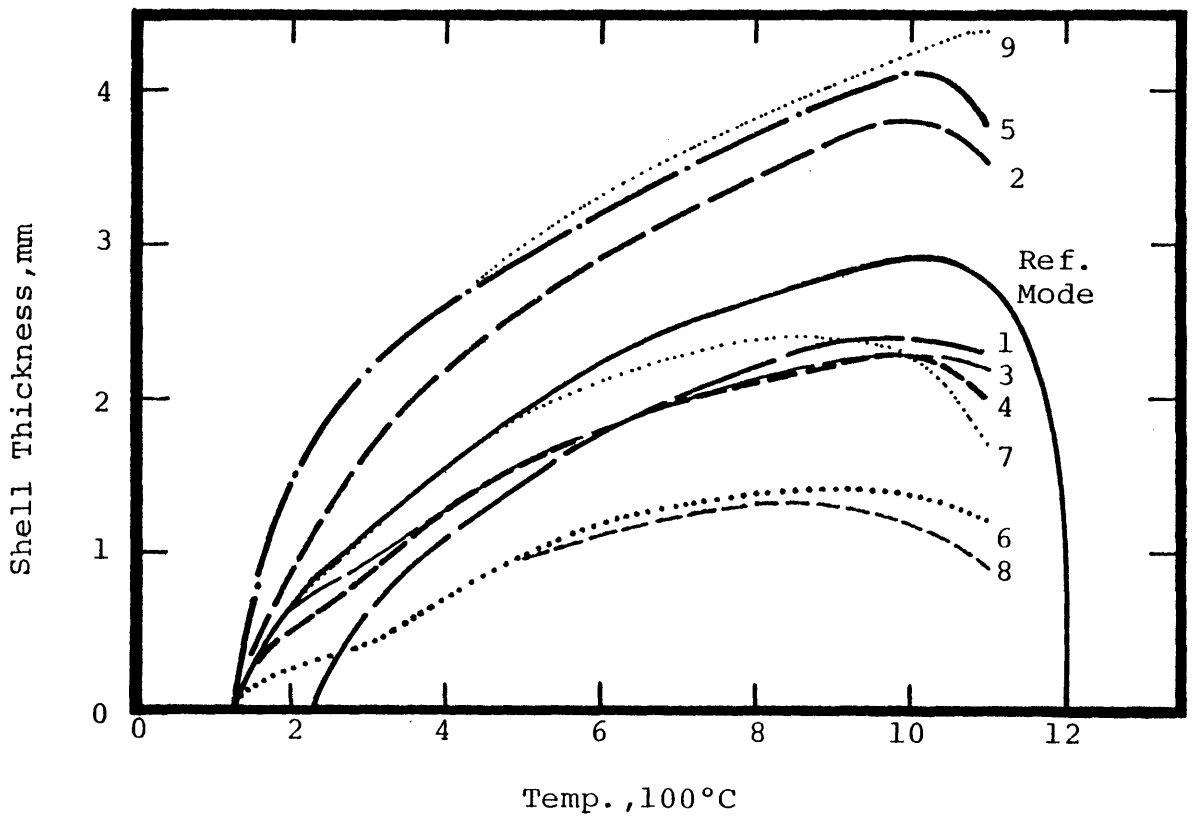


Fig. 6-19 Variation of Thickness of Solid Shell Against Changes Specified in Table 6-3.

Table 6-4 Sensitivity of Shell Thickness and Center Temp. of 1.8 cm Ni Sphere to Changes of Parameters Specified.

| Property | Quantity | | Percent Increase | |
|---|---|---|---|---|
| | reference | current | thickness | temp. |
| Porosity of particle, fraction | 0.02 | 0.10 | 0 | 0 |
| Pore diameter in particle, cm | 0.01 | 0.10 | 0 | 0 |
| Density of particle, $g/cm^3$ | 8.29 | 7.29 | -12 | 3 |
| Density of solid slag, $g/cm^3$ | 3.7 | 4.7 | -10 | 0 |
| Porosity of solid slag, fraction | 0.06 | 0.12 | -4 | -3 |
| Pore diameter in solid shell, cm | 0.02 | 0.10 | 3 | 2 |
| Conductivity of solid slag, cal/cm. sec.°C | 0.0059 | 0.0069 | 4 | 0 |
| Specific heat of solid slag, cal/g. °C | 0.25 | 0.50 | 6 | -4 |
| Solidus Temp. of slag, °C | 1413 | 1488 | 7 | 4.5 |
| Density of liquid slag, $g/cm^3$ | 3.6 | 4.6 | 0 | 0 |
| Specific heat of liquid slag, cal/g. °C | 0.28 | 0.56 | -3 | 0 |

b. At about 750°C, the thermodynamics of the reactions favor the $Fe_3O_4$/"FeO" conversion dramatically and a maximum in the rate of gas evolution is observed. Since the amount of magnetite is limited in the sample, the evolution of gas because of the reduction of magnetite to wustite decreases above 750°C.

c. Because of the favorable thermodynamics of "FeO"/Fe reduction, a peak in the rate of evolution gas occurs at about 1000°C above which the gas evolution rate drops with increasing progress of reactions and removal of the last traces of oxygen or carbon from DRI.

d. The effect of grain size on evolution of gas from DRI is not considerable. The slight shift of gas rate patterns when DRI grain size changes is due to: (1) change of chemical composition and (2) change of the thermal conductivity of the samples.

e Heating rate does not appreciably affect the evolution of gas from DRI.

2. Heat Transfer.

a. The growth of the shell of solid slag on surface of a particle immersed in liquid slag prevents the rapid rise of temperature of the particle.

b. When the bath of liquid slag is not exogenously mixed, short-term conduction is the dominant mechanism for transfer of heat to an immersed inert particle.

c. The local evolution of gas from a particle into the slag decreases the thickness of the shell of slag which may freeze immediately after immersion, but does not appear to have a significant influence

on the shell thickness or the Nusselt number of the bath long after immersion.

d. The temperature and rate of heating of a particle with gas evolution are greater than those of a particle without gas evolution due to the thinner slag shell formed on the former.

e. The formation of gas in a D-R pellet increases the heat capacity of the pellet and decreases the rate of rise of its temperature (if the produced gas is not allowed to evolve into the bath). The thickness of the slag shell will be greater in this case.

# CHAPTER VII

## MELTING D-R PELLETS

The mathematical model described in Chapter V is utilized to determine the temperature distribution, the change of chemical composition, the volume of gases evolved, the movements of the solid-liquid interface and the melting time of DRI pellets heated in a hot bath of slag. The calculations are carried out on pellets of different sources and specifications. The effects of various parameters and conditions on the rate of melting of pellets are determined. The impact of a combination of these parameters on the efficiency of the steelmaking operation is given. The optimum conditions for maximum melting rate of D-R pellets are also summarized.

Since the densities of commercial pellets and steelmaking liquid slags do not differ appreciably, it may be assumed that the pellets, after being charged into the furnace, sink in the slag long enough to be melted. The effect of the immediate submersion of the pellets, when charged, on the rate of transfer of heat and melting of the pellets is small and therefore neglected (see Section VII.C). Since the probable effect of evolution of gas on removal of melted or solid portions of D-R pellets when heated in a hot bath of slag (according to a physical model similar to the one shown in Figure 6-8) is not certain, it is also neglected. Observations made of DRI pellets heated in a levitation furnace indicate that the pellets neither break nor explode (as may appear to happen because of gas evolution) until they melt completely. If this is the case, the predictions of the model can conveniently be used to optimize arc furnace steelmaking operation as

is discussed in the last portion of the chapter.

A. Stagnant Slag

A similar procedure to that used in Chapter VI was employed to calculate the rate of heating and melting of a typical Midrex pellet (column E, Table 5-2) and a typical HYL pellet (Column D, Table 5-2) in a synthetic steelmaking slag (column C, Table 5-1) that is initially at rest. The results are illustrated in Figure 7-1. The overall Nusselt quantities of the slag was calculated from Equations (5.11) and (5.12) for short and long times after immersion, respectively. It was assumed that the effect of the motion of slag relative to the particle which may be generated as a result of the sudden drop of the pellet into the slag on the Nusselt number of the bath is negligible (cf. Section VII.C).

Because of the large quantity of heat transferred to the surface of the pellets immediately after immersion--Eq. (5.11)-- and the great difference between the temperature of the bulk and the solidus temperature of the slag, the liquid does not freeze on either of the pellets and the calculated thickness of the shell of slag remains equal to zero throughout the heating period. Since the major influence of the evolution of gas from the pellets is on the thickness of the shell of solid slag, and the Nusselt number of the bath does not appreciably change by gas evolution, as was concluded from the experimental results discussed in the previous chapter, the evolution of gas does not appear to affect the heating conditions of the system in this case. The essential influences are, however, on properties of materials, such as chemical composition and heat capacity of the pellets or thermal con-

ductivity and effective density of the pellets and the slag. The differences in properties of DRI materials result in faster heating and shorter life-time of pellet E when both pellets E and D are heated under the same circumstances, as illustrated in Figure 7-1.

B. Mixed Slag

The practical steelmaking slags are mixed by rising gases which evolve from DRI materials, enter the furnace as blast or form by the refining reactions. The active mixing of the slag can increase the Nusselt number of the bath as is described in reference 58. Effects of conditions and properties of the liquid slag and D-R materials on the rate of melting of the pellets are described in the following sections.

1. Condition of Slag

Effects of the degree of mixing and the melting temperature of slag on the melting time of the D-R pellets are discussed in the following articles.

a. Degree of Mixing

The degree of agitation of the slag can be inserted into the model by quantifying the dimensionless Nusselt number of the bath. The effects of agitation of the slag on the total melting time of pellet E is illustrated in Figure 7-2. The Nusselt numbers employed for calculations are also shown as a function of the time after immersion in the same Figure.

As is seen in Figure 7-2, the long-term agitation of the slag decreases the melting time of the pellet from about 90 seconds for natural convection to about 25 seconds for a violently stirred slag.

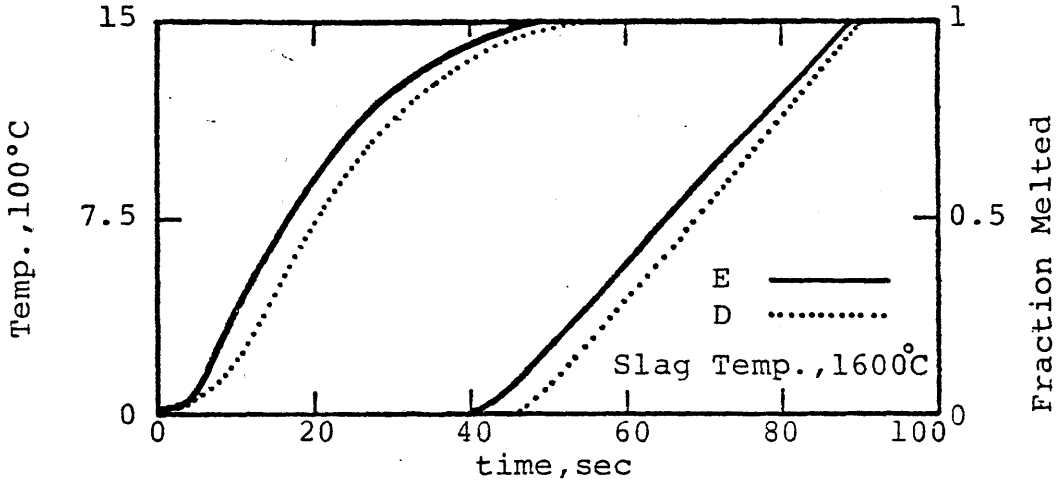


Fig. 7-1 Temp. at Center and Melted Fraction of Pellets E and D Heated in Slag C. Slag Temp., 1600°C.

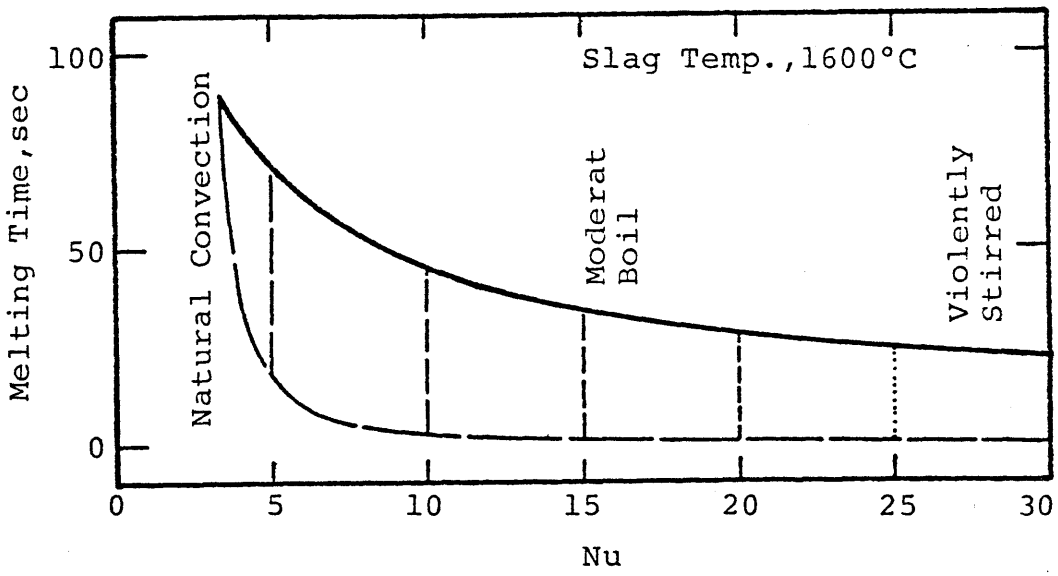


Fig. 7-2 Effect of Mixing of Slag on Melting Time of Pellet E Heated in Slag C. Broken Lines Illustrate Nusselt Number of Slag.

The melting time however does not significantly change when the slag becomes overwhelmingly violent (Nu 25). The insensitivity of the melting time to the mixing of the bath at high levels of violence is due to the excessive rise of temperature at the surface of the pellet which decreases the difference between the temperature of the bulk and that of the surface of the pellet. Under such conditions, the thermal conductivity of the pellet controls the rate of heating of the pellet and its total melting time.

b. M.T. of Slag

The melting temperature of the slags changes with their chemical composition dramatically. For the synthetic steelmaking slag C (basicity 1) identified in Table 5-1, the solidus temperature is low enough that no solid shell may form on immersed DRI pellets of ordinary specifications when the bulk temperature is maintained at 1600°C, as was described earlier. For slags of different compositions and higher basicities, however, the solidus temperature may be greater resulting in the growth of the shell of solid slag on periphery of the pellet and a decrease in the rate of flow of heat to the surface of the pellet. (Notice that the solid-liquid mushy interface is assumed to be sheared off).

The effects of the change of the melting temperature of the slag on the thickness of the frozen shell and the melting time of pellet E are demonstrated in Figure 7-3. As is seen from the figure, a rise of 200 °C in the solidus temperature of the slag increases the life-time of the pellet only for 7 seconds. The difference will be even less when the effects of gas evolution on the thickness of the shell of slag are included (Figure 7-3).

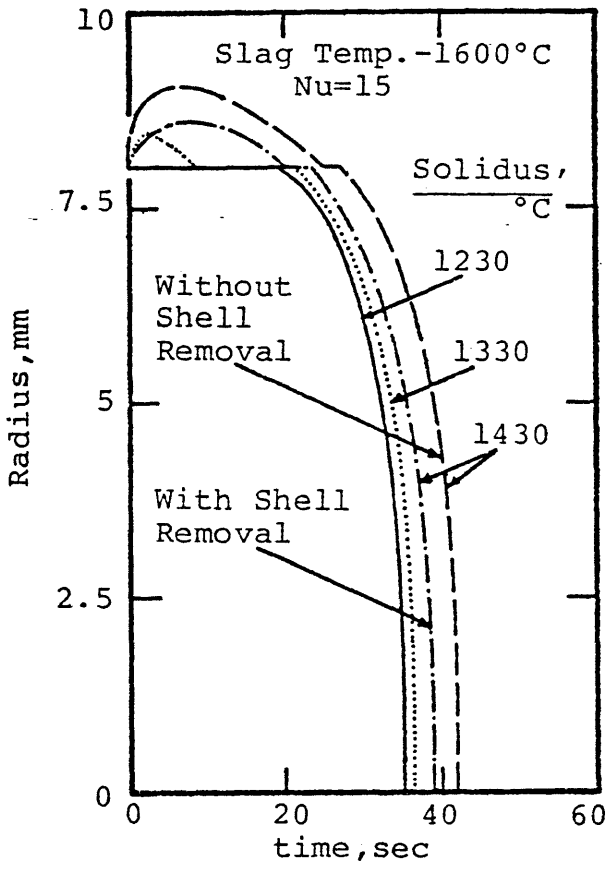


Fig. 7-3 Effect of Melting Temp. of Slag on Solidification and Melting of Slag and Pellet.

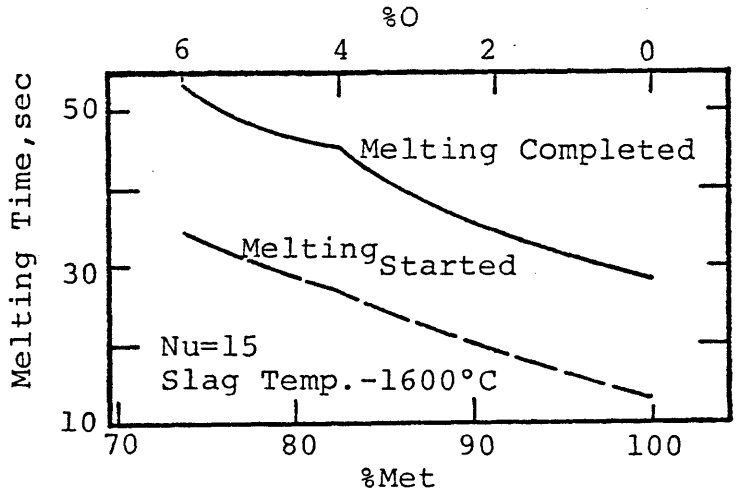


Fig. 7-4 Effect of Degree of Metallization on Melting Time of Pellet E when Heated in Slag C.

2. Properties of Pellet

A moderately mixed slag (Nu=15) is employed to investigate the influence of the properties of DRI on the melting time of the pellets fed into the slag.

a. Degree of Metallization

The effect of the degree of Metallization on the melting time of the DRI pellets is illustrated in Figure 7-4. A balanced content of carbon is assumed for the total reduction of the pellets. As is seen, the melting time of the D-R pellets decreases up to about 10 percent for each 5 percent increase in the metallization degree. The enthalpies of the reduction reactions and the change of properties of materials are responsible for this decrease.

b. Carbon Content

The effect of the carbon content of DRI on the melting time of the pellets is demonstrated in Figure 7-5. An excessive content of carbon to that necessary for the total reduction of the pellets is considered. The oxygen conrent is however maintained the same (1.99%). As is shown, the life-time of a pellet with a greater content of carbon is longer. Since the total reduction of DRI can occur with all carbon contents that are assumed, the enthalpies absorbed by the reactions do not contribute in change of the melting time of the pellet. Hence, the melting time of the pellet is not as sensitive to the change of the percentage of carbon as to that of oxygen, as can be concluded from comparison of Figures 7-5 with 7-4.

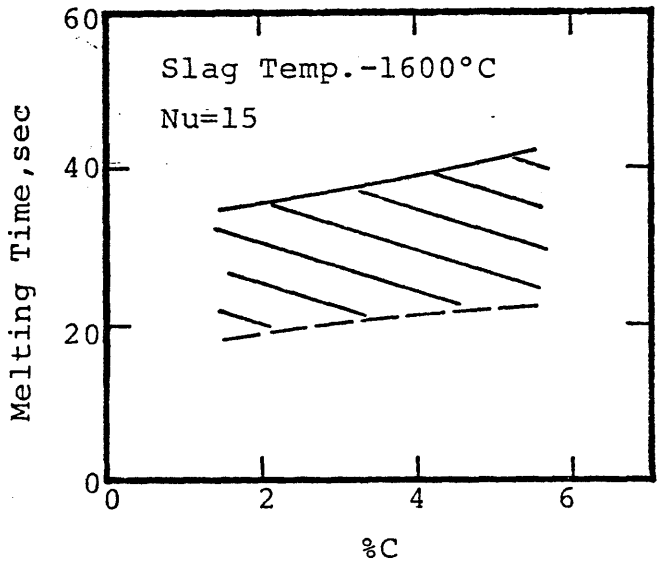


Fig. 7-5 Effect of Carbon Content on Melting Time of Pellet E when Heated in Slag C.

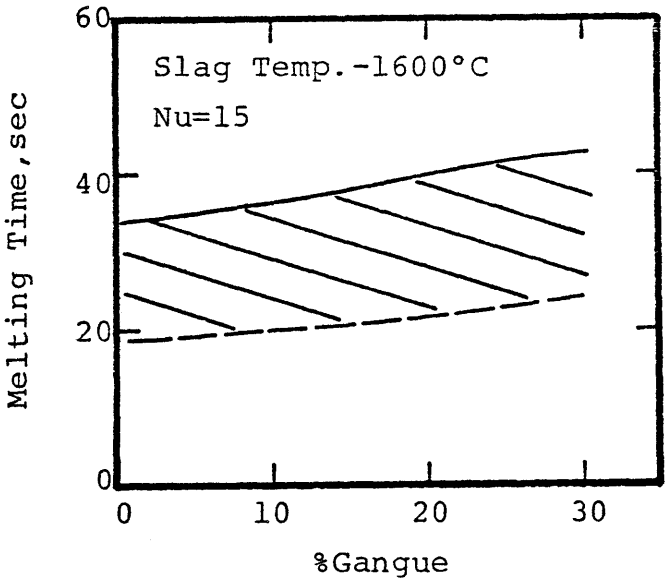


Fig. 7-6 Effect of Gangue Content on Melting Time of Pellet E when Heated in Slag C.

c. Gangue Content

The effect of the content of gangue ($Al_2O_3$, $SiO_2$) on the melting time of the pellets is illustrated in Figure 7-6. For each 1 percent increase in the content of gangue of DRI, less than 1 percent increase in the melting time of the pellet is observed.

d. Size and Density

Since the area/volume ratio of a sphere is inversely proportional to its diameter, the rate of heating and melting of the pellets decreases as their size increases, as shown in Figure 7-7. The melting-time however increases faster than the diameter because of the resistance to transport of heat within the pellets. Susceptibility to reoxidation and convenience in shipping, storage and handling are other criteria in determining the size of the pellets.

The melting time of large pellets decreases dramatically when their density exceeds that of liquid slag because of the tendency of such pellets to pass rapidly to the slag-metal interface were melting can be completed rapidly, as is discussed in detail in references 58 and 31. If sintering or partial fusion of the pellets results in an increase in their density, similar results are expected.[58] Pellets of high density are not however necessarily desirable because of the difficulties in maintaining the temperature of the metal bath well above the melting point of D-R pellets, especially when a large quantity of cold DRI descends to the slag-metal interface immediately after submersion.[31]

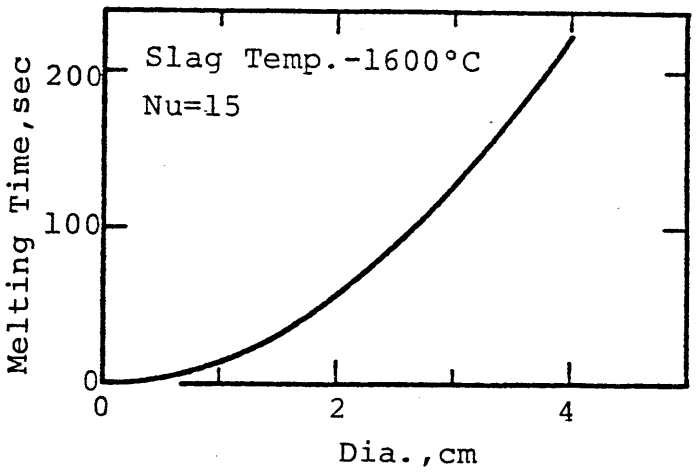


Fig. 7-7 Effect of Size on Melting Time of Pellet E Heated in Slag C.

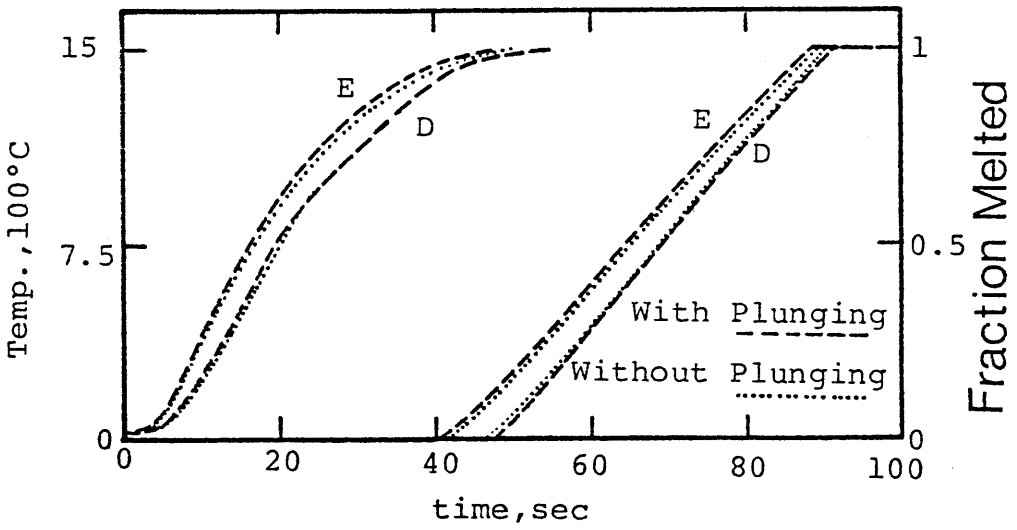


Fig. 7-8 Effect of Sudden Submersion on Center Temp. and Melted Fraction of Pellets E and D Heated in Slag C.

C. Sudden Submersion

The effect of the sudden submersion on the heating rate of the pellets is investigated by employing the same Nusselt number as was used to identify the plunging effect during the experimental studies described in Section VI.B.3. The plunging effect was assumed to last for 2 seconds during which the contribution of the transient forced convention on the Nusselt number drops from 70 to 0. As is seen from Figure 7-8, although the temperature at the center of the pellets slightly increases, when a greater initial Nusselt number is utilized, the melting time of the pellets does not necessarily decrease. A small increase in the melting time of pellet D, for instance, is observed in Figure 7-8 when the effect of the sudden submersion is included.

The relatively large initial Nusselt number causes a rapid rise of the temperature at the surface of the immersed pellet which lowers the difference between the temperature of the bulk and that of the surface of the pellet. Since the thermal conductivity of pellet D is less than that of pellet E, this difference is greater for pellet D. The small temperature difference may result in a small rate of transfer of heat to the particle when effects of sudden immersion is eliminated, and may increase the life-time of the immersed pellet, as happens for pellet D.

D. Melting Efficiency

The rate of production of steel from DRI in a steelmaking furnace is controlled by the rate of feeding and the iron content of D-R materials. The rate of feeding cannot exceed the rate of melting of the charge and is controlled by the melting time of the DRI pellets. Assuming an ideal

case with uniform distribution of the pellets in the slag (so that the interaction between the pellets can be neglected and the pellets do not make cold islands in the bath) the maximum rate of feeding of the D-R pellets, $\dot{F}$, will be proportional to the rate of melting of the pellets provided that the arcs can produce enough heat that the bulk slag does not cool off.

$$\dot{F} = C/t_m \tag{7.1}$$

In the above equation, C is a proportionality constant and is determined from the specifications of the furnace and $t_m$ is the life-time of the pellets fed into the slag.

The iron content of DRI is related to the degree of metallization, percent carbon and the content of gangue of the pellets. Assuming 6 percent gangue and a sufficient content of carbon to reduce all of oxygen and add 1 percent carbon to the iron that can be produced from reduction of DRI, the quantity of iron produced per unit weight of D-R materials can be calculated as follows:

$$M = 0.93 - \frac{100-\%Met}{269.8 - 1.07\%Met} \tag{7.2}$$

Combining Equations (7.1) and (7.2) results in the rate of production of iron from DRI.

$$\dot{p} = C(0.93 - \frac{100-\%Met}{269.8 - 1.07\%Met})/t_m \tag{7.3}$$

The effect of the degree of metallization on the rate of production of iron from typical Midrex pellets is demonstrated in Figure 7-9. The melting times of the pellets are determined from the model calculations

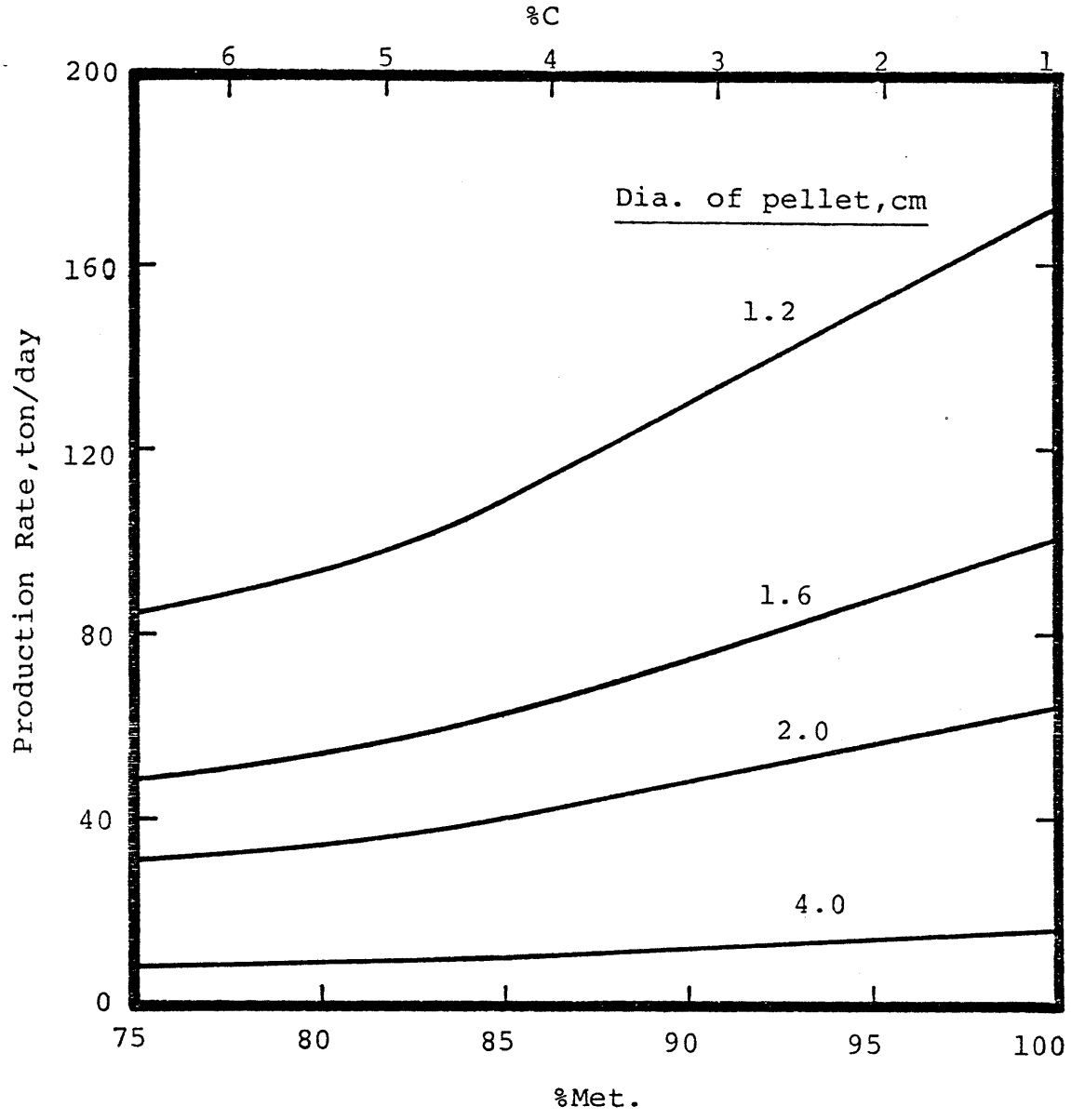


Fig. 7-9 Effects of Degree of Metallization and Size of D-R Pellets on Rate of Production of Iron.

(Figure 7-4). The quantity C is arbitrarily chosen for a medium size electric furnace.

Effects of the other specifications of the D-R pellets on the rate of production of iron can also be included. As is seen from Figures 7-5 and 7-6, the melting time of the pellets does not change appreciably with carbon and gangue contents of DRI. The effect of the pellet size on the rate of production of iron from DRI is calculated from the information given in Figure 7-7 based on the assumption that C is the same for all sizes employed, as illustrated in Figure 7-9.

E. Optimal Conditions

From discussions in this chapter, the following conclusions may be derived:

1. The life-times of the immersed D-R pellets are substantially less for mildly stirred slags than for slags at rest. Violently stirred slags are not necessarily desirable because of the relatively small change they create in the melting time of the pellets and the difficulties they may produce in proper operation of the bath (e.g. slag over-flow as a result of evolution of large volumes of gas).

2. Small changes of the chemical composition of the steel making slags do not influence the melting time of DRI pellets substantially.

3. Highly metallized pellets melt appreciably faster than less metallized pellets.

4. The influence of the carbon and gangue contents of DRI on the life-time of pellets is relatively small.

5. The pellets of smaller size melt much faster.

# CHAPTER VIII

## SUMMARY

Evolution of gas from DRI materials as a result of their final reduction was studied by heating crushed DRI samples in a sealed capsule isothermally or in a steel bomb with varying temperature. Changes of the chemical composition and the thermophysical properties of DRI materials when their temperature rises were determined from the gas evolution results and the differential thermal analysis of DRI and were utilized in modification of the computer model originally described in reference 58. The modified model can determine the rate of transfer of heat into the inert spheres as well as the DRI pellets of all types and specifications.

Experimental studies on transfer of heat into the immersed metallic particles were made by heating cold nickel spheres, sintered iron spheres and prereduced iron pellets in hot liquid slags of different compositions and temperatures. The growth of the shell of solid slag on inert particles and the rate of evolution of gas from DRI pellets were experimentally determined by withdrawing the heated particles from slag, cracking the solid skull and measuring the thickness of the shell by calipers. Effects of evolution of gas on thickness of the frozen shell of slag were investigated by blowing nitrogen from gas ports bored in the nickel spheres into the slag and measuring the thickness of the slag shell.

The computer model was tested against empirical information on the thickness of the slag shell, the rate of heating of immersed particles

and the evolution of gas from DRI pellets. Physical transfer models were suggested to describe the results obtained from comparisons of the experimental and mathematical results. The dominant transfer mechanisms were determined from the best fits of the experimental and computational data.

The information available on the thermodynamics of reduction reactions was successfully utilized to explain the results of the evolution experiments. Effects of the test conditions and the sample specifications on these results were verified.

The simulation model was exploited to determine the rate of heating and melting of D-R pellets of different sources when immersed in hot slags of various conditions. Effects of the conditions of the bath of slag and the specification of pellets were determined. The optimum melting conditions were summarized.

# CHAPTER IX

## CONCLUSION

The experimental results on evolution of gas from D-R materials of various sources indicate that the volume of the gases evolved is proportional to the degree of metallization of DRI provided that there is sufficient amount of carbon in D-R materials to react with oxygen. The volume of the gases evolved is however independent of the rate of heating and the size of DRI grains utilized for evolution studies. The final reduction of D-R materials becomes complete before they reach their melting point. The principal component of the gas is CO with less than 10 percent $CO_2$.

The results of the studies on transfer of heat into inert spheres and DRI pellets immersed in a liquid slag which is initially at rest indicate that the short-term conduction is the dominant mechanism for transfer of heat to the immersed particles. The local evolution of gas from the particles decreases the thickness of the shell of slag that freezes on the particles. Although the local evolution of gas increases the rate of heating of the inert spheres, because of the changes of the thermal properties of the partially reduced pellets during final reduction, the rate of heating of the fully reduced pellets with no gas evolution is greater than that of the low metallized ones with gas evolution.

The predictions of the simulation model indicate that the melting rate of DRI pellets is substantially greater for mildly stirred slags (Nu=15) than for slags at rest. Vigorously boiled slags (Nu=30) are not necessarily desirable because of the relatively small increase they

create in the melting rate of the pellets and the difficulties they may produce in proper operation of the bath. The influence of the carbon (in excess to that necessary for total reduction of oxygen) and gangue contents of D-R materials on the melting rate of the pellets is relatively small. The rate of production of steel in an arc electric furnace can increase when highly metallized DRI materials are utilized. Pellets of smaller size and higher density can melt faster if the temperature of the bath can be maintained uniform and well above the melting point of the pellets.

# CHAPTER X

## FURTHER RESEARCH

More studies on thermal properties of slags and DRI materials should be made to provide the information necessary for further study of the DRI melting systems. The assumptions made to calculate the thermo-physical properties of materials may be verified and proper corrections be proposed.

Since the difference between the temperature of the bulk and the melting temperature of the slags employed for experimental studies on transfer of heat into the immersed particles was relatively small, the measured growth of the shell of solid slag that freezes on the particles appears to be much greater than that which solidifies in practical steelmaking slags. Further studies can be made on transfer of heat into DRI particles heated in steelmaking slags of sufficiently high temperatures that may lead to a typical set of results corresponding with the practical DRI melting system.

Effects of the shape on the rate of melting of DRI particles can be determined experimentally and included in the model. Effects of the interaction of pellets and the local evolution of gas when swarms of DRI particles are charged into a steelmaking slag on the rate of melting of DRI can be investigated experimentally and theoretically. The computer model developed can be generalized for melting of multi-particles in slags.

Effects of local gas evolution on the overall condition of the bulk slag can be investigated and substituted in the model. A simulation model can also be developed to combine the specifications of

the melting bath, the rate of consumption of the electrical power, the rate of feeding of particles, the physical and chemical properties of DRI particles, and the rate of production of steel in an electric arc furnace.

# Appendix A

## Sample Calculation for the $H_2$ Extraction

The weight changes obtained from the hydrogen extraction of a granular 2 mm size D-R sample of the type D pellets are given in Table A-1. The reduction reactions associated with these weight changes are basically of $C/H_2$ combustion type:

$$O + C = CO \tag{A.1}$$

$$2O + C = CO_2 \tag{A.2}$$

$$O + H_2 = H_2O \tag{A.3}$$

Table A-1. $H_2$ Extraction Data for Type D Pellets. Grain Size, 2 mm.

| Weights (Gram) | Initital | Final | Gain |
|---|---|---|---|
| Sample | 4.1971 | 3.9752 | -0.2219 |
| $H_2O$ absorbent | 64.9596 | 64.9804 | 0.0208 |
| correction | - | - | -0.0138 |
| total | - | - | 0.0070 |
| $CO_2$ absorbent | 64.3738 | 64.3856 | 0.0118 |
| correction | - | - | 0.0133 |
| total | - | - | 0.0251 |
| CO* | - | - | 0.1906 |

*Calculated from Equation (A.4).

The reacting contents of oxygen and carbon can be calculated from the given data as follows:

$$W_{CO} = \Delta W_S - W_{CO_2} - w_O \tag{A.4}$$

$$W_O = W_{H_2O}\left(\frac{M_O}{M_{H_2O}}\right) + W_{CO_2}\left(\frac{2M_O}{M_{CO_2}}\right) + W_{CO}\left(\frac{M_O}{M_{CO}}\right) \tag{A.5}$$

$$W_C = W_{CO_2}\left(\frac{M_C}{M_{CO_2}}\right) + W_{CO}\left(\frac{M_C}{M_{CO}}\right) \tag{A.6}$$

$$\%O = 100\left(\frac{W_O}{W_S}\right) \tag{A.7}$$

$$\%C = 100\left(\frac{W_C}{W_S}\right) \tag{A.8}$$

$W_i$ is the weight gain of the specie i, $\Delta W_S$ is the weight loss of the sample, $w_O$ is the weight of oxygen in the water vapor evolved, $M_i$ is the molar weight of the specie i, and %i is the reacting content of i in the sample.

$$W_{CO} = 0.2219 - 0.0251 - 0.0070\left(\frac{16}{18}\right) = 0.1906$$

$$W_O = 0.0070\left(\frac{16}{18}\right) + 0.0251\left(\frac{32}{44}\right) + 0.1906\left(\frac{16}{28}\right) = 0.1334$$

$$W_C = 0.0251\left(\frac{12}{44}\right) + 0.1906\left(\frac{12}{28}\right) = 0.0885$$

Hence:

$$\% O = 3.18$$

$$\% C = 2.10$$

## Appendix B

## Volumetric Measurement of Evolved Gas

Volumetric flow rate of the gases evolved from DRI was measured by an integrating flowmeter similar to the one described by Naci Seving.[93] After the evolved gas passed through a mercury manometer, a dibutyl phthalate bubbler and a glass bulb held in a water tank, it entered the flowmeter. The temperature of the gas was kept constant at 25°C by controlling the temperature of the water in the tank. The pressure drop in the gas stream, measured by the mercury manometer, was less than 5 mm of mercury. A negative pressure of about 5 mm mercury was applied to the system by suction of the outlet of the flowmeter to facilitate the evolution of gas when a D-R pellet was heated in liquid slag.

The flowmeter translated the rate of flow of gas into a characteristic frequency (Figure B-1). The spread of data at flow rates greater than 200 $cm^3$/min is because of the abrupt pressure drop in the stream when the instrument was discharged of the trapped gas (see Ref. 93). At flow rates greater than 450 $cm^3$/min, the flowmeter became unstable and did not operate properly.

For simplicity, the rate of evolution of gas was expressed in terms of the characteristic frequency of the instrument as follows:

$$\dot{V} = 19f + 1/9\ f^{2.7} \qquad f \leq 8 \qquad \text{(B.1)}$$

$$\dot{V} = 33f - 81 \qquad f \geq 8 \qquad \text{(B.2)}$$

where $\dot{V}$ is the gas rate in $cm^3$/min and f is the frequency in Cycles/min.

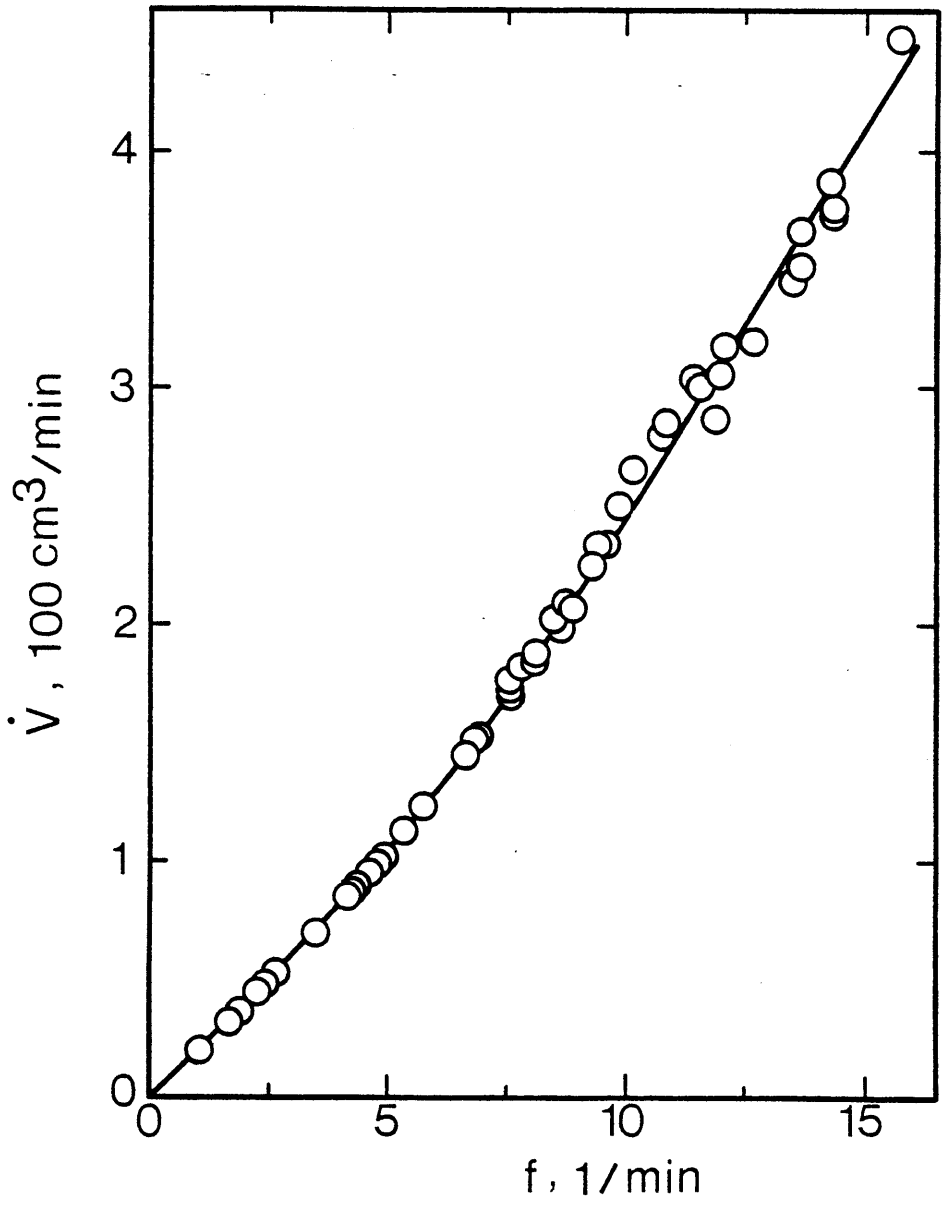


Fig. B-1 A Calibration Curve for Flowmeter.

## Appendix C

## Data Analysis for Bomb Extraction

The gas flow rates obtained from bomb evolution experiments were corrected for the actual rate of change of temperature of DRI. For a small temperature change T, the rate of evolution of gas may be expressed as a linear function of the heating rate (Figure C-1):

$$\dot{V} = a\dot{T} + b \qquad (C.1)$$

where $\dot{V}$ and $\dot{T}$ are the rates of evolution of gas and rise of temperature, a is the proportionality constant and b is the rate of flow of gas at zero temperature rate. Assuming b small, Equation (C.1) reduces to the following equation:

$$\dot{V} = (\dot{V}_a/\dot{T}_a)\ \dot{T} \qquad (C.2)$$

in which $\dot{V}_a$ is the measured flow rate and $\dot{T}_a$ is the corresponding temperature rate.

A schematic plot is made of temperature fluctuations of a DRI sample in Figure C-2. The response of the flowmeter to the passage of the gases evolved is sketched in the same figure. The actual gas rate at time $t = (t_i+t_{i+1})/2$ is evaluated by substituting f into Equations (B.1) and (B.2):

$$f = 1/(t_{i+1}-t_i) \qquad (C.3)$$

$$\dot{V}_a = 19(t_{i+1}-t_i)^{-1} + (t_{i+1}-t_i)^{-2.7}/9 \quad t_{i+1}-t_i \geq .25 \text{ min} \qquad (C.4)$$

$$\dot{V}_a = 33(t_{i+1}-t_i)^{-1} - 81 \quad t_{i+1}-t_i < .25 \text{ min} \qquad (C.5)$$

The temperature of the sample and its actual rate at time t can be

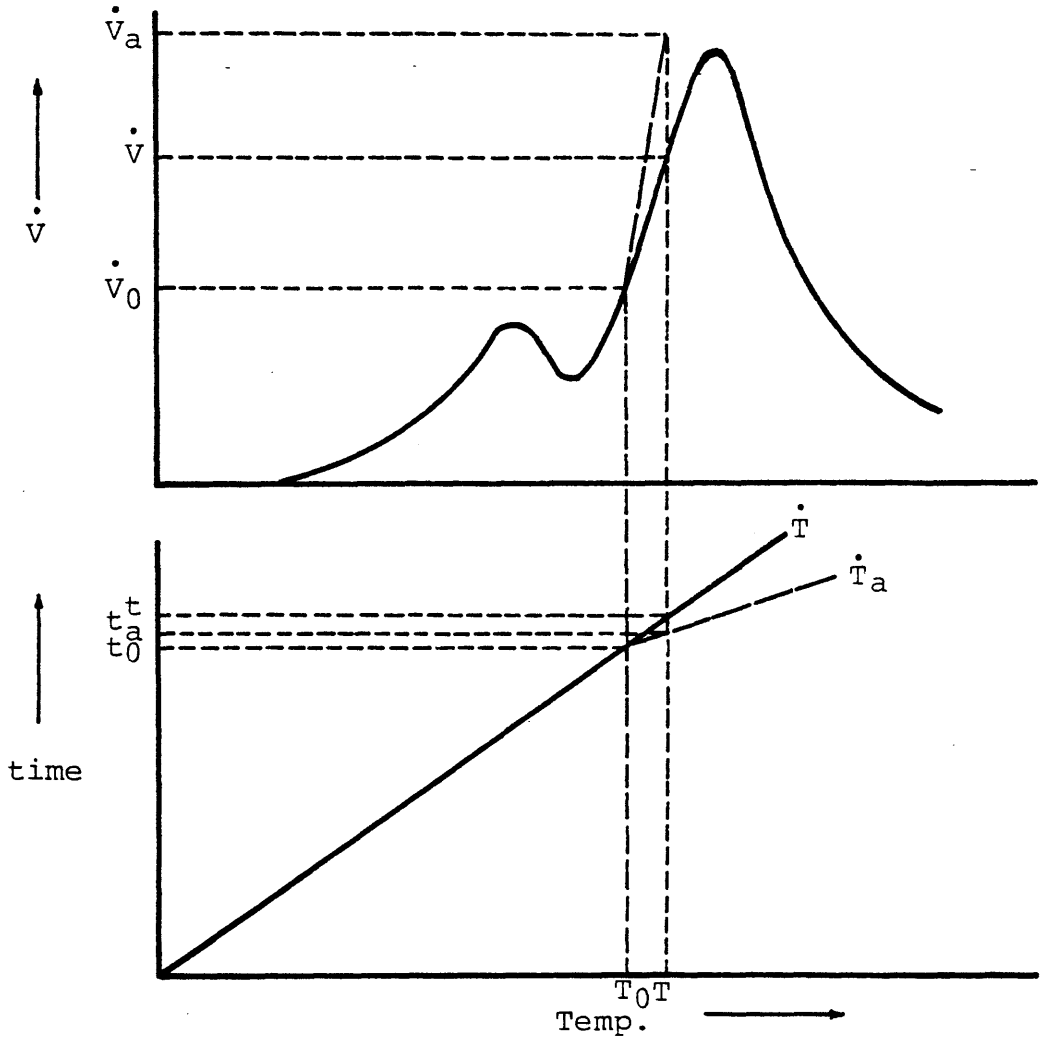


Fig. C-1 Temp. Profile for a Schematic Gas Evolution Pattern.

evaluated from the following equations:

$$\bar{T} \simeq \frac{T_i + T_{i+1}}{2} \qquad (C.6)$$

$$\dot{T}_a = \frac{T_{i+1} - T_i}{t_{i+1} - t_i} \qquad (C.7)$$

Substituting into Equation (C.2) results in the corrected rate of evolution of gas for temperature rate $\dot{T}$:

$$\dot{V} = \left[\frac{19(t_{i+1}-t_i)^{-1} + (t_{i+1}-t_i)^{-2.7}/9}{(T_{i+1}-T_i)/(T_{i+1}-T_i)}\right] \dot{T}$$

$$T_{i+1} - t_i \geq .25 \text{ min} \qquad (C.8)$$

$$\dot{V} = \left[\frac{33(t_{i+1}-t_i)^{-1} - 81}{(T_{i+1}-T_i)/(t_{i+1}-t_i)}\right] \dot{T} \quad t_{i+1} - t_i < .25 \text{ min} \qquad (C.9)$$

These expressions were used to calculate the corrected rate of flow of the gases evolved from DRI. This rate was corresponding to the time between two sequential cycles at $t_i$ and $t_{i+1}$. It was plotted against the mean sample temperature $\bar{T}$.

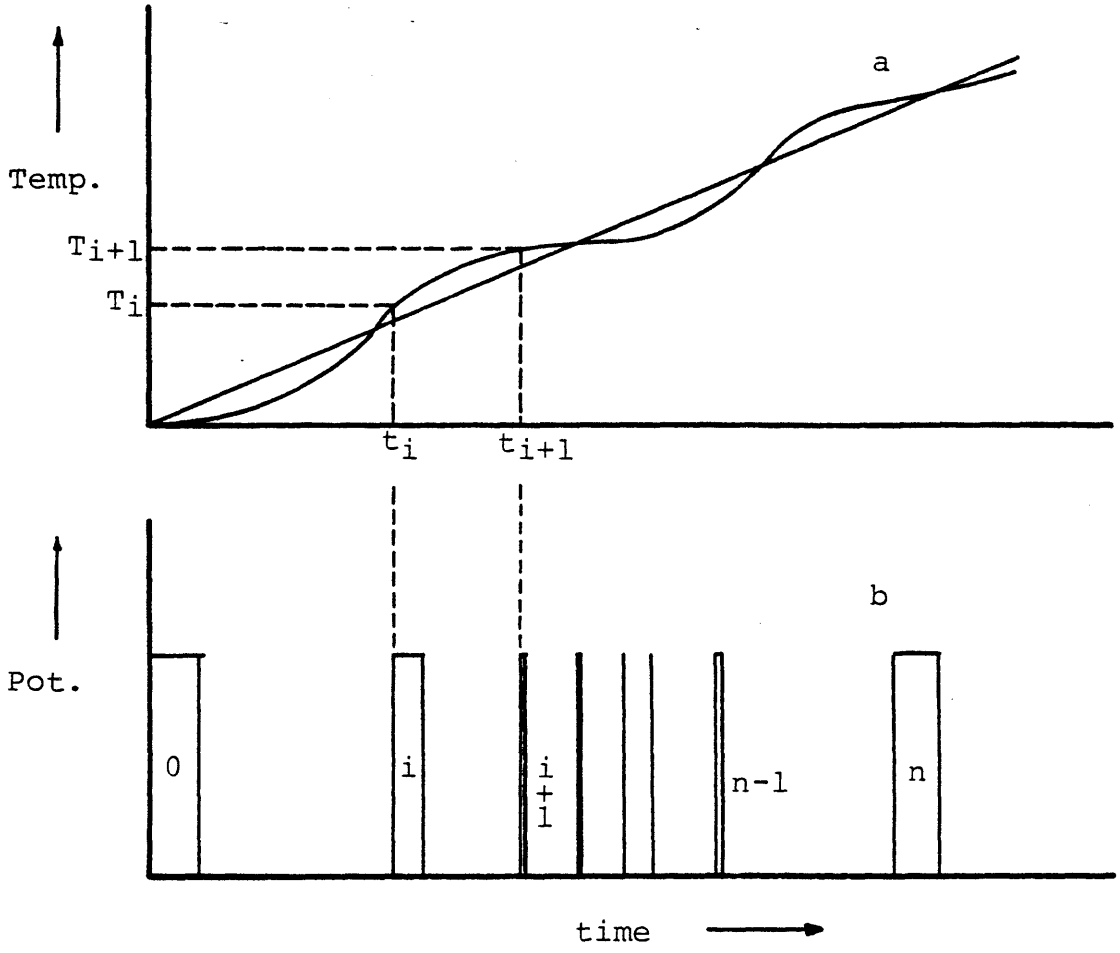


Fig. C-2 Temp. Fluctuations of Bomb Sample (curve a) and Response of Flowmeter to Flow of Gases Evolved (curve b).

## Appendix D

## Properties of Slag

The thermal expansivity of the liquid slags, defined by Equation (D.1), has been assumed equal to the thermal expansivity of similar ferrous-silicate slags given in reference 84.

$$\beta = \frac{1}{V} \left(\frac{\partial V}{\partial T}\right)_p \tag{D.1}$$

In the above equation V is volume of slag and p is pressure of the system.

The thermal diffusivity, $\alpha$, and the kinematic viscosity, $\nu$, are defined by the following equations:

$$\alpha \equiv k/\rho\ C_p \tag{D.2}$$

$$\nu \equiv \mu/\rho \tag{D.3}$$

where k is thermal conductivity, $\rho$ is density, $C_p$ is specific heat and $\mu$ is viscosity of the slag. The dimensionless Prandtl number is defined as follows:

$$Pr = \nu/\alpha \tag{D.4}$$

The dimensionless Grashof number, Gr, for a liquid slag at temperature $T_\infty$ can be determined from the following relationship:

$$Gr = \frac{g\ \beta(T_\infty - T_s)(R+\theta)^3}{\nu^2} \tag{D.5}$$

where g is gravitational acceleration, $T_s$ is temperature of solid-liquid interface, R is radius of immersed particle and $\theta$ is thickness of solid shell of slag. The combination of Prandtl and Grashof groups is called

the Rayleigh number:

$$Ra = Pr \cdot Gr \tag{D.6}$$

The heats of fusion of the slags are assumed equal to the weighted mean of the heats of fusion of the components.

The evolution of gas from DRI pellets into the slag results in a change in the density and porosity of the solid and liquid slag phases. The thermal conductivity of the porous substance, k, is equal to the geometric mean of the thermal conductivities of the pores, $k_p$, and of the substratum, $k_s$:[79]

$$k = k_p^{1-\psi} \cdot k_s^{\psi} \tag{D.7}$$

where $\psi$ is the porosity (volume fraction) of the substance. Ben-Amoz[79] derived the above formula by solving the heat conduction equation with space fluctuating properties and showed that the effective thermal conductivity and diffusivity of a multiphase material can similarly be predicted from a geometric mean formula. The predicted conductivities have been consistent with the results of Kon and Fortini,[83] and Woodside and Messmer[90] for oxides and metals of less than 50 percent porosity.

The thermal conductivity of the pores is equal to the sum of the radiation, $k_r$, and conduction, $k_c$, components:

$$k_p = k_r + k_c \tag{D.8}$$

For homogeneously distributed pores, the approximation suggested by Marino[80] and Loeb[81] may be used to calculate the radiative component of the thermal conductivity:

$$k_r = 3\,\sigma\,d\,T^3 \qquad (D.9)$$

in which $\sigma$ is the Stephan-Boltzman constant and d is the diameter of the spherical pores. The conduction contribution may be evaluated from the information available on the thermal conductivity of air between 500 and 1500°K:[82]

$$k_c = 3.04 \times 10^{-4}[1-\exp(-7.65 \times 10^{-4}T)] \ (\text{Cal/cm.sec.°K}) \qquad (D.10)$$

The overall thermal conductivity of the pores can therefore be calculated from the following expression:

$$k_p = 4.08 \times 10^{-12}\ d\ .\ T^3 + 3.04 \times 10^{-4}\ [1-\exp(-7.65 \times 10^{-4}T)]$$

$$(\text{Cal/cm.sec.°K}) \qquad (D.11)$$

Equations (D.7) and (D.11) were inserted in the model for calculation of the thermal conductivity of the slags. A summary of the thermo-physical properties of the slags employed in heat transfer studies is given in Table 5-1.

## APPENDIX E

### Thermal Properties of Specimen

The effective thermal conductivity of DRI pellets may be calculated from the geometric mean of the thermal conductivities of the constituents and the pores, as described in Appendix D:[79]

$$k = k_p^{\psi_p} \cdot k_{Fe}^{\psi_{Fe}} \cdot k_{"FeO"}^{\psi_{"FeO"}} \cdot k_{Fe_3C}^{\psi_{Fe_3C}} \cdot k_{Al_2O_3}^{\psi_{Al_2O_3}} \cdot k_{SiO_2}^{\psi_{SiO_2}} \tag{E.1}$$

where $k_M$ is the thermal conductivity of constituent M. The volume fraction of M denoted by $\psi_M$ is assumed to be proportional to the weight fraction of M designated by $W_M$:

$$\psi_M = W_M (1 - \psi_p) \tag{E.2}$$

For simplicity, the change of $\psi_p$ when DRI pellets are heated is assumed negligible.

The heat of fusion of DRI materials, $\Delta H$, may be estimated from the heats of fusion of the constituents. Since at the melting point the oxygen and carbon contents of the samples are negligible, $\Delta H$ can be calculated from the following equation:

$$\Delta H = W_{Fe} \Delta H_{Fe} + W_{Al_2O_3} \Delta H_{Al_2O_3} + W_{SiO_2} \Delta H_{SiO_2} \tag{E.3}$$

in which $\Delta H_M$ is the heat of fusion of the component M of DRI. The specific heat of DRI is calculated in Appendix F.

Typical quantities of the constants used for calculation of the rate of transfer of heat to the thermocouple bead embedded inside the specimens

are given in Table E-1. These coefficients are derived from the following equations which include the terms for transfer of heat by radiation and conduction from the surface of the insertion well to the thermocouple bead and the change of the temperature of the bead with time:[58]

$$\dot{Q} = \chi A_1 F \sigma (T_{W,j}^4 - T_{b,j}^4) + y A_2 k (T_{W,j} - T_{b,j})/\Delta r \qquad (E.4)$$

$$T_{b,j+1} = T_{b,j} + \dot{Q} \Delta t/m C_p \qquad (E.5)$$

where $\chi A_1$ is the area of the thermocouple well that radiates heat to the thermocouple bead or to the platinum foil used to protect the bead, $T_{W,j}$ is the temperature of the surface of the well, $T_{b,j}$ and $T_{b,j+1}$ are the present and future temperatures of the bead, $y A_2$ is the area of the bead or the platinum foil that contacts the particle, m is the mass of the thermocouple bead and the platinum foil if present, $C_p$ is the heat capacity of platinum and F is calculated from the following equation:

$$F = 1/(1/\varepsilon_w + 1/\varepsilon_b - 1) \qquad (E.6)$$

where $\varepsilon_w$ and $\varepsilon_b$ are the emissivities of the surfaces of the well and the platinum foil when used to protect the bead, respectively. For a small thermocouple bead enclosed in the well, the emissivity of the well is unity and F is equal to the emissivity of the bead. Equations (E.4) and (E.5) may be rewritten in the following form:

$$\dot{Q} = A(T_{w.j}^4 - T_{b,j}^4) + B(T_{w,j} - T_{b,j}) \qquad (E.7)$$

$$T_{b,j+1} = T_{b,j} + \dot{Q} \Delta t/D \qquad (E.8)$$

where the coefficients A, B and D are defined as follows:

$$A \equiv \chi A_1 F \sigma \qquad (E.9)$$

$$B \equiv y A_2 k \qquad (E.10)$$

$$D \equiv m C_p \qquad (E.11)$$

Table E-1 Typical Constants Used for Temperature Calculations (See Equations E.9 to E.11).

| Coefficient | Nickel Sphere | | DRI Pellet | |
|---|---|---|---|---|
| | Small | Large | E | D |
| A, $10^{14}$ Cal/sec. $°K^4$ | 2 | 6 | 1 | 1 |
| B, $10^4$ Cal/sec. °K | 3 | 1 | 6 | 6 |
| D, Cal/°K | 0.0030 | 0.0037 | 0.0016 | 0.0011 |

# Appendix F

## Overall Specific Heat of DRI

The contribution of various items explained in Section V.B.2 to the overall specific heat of sponge materials is evaluated at different temperature ranges determined from the equilibrium phase diagram (see Figure F-1). The results are summarized in Table 5-3.

1. Specific Heat of Materials

The specific heat of iron-bearing sponge pellets can be evaluated by summing up the specific heats of the components of the sponge. The principal components are: Iron, Oxygen, Carbon, Gangue, Sulphur and Phosphorous. The dominant portion of the gangue is generally the "acid gangue" ($SiO_2 + Al_2O_3$), while the sulphur and phosphorous contents of the sponge are negligible.

To calculate the specific heat of a D-R pellet, let us assume, for simplicity, that oxygen and carbon are in form of "FeO" and $Fe_3C$ chemical compounds. The reaction between these compounds below the carbide decomposition temperature $T_a$ (see Figure F-1) may be written as follows:

$$\text{"FeO"} + Fe_3C = 3.95\ Fe + CO \qquad (F.1)$$

$$2\text{"FeO"} + Fe_3C = 4.9\ Fe + CO_2 \qquad (F.2)$$

For a gaseous product composed of 90% CO and 10% $CO_2$, the stoichiometric quantities of reactants and products are as demonstrated in Eq. (F.3):

$$1.1\ \text{"FeO"} + Fe_3C = 4.05\ Fe + 0.9\ CO + 0.1\ CO_2 \qquad (F.3)$$

$$3.53 \times 10^{-3}\,g + 8.02 \times 10^{-3}\,g = 1.01 \times 10^{-2}\,g + 1\ cm^3$$

The weights of the components participating in these reactions can be subtracted from the initial values to obtain the chemical analysis of the pellet:

$$W_{Fe} = W_{i,Fe} - (-1.01\ E\text{-}2)V \qquad (F.4)$$

$$W_{"FeO"} = W_{i,"FeO"} - (3.53\ E\text{-}3)V \qquad (F.5)$$

$$W_{Fe_3C} = W_{i,\ Fe_3C} - (8.02\ E\text{-}3)V \qquad (F.6)$$

where $W_{i,M}$ and $W_M$ are initial and present weights of component M, and V is the volume of the released gas, all per gram of DRI.

The specific heats of the species present in DRI are given in Table E-1. From the data given, the specific heats of D-R materials are computed for the specified temperature ranges, based on the assumption that the Neumann-Kopp rule is valid at elevated temperatures:

$$CM = W_{Fe} \cdot C_{Fe} + W_{"FeO"} \cdot C_{"FeO"} + W_{Fe_3C} \cdot C_{Fe_3C} + W_{Al_2O_3} \cdot C_{Al_2O_3} + W_{SiO_2} \cdot C_{SiO_2} \qquad (F.7)$$

Table F-1. Specific Heat of Materials.[94]

| Material | Relationship (Cal.°K$^{-1}$.g$^{-1}$) | Temp. Range (°K) |
|---|---|---|
| $Fe_{\alpha}$ | 7.48 E-2 + 1.06 E-4 T | 273 - 1033 |
| $Fe_{\beta}$ | 1.61 E-1 | 1033-1181 |
| $Fe_{\gamma}$ | 3.29 E-2 + 8.34 E-5T | 1181-1674 |
| $Fe_{0.95}O$ | 1.69E-1 + 2.90E-5T - 9.70E2 $T^{-2}$ | 298 - m.p. |
| $Fe_3C)_{\alpha}$ | 0.109 + 1.11E-4T | 273-463 |
| $Fe_3C)_{\beta}$ | 0.143 + 1.67E-5T | 463-1500 |
| $Al_2O_3$ | 0.25 + 4.17E-5T - 6.69E3$T^{-2}$ | 298 - 1800 |
| $SiO_2)_{\alpha}$ | 1.87E-1 + 1.36E-4T - 4.49E3$T^{-2}$ | 298-848 |
| $SiO_2)_{\beta}$ | 2.40E-1 + 3.23E-5T | 848-2000 |

2. Enthalpy of Reactions

Equation (F.3) illustrates the final reduction of the sponge material below the carbide decomposition temperature Ta (see Figure F-1), where the total carbon content of the sample is in carbide form. A comparison of the free energy of the reduction reactions (F.3) and (F.8) is made in Table F-2.

$$1.1\ \text{"FeO"} + \underline{C} = 1.05Fe + 0.9CO + 0.1CO_2 \qquad (F.8)$$

The results indicate that above $T_a$, the reduction of the sample according to the reaction (F.3) occurs more favorably.

The reduction reactions specified in Eqs. (F.3) and (F.8) are endothermic. The associated enthalpies may be converted into specific

heat terms for the sponge material, as shown in Table F-2. Multiplying the heats of reduction of the sponge by a "Specific Gas Volume", G, (the total volume of the released gases per unit weight of the sample per unit temperature increment) results in the specific heat terms required. The specific gas volume is determined as a function of temperature, from the bomb extraction results:

$$G(T) = \partial V/\partial T \simeq V_{T+0.5} - V_{T-0.5} \qquad (F.9)$$

Table F-2 Enthalpies and Free Energies of Reactions.[77,94]

| Temp. Range (°K) | Enthalpy (Cal. $cm^{-3}$) (F.3) | Enthalpy (Cal. $cm^{-3}$) (F.8) | Standard Free Energy (Cal. $cm^{-3}$) F.3) | Standard Free Energy (Cal. $cm^{-3}$) (F.8) | $C_R$ ($Cal.k^{-1}.g^{-1}$) |
|---|---|---|---|---|---|
| $T < T_a$ | 1.29 | - | - | - | 1.29 G(T) |
| $T_a \leq T \leq T_a+8$ | 1.35 | - | -0.02* | 0.22* | 1.35 G(T) |
| $T_a+8 < T < T_b$ | 1.47 | - | -0.60≠ | -0.24≠ | 1.47 G(T) |
| $T \geq T_b$ | - | 1.35 | - | - | 1.35 G(T) |

*Calculated at 1000°K. ≠Calculated at 1400°K.

3. Heat of Phase Transformation

The formation of Austenitic iron phase in D-R sponge pellets at eutectoid temperature, $T_a$, is exothermic:[77]

$$Fe_3C = 3Fe + \underline{C} \quad -1.23 \ (cal.\ g_{Fe_3C}^{-1}) \qquad (F.10)$$

The contribution of the associated enthalpy to the specific heat of the sponge materials is determined as a function of the sponge composition.

The iron rich portion of the iron-iron carbide equilibrium diagram

is reconstructed in Figure F-1 (cf. Figure 4-20). The variation of the carbon content of a DRI pellet is also schematically shown as a function of temperature. The loci of the transformation temperatures are given in Table 4-10. The change in the amount of the structural constituent, $Fe_3C$, at the eutectoid temperature can be calculated from Eq. (F.13):

$$W_{i,\ Fe_3C} = (CA - 0.02)/6.66 \qquad (F.11)$$

$$W_{Fe_3C} = (CA - 0.77)/5.92 \qquad (F.12)$$

$$\Delta W_{Fe_3C} = 1.88 \times 10^{-2}\ CA - 0.127 \qquad (F.13)$$

in which CA is the carbon content of the sponge at temperature T.

Assuming the completion of the phase change be achieved within eight degrees above eutectoid point allows the transformation enthalpy to be divided into this range, in order to yield the specific heat of the sponge due to the phase change.

$$C_T = 2.89 \times 10^{-3} CA - 1.95 \times 10^{-2} \qquad (F.14)$$

Above the eutectoid temperature, the austenitizing process continues until the chemical composition of the particle reaches the curve separating austenite and austenite-cementite phase region. It is assumed that the influence of the enthalpy change due to the completion of the austenitizing process on the specific heat of the sponge is negligible. The thermodynamic data available justify such an assumption.

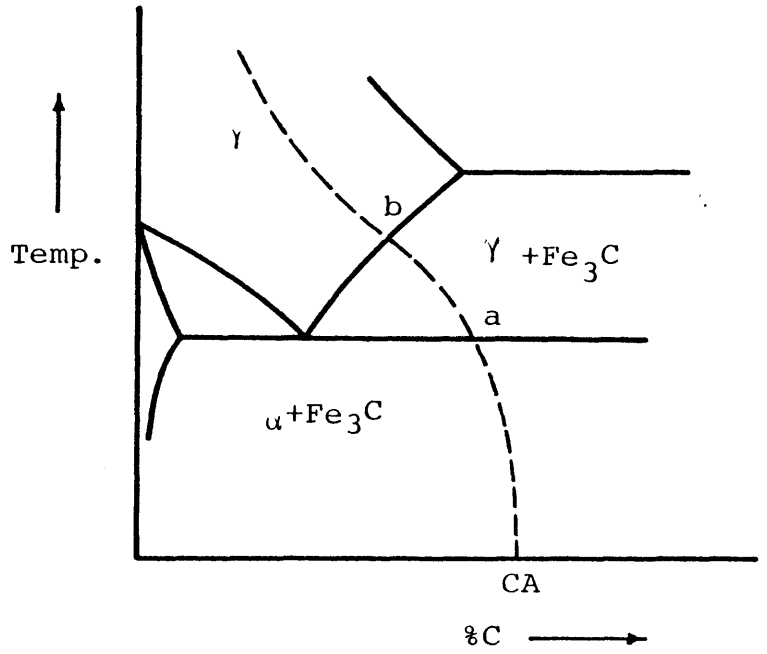


Fig. F-1 Schematic $Fe-Fe_3C$ Phase Diagram and DRI Extraction Path.

## Appendix G

## Thickness of Thermal Boundary Layer

At steady state, the Nusselt number of the slag bath can be calculated from Equation (5.12). If $T_\infty$ is the temperature of bulk liquid slag and $T_i$ is the temperature at the solid-liquid slag interface, the following equation can be written for transfer of heat into the surface of an immersed specimen:

$$-k\left(\frac{\partial T}{\partial r}\right)_{i^+} = h\ (T_\infty - T_i) \qquad (G.1)$$

Substituting for partial derivative in terms of the thickness of the thermal boundary layer, $\delta_T$, and from Equation (5.9 ) for h results in the following correlation:

$$\delta_T = 2(R + \theta)/Nu \qquad (G.2)$$

From the data given in Table 5-4 the thickness of the thermal boundary layer can be calculated for various specimens. The ratio of $\delta_T/\theta$ is generally greater than three.

## Appendix H

## Conduction Heat Transfer

The conduction equation in spherical coordinates can be written as follows:

$$\frac{\partial T}{\partial t} = \alpha\left[\frac{\partial^2 T}{\partial r^2} + \frac{2}{r}\frac{\partial T}{\partial r}\right] \qquad (H.1)$$

Substituting $\xi = r(T-T_\infty)$ in Eq. (H.1) yields:

$$\frac{\partial \xi}{\partial t} = \alpha \frac{\partial^2 \xi}{\partial r^2} \qquad (H.2)$$

where:

$$\xi = 0 \qquad t = 0 \qquad (H.3)$$

$$\xi = (R+\theta)(T_i-T_\infty) \qquad r = R + \theta \qquad (H.4)$$

Solving (H.2) for boundary conditions (H.3) and (H.4) yields:[85]

$$T - T_\infty = (T_i-T_\infty)\frac{R+\theta}{r}\operatorname{erfc}\frac{r-R-\theta}{\sqrt{\pi\alpha t}} \qquad (H.5)$$

The rate of transfer of heat to the particle is calculated from the following expression:

$$\left(\frac{q}{A}\right)_{R+\theta^+} = -k\left(\frac{\partial T}{\partial r}\right)_{R+\theta^+} = -k\,(T_i-T_\infty)\left[\frac{1}{R+\theta} + \frac{1}{\sqrt{\pi\alpha t}}\right] \qquad (H.6)$$

which leads to the coefficient of transfer of heat in the liquid slag:

$$h = k\left[\frac{1}{R+\theta} + \frac{1}{\sqrt{\pi\alpha t}}\right] \qquad (H.7)$$

Substituting for h from Equation (5.33) the Nusselt number of the slag is obtained:

$$Nu = 2 + 2(R+\theta)/\sqrt{\pi\alpha t} \qquad (H.8)$$

# Appendix I

## Porosity of Liquid Slag

Porosity of the liquid slag of around an immersed particle with local gas evolution was calculated from the information given in Table 3-5. The number of gas bubbles evolved from a gas port that cover the surface of the particle can be calculated from the following equation:

$$n = f \frac{\ell}{v} \qquad (I.1)$$

where f and v are frequency and velocity of gas bubbles and $\ell$ is the length of coverage (Figure I-1). For a thickness of $D_b$, the porosity of the forced convection layer of around the particle can then be estimated from the following correlation:

$$P = N \frac{f\ell}{6v} \left(\frac{D_b}{D}\right)^2 \qquad (I.2)$$

where N is the number of active bubbling sites, $D_b$ is the average diameter of the bubbles and D is the diameter of the particle.

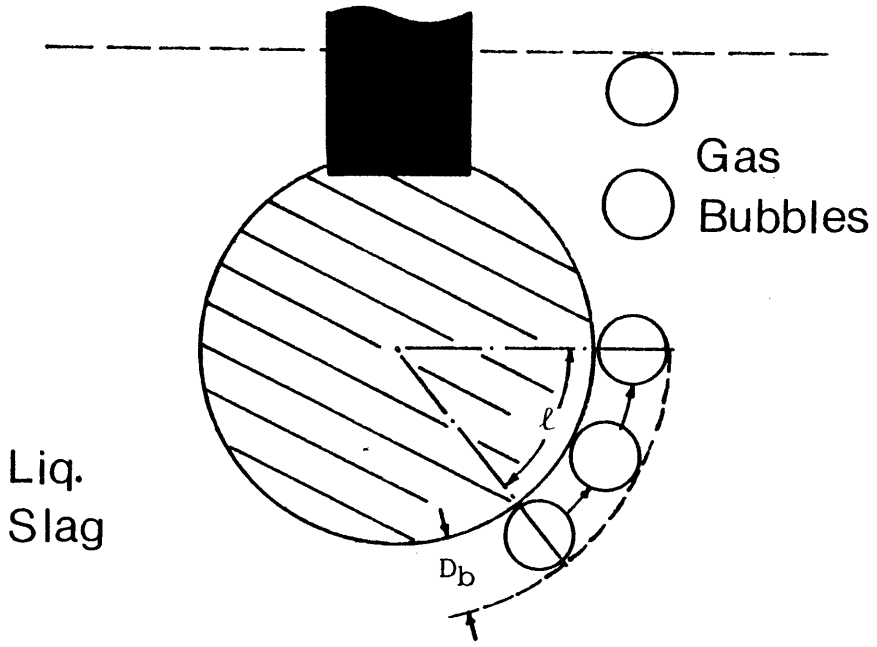


Fig. I-1 Immersed Particle with Gas Evolution.

# Appendix J

## Computer Program

A listing of the computer model transcribed in Fortran IV is provided in the following sections with brief commentary statements to clarify the procedures employed to compute the rate of heating and melting of submerged particles. Copies of the subprograms used to calculate properties of materials are also included. The definition of the terms used is given in the last section.

The model has been originally developed in reference 58 for melting an immersed inert sphere in slag. It is generalized for evolution of gas from particles, changes of properties of materials with temperature and time, and condition of liquid bath as related to the solidification and melting of slag and particle and to the heat transfer mechanisms that dominate the Nusselt quantity of the slag. Those properties which vary the most with temperature are supplied in form of table functions. The model is applicable to both inert spheres and DRI pellets heated in hot fluid media.

The approach is in general the same as that described in reference 58. Slight changes are however made to increase the accuracy of results. First, the temperatures and gas volumes of the space elements are initialized, the areas and volumes attributed to these elements are calculated and a small initial shell thickness is set. The calculations are then carried out on an iterative basis. The Nusslt number of the bath, the temperature and properties of the elements, the thickness of the frozen shell or the fraction of the particle that may melt are calculated at each iteration.

1. Main Program

```
C..............INPUT  DATA
      REAL    IDT,IDR,NU ,K2,K3,K4,K5
      COMMON VG(20), GG(20),PS,TA,CA,TB,F1 ,F2,F3 ,F4,F5,W1,W2,W3
     C,S,CKS ,CKL,     DP,DB ,K2,K3,K4,K5 ,DDD,FF2
      DIMENSION A(99),V(99),I(99),E(99),  EV(99),TT(99),GV(99)
      AF=0
200   IF(AF.EQ.0) GO TO 77
      IF(AF-CJ)66,98,77
98    AF=0
77    READ(5,100)NO, NOT, NOS,N1,IDR,IDT,BB,TO,TMS,TMSP,CA,K3 ,S,R,D,K2,
     CCPL,CPS,U,XX,DL,TM ,DD, ZT ,CJ ,DSS,RR,TR,CB , TA, TB, (VG(I),I=1,
     CN1),CKS,F, PS, (GG(I),I=1,N1),DS1, ACRM,GNU,AA,H ,DDD,K4, K5 ,TTT
      IF(NO.EQ.0.)GO TO 201
100   FORMAT(4I5/ (8F10.4))
      WRITE(6,111)NO,NOT, NOS,N1,IDR,IDT,BB,TO,TMS,TMSP,CA,K3 ,S,R,D,K2,
     CCPL,CPS,U,XX,DL,TM ,DD,ZT  ,CJ ,DSS,RR,TR,CB , TA, TB, (VG(I),I=1,
     CN1),CKS,F, PS, (GG(I),I=1,N1),DS1 ,ACRM,GNU,AA,H , DDD,K4, K5,TTT
111   FORMAT(4I5/5X,'IDR',T15,'IDT',T25,'BB',T35,'TO',T45,'TMS',T55,'TMS
     CP',T65,'CA',T75,'K3'/8F10.4/5X,'S',T15,'R',T25,'D',T35,'K2',T45,'C
     CPL',T55,'CPS',T66,'U',T75,'XX'/8F10.4/5X, 'DL',T15,'TM ',T25,'DD',
     CT35,' ZT',T45,'CJ',T55,'DSS',T65,  'RR',T75,'TR'/8F10.4/5X,  'CB'
     C,T15,'TA',T25,'TB',T35,'VG(1)',T45, '2',T55,'3',T65,'4',T75,'5'
     C/8F10.4/5X,'6',T15,'7',T25,'8',T35,'9',T45,'10',T55,'11',T65,'12'
     C,T75,'13'/8F10.4/5X,'14 ..... 15 ..... 16 .....  CKS ....  F
     C... PS .....  GG(1)  .. 2'/8F10.4/5X,'3',9X,'4 ..... 5  .....  6
     C ..... 7   ....  8  ..... 9   ..... 10'/8F10.4/5X,'11',9X,'12
     C ... 13  ..... 14 .....  15 ..... 16 .....DS1 ...  ACRM'/8F10.4/
     C5X,'GNU        AA         H          DDD        K4         K5' /8F10.4)
66    READ(5,10) F1,F2,F3,F4,F5,TI,CKL,YYY,FF2 ,FNU,TMS,TMSP,NU,DP,FR,WT
     C,R
10    FORMAT(8F10.4)
      IF(F1 )201,201,11
11    WRITE(6,12) F1,F2,F3,F4,F5,TI,CKL,YYY,FF2,FNU,TMS,TMSP,NU,DP,FR,WT
     C,R
12    FORMAT(//// 5X,'PELLET COMPOSITION :',10F10.4/ (12F10.4))
```

```
C..............CALCULATE  CONSTANTS
      DR=(R-RR    )/(NO-NOS   )
      XX=DR
      DS=DS1* (1.-S)
      AF=AF+1
      NOM=NO-1
      MM=NOS+1
      M=NOS-1
C..............INITIALIZE  VARIABLES
      KL=0
      LLL=0
      TFM=0.
      TGV=0
      J=0
      TIME1=0
      GR=0
      TGV1=0.
      Y=0.
      W1=F1
      W2=F2
      W3=F3
C..............INITIALIZE  GAS  VOLUMES  AND  TEMPERATURES ,
C..............AND  CALCULATE  AREA  AND  VOLUMES  OF  ELEMENTS
      DO  400 I=1,NO
      GV(I)=0.
400   EV (I)=0.
      DO 101 N=1,M
      T(N)=TMS
      E(N)=TMS
      A(N)=((N-.5)*IDR+R)**2
101   V(N)=.333*((N-.5)*IDR+R)**3 -.333*((N-1.5)*IDR+R)**3
      A(1)=A(1)*F
      DO 102 N=NOS,NUM
      T(N)=TO
      TT(N) =TO
      A(N)=((N-NOS- .5)*DR+RR )**2
102   V(N)=.333*((N-NOS-.5 )*DR+RR )**3-.333*((N-NOS-1.5)*DR+RR )**3
      V(NOS+1)   =   ((RR+DR/2)**3-RR**3)/3
```

```
      T(NO)=TO
      TT(NO)=TO
      T(1)=TO
      A(NO)=(R-XX/2)**2
      V(NO)=  (R** 3-(R-XX-DR/2) **3)/3
C.............SET  INITIAL  SHELL  THICKNESS
      BOND=R
      X=.10*IDR
      DM = X
      XN=X
      TIME=0.
C.............CALCULATION  OF  HEAT  TRANSFER  COEFFICIENT
88    ENU= GNU
      PNU=0.
      IF(TIME.LT.TTT) PNU=ENU*(1-TIME/TTT)
      IF (TIME.GT.0)ENU=2*BOND/(3.1416*     CKL/ DL/CPL*TIME)**.5+2+PNU
      IF (ENU.LT. NU      ) ENU=NU
      HTRANS=ENU*  CKL      /BOND/2.
      BCND=BOND+XN
      TIME= J * IDT
87    IF(T(1)-TI)85,90,9
85    IF(T(1)) 90,90,84
90    WRITE(6,73) TIME,T(1),T(NC),T(NOS)
73    FORMAT(' CHANGED    ',4F12.4)
      GO TO 200
84    KL = KL + 1
      J=J+1
      THICK=BOND-R
6     IF(TIME  .LT.Y) GO TO 4
      Y=Y+1
15    IF (TIME-TIME1) 16,16,17
C.............CALCULATION  OF  VOLUME  AND  RATE  OF  EVOLUTION  OF  GAS
17    TGV  =  0.
      DO  300  I=MM,NO
      EV(I)  =  VVV(T(I))
      GV(I)  =  EV(I) *3 *V(I)/(R**3-RR**3)
      TGV  =  TGV+GV(I)
```

```
300   TT(I) =T(I)
      GR  =  (TGV-TGV1)/(TIME-TIME1)*60.
      TGV1=TGV
      TIME1 = TIME
16    THICKN =(THICK    )*100.
      WW1=W1*100.
      WW2=W2*100
      WW3=W3*100.
      WRITE(6,70)TIME, THICKN ,TGV,GR,(T(I),I=1,NO),(GV(I),I=MM,NO),TFM
     C,WW1,WW2,WW3,ENU
70    FORMAT(/(10F12.2))
      IF(T(NOS).GE.1373.AND.TI.LT.1773.) GO TO 200
C.............CALCULATION  OF  TEMPERATURE  OF  THERMOCOUPLE
C.............AND  PARTICLE  ELEMENTES
4     HIN=AA*1E-14*(T(NOS+1)**4-T(NOS)**4)+BB*1E-4*(T(NOS+1) -T(NOS))
      E(NOS)=HIN*IDT/  DD+T(NOS)
      CALL  FFF (CPM,T(NOS+1), CKM , CS )
      HOUT=A(NOS+1)*(T(NOS+2)-T(NOS+1))*CKM        /DR
      E(NOS+1)=T(NOS+1)+(HOUT    -HIN)*IDT*3/((DR*.5+RR)**3-RR**3)/CPM/D
      NA=NOS+2
      DO 51 N=NA,NOM
      HIN=A(N-1)*(T(N-1)-T(N))
      HOUT=A(N)*(T(N+1)-T(N))
      CALL  FFF (CPM,T(N)     , CKM , CS )
51    E(N)=  T(N)    +CKM/D/CPM*IDT /V(N)  / DR*(HIN+HOUT)
      CALL  FFF (CPM,T(NO)    , CKM ,CS )
      HIN=-HOUT*CKM/DR
      HOUT=A(NO)*CS*(T(1)-T(NO))/XX
      CPC=CPM
      VV =(CPM*D*((R-XX)**3-(R-XX-DR/2)**3)+CPO*DSS*((R-XX/2)**3-(R-XX)
     S**3))/3
      E(NO)=(HIN+HOUT                                  )*IDT/VV+T(NO)
      N=1
C.............CALCULATION  OF  TEMPERATURE  AT  SURFACE  OF  PARTICLE
      IF(R+IDR-BCND)108,108,103
103   HIN=-HOUT
      CALL  FFF (CPO,T(1), CKM ,CS)
      VU = (DS*CPS*((R+X/2) **3-R**3)+ CPO *DSS*(R**3-(R-XX/2) **3))/3
```

```
      IF (BOND-R) 1,2,3
1     BOND=R
2     XN=0.
      X=0.
      IF (T(1)-TM) 1007,1008,1008
1007  HOUT = R**2*HTRANS* (TI-T(1))
      E(1) = (HIN+HOUT)*IDT/VU+T(1)
      IF (E(1)-TM) 203,203,1009
C.............CALCULATION OF MELTED FRACTION OF PARTICLE
1009  QR= (E(1)-TM)*VU/IDT
      GO TO 1010
1008  QR=R**2*HTRANS*(TI-TM)+HIN
1010  FM = QR*IDT*3/(R**3*D*ACRM)
      TFM=TFM+FM
      IF (TFM.LT.0.) E(1)=TM+QR*TFM/FM*IDT/VU
      IF (TFM.GE.0.) E(1)=TM
      IF (TFM-1.) 203,1005,1005
1005  WRITE (6,1006) TIME,TFM
1006  FORMAT(////10X,'TOTAL MELTING TIME =',2F10.2)
      GO TO 200
C.............CALCULATION OF TEMPERATURE AT SURFACE OF PARTICLE
C.............WITH SLAG SHELL THICKNESS LESS THAN IDR
3     A1 = ( R+.5*X )**2
      HOUT=A1*F*(TMS  -T(1))*CK(T(1))/X
      E(1)=(HIN+HOUT)*IDT/VU       +T(1)
      IF(E(1)-E(NO))29,30,30
29    E(1)=E(NO)
30    XN =-IDT/H/DS*(CK(T(1))*(E(1)-TMS)/X + (TI-TMSP) *HTRANS)
      IF(TIME.LE. WT.AND.YYY.GT.0.) XN=XN*FR
      BA=BOND+XN-R
      L=BA/IDR
      X=IDR*(BA/IDR-L)
      IF(DM - IDR/10.)9,8,8
9     DM = IDR/10.
8     IF(X-IDR/10)7,203,203
7     X = IDR/10.
203   IF(NOT - KL)2  ,2  ,99
```

```
C..............SUBSTITUTE FOR TEMPERATURES AND START A NEW ITERATION
99     DO 705 K=1,NO
705    T(K)=E(K)
       GO TO 88
C..............CALCULATION OF  TEMPERATURE AT SURFACE OF PARTICLE
C..............AND  THROUGHOUT  SOLID  SLAG  SHELL
108    HIN=-HOUT
       HOUT=A(1)*(T(2)-T(1))* CK(T(1))/IDR
       CALL  FFF (CPO,T(1)     , CKM , CS)
       VOL =(DS*CPS*((R+IDR/2)**3-R**3)+CPO*DSS*(R**3-(R-XX/2)**3))/3
       E(1)=(HIN+HOUT)*IDT/VOL      +T(1)
109    N=N+1
       IF (R+(N  )*IDR-BOND)115,115,110
110    AX=(BOND-X/2.)*(BOND-X/2.)
       VX=.333*(BOND-X/2)**3-.333*(BOND-IDR/2-X)**3
       HIN=A(N-1)*(T(N-1)-T(N))/IDR
       HOUT=AX*(TMS -T(N))/X
       E(N)=(HIN+HOUT)* CK(T(N))/DS/ CPS*IDT/VX+T(N)
       QQ= (E(N)+TMS)/2.
       XN=  -IDT/H/DS *(CK(QQ)*(E(N)-TMS) / X+ (TI-TMSP)* HTRANS)
       IF(TIME.LE. WT.AND.YYY.GT.0.) XN=XN*FR
       BA=BOND+XN-R
       L=BA/IDR
       X=IDR*(BA/IDR-L)
       IF(DM - IDR/10.)9,8,8
115    IF(N-NOS+1)116,90,90
116    A9 = (T(N+1)-T(N))*A(N) - (T(N)-T(N-1))*A(N-1)
       E(N) =CK(T(N))/DS/CPS/V(N) * IDT/ IDR*A9+ T(N)
       IF(E(N)-TMS  )109,109,402
402    E(N)=TMS
       GO TO 109
201    STOP
       END
```

2. Subprogram 1

```
C..............VOLUME  OF  GAS  EVOLVED  AT  TEMP.  Q
      FUNCTION  VVV(Q)
      COMMON VG(20), GG(20),PS,TA,CA,TB,F1 ,F2,F3 ,F4,F5,W1,W2,W3
     C,S,CKS ,CKL,    DP,DB ,K2,K3,K4,K5  ,DDD,FF2
      IF (F2.LE.0.OR.F3.LE.0) GO TO 1011
      I=( Q-273. )/ 100.
      IF (I.GT.0.)VVV=(VG(I)+(VG(I+1)-VG(I))*((Q-273.)/100.-I))*F2/FF2
      IF (I.EQ.0.) VVV= VG(1)*(Q-273.)/100.
      RETURN
1011  VVV=0.
      RETURN
      END
```

3. Subprogram 2

```
C..............SPECIFIC  HEAT  AND  THERMAL  CONDUCTIVITY OF DRI  PELLET
      SUBROUTINE  FFF (CPM,Q,CKM,CS)
      REAL K2,K3,K4,K5
      COMMON VG(20), GG(20),PS,TA,CA,TB,F1 ,F2,F3 ,F4,F5,W1,W2,W3
     C,S,CKS ,CKL,    DP,DB ,K2,K3,K4,K5  ,DDD,FF2
      J=Q/100.-1.
      CHECK=CM(Q)
      OO  = 3.04E-4*(1-EXP(-7.65E-4*Q))+ 4.08E-12*Q**3 *DDD
      CKM   =OO**PS*GG(J)**(W1*(1-PS))*K2** (W2*(1-PS))*K3**(W3 *(1-PS))
     C*K4**(F4*(1-PS))*K5**(F5*(1-PS))
      CS = CKM
      G= VVV(Q+.5) - VVV(Q-.5)
      IF(Q-TA)1001,1002,1002
1001  CPM = CHECK+1.29*G
      RETURN
1002  IF(Q-TA-8)1003,1003,1004
1003  CPM = CHECK+1.35*G+2.89E-3*CA-1.95E-2
      RETURN
1004  IF( Q.LT.TB) CPM=CHECK+1.47*G
      IF( Q.GE.TB ) CPM=CHECK+1.35*G
      RETURN
      END
```

4. Subprogram 3

```
C..............SPECIFIC  HEAT  OF  MATERIALS  USED  IN  CALCULATION
C..............OF  SPECIFIC  HEAT  OF  DRI  PELLET
      FUNCTION  CM(Q)
      COMMON VG(20), GG(20),PS,TA,CA,TB,F1 ,F2,F3 ,F4,F5,W1,W2,W3
     C,S,CKS ,CKL,    DP,DB ,K2,K3,K4,K5  ,DDD,FF2
      W1 = F1+1.01E-2*VVV(Q)
      W2 = F2-3.53E-3*VVV(Q)
      W3 = F3-8.02E-3* VVV(Q)
      IF (Q.LE.1033) C1=7.48E-2+1.06E-4*Q
      IF (Q.GT.1033.AND.Q.LE.1181)  C1=.161
      IF (Q.GT.1181) C1= 3.29E-2    +8.34E-5*Q
      C2 = .169+2.9 E-5*Q-9.7E2/Q**2
      IF (Q.LE.463) C3=.109+1.11E-4*Q
      IF (Q.GT.463) C3=.143+1.67E-5*Q
      C4 = .25+4.17E-5*Q-6.69E3/Q**2
      IF (Q.LE.848) C5=1.87E-1+1.36E-4*Q-4.49E3/Q**2
      IF (Q.GT.848) C5= 2.4 E-1+3.23E-5*Q
      CM = W1*C1+W2*C2+W3*C3+F4*C4+F5*C5
      RETURN
      END
```

5. Subprogram 4

```
C..............CONDUCTIVITY  OF  SOLID  SLAG  SHELL
      FUNCTION CK(Q)
      COMMON VG(20), GG(20),PS,TA,CA,TB,F1 ,F2,F3 ,F4,F5,W1,W2,W3
     C,S,CKS ,CKL,     DP,DB ,K2,K3,K4,K5  ,DDD,FF2
      PC = 3.04E-4*(1-EXP(-7.65E-4* Q))+4.08E-12* Q**3 *DP
      CK = CKS **(1-S)*PC**S
      RETURN
      END
```

6. Subprogram 5

```
C.............SPECIFIC HEAT AND THERMAL CONDUCTIVITY OF NI PARTICL
      SUBROUTINE FFF (CPM,Q, CKM ,CS)
      COMMON VG(20), GG(20),PS,TA,CA,TB,F1 ,F2,F3 ,F4,F5,W1,W2,W3
     C,S,CKS ,CKL,SG, DP,DR ,K2,K3,K4,K5 ,DDD
      J=Q/100.-1.
      GG  = 3.04E-4*(1-EXP(-7.55E-4*Q))+ 4.08E-12*Q**3 *DDD
      CKM=GG**PS*GG(J)**(1-PS)
      CS = CKM
      IF(Q.LT.903)CPM=.13-8.01E-5*Q-2.27E3/Q**2
      IF(Q.GE.903)CPM=.12+1.70E-5*Q-3.80E3/Q**2
      RETURN
      END
```

7. Definition of Terms

A(N) = AREA BETWEEN NODES N AND N+1 AT DISTANCE IDR/2
AA = CONSTANT FOR HEAT TRANSFER TO THERMOCOUPLE
ACRM =HEAT OF FUSION OF PARTICLE
ALL = TERMAL DIFUSIVITY OF LIQ. SLAG
ALP = TERMAL DIFUSIVITY OF SOLID SLAG

BB = CONSTANT FOR HEAT TRANSFER TO THERMOCOUPLE
BK =THERMAL CONDUCTIVITY OF POROUS LIQ. SLAG
BOND = R + THICKNESS OF SHELL

C1 = SPECIFIC HEAT OF IRON
C2 = SPECIFIC HEAT OF "FEO"
C3 = SPECIFIC HEAT OF FE3C
C4 = SPECIFIC HEAT OF AL203
C5 = SPECIFIC HEAT OF SI02
CA = CARBON CONTENT OF PARTICLE AT TEMP. TA
CB = CARBON CONTENT OF PARTICLE AT TEMP. TB
CC = CONSTANT FOR HEAT TRANSFER TO THERMOCOUPLE
CK = THERMAL CONDUCTIVITY OF POROUS SOLID SHELL
CKL =THERMAL CONDUCTIVITY OF LIQ. SLAG
CKM =THERMAL CONDUCTIVITY OF PARTICLE
CKS =THERMAL CONDUCTIVITY OF SOLID SLAG
CM = SPECIFIC HEAT OF D-R MATERIAL
CPL =SPECIFIC HEAT OF LIQ. SLAG
CPM =SPECIFIC HEAT OF PARTICLE
CPO =SPECIFIC HEAT OF EXTERNAL ELEMENT OF PARTICLE
CPS =SPECIFIC HEAT OF SOLID SHELL
CS =CONDUCTIVITYT OF EXTERNAL ELEMENT OF PARTICLE

D = DENSITY OF PARTICLE
DB = PORE DIAMETER IN LIQ. SLAG
DD = CONSTANT FOR HEAT TRANSFER TO THERMOCOUPLE
DDD = PORE DIAMETER IN PARTICLE
DL = DENSITY OF LIQ. SLAG
DP = PORE DIAMETER IN SOLID SLAG
DR =WIDTH OF AN ELEMENT IN PARTICLE
DS = DENSITY OF POROUS SOLID SHELL
DS1 = DENSITY OF SOLID SLAG
DSS = DENSITY OF EXTERNAL ELEMENT OF PARTICLE

E(N) = TEMP. AT NODE N FOR PRESENT TIME
EE = CONSTANT FOR HEAT TRANSFER TO THERMOCOUPLE
EV(N)= GAS VOL. PER GRAM OF SPONGE ELEMENT N

```
F     =  CORRECTION  FACTOR  FOR  PARTICLE-SLAG  INTERFACE
F1    =  INITIAL  WT.  FRACTION  OF  IRON  IN  D-R  PELLET
F2    =  INITIAL  WT.  FRACTION  OF  "FEO"  IN  D-R  PELLET
F3    =  INITIAL  WT.  FRACTION  OF  FE3C  IN  D-R  PELLET
F4    =    WEIGHT      FRACTION  OF  AL2O3  IN  D-R  PELLET
F5    =    WEIGHT      FRACTION  OF  SIO2  IN  D-R  PELLET
FNU   =  NUSSELT  NUMBER


G     =  SPECIFIC  GAS  VOLUME
GG    =  THERMAL CONDUCTIVITY OF METAL AS A FUN. OF TEMP.
GR    =  RATE OF GAS EVOLUTION FROM PARTICLE
GV(I)=  VOL.  FRACTION  OF  GAS  EVOLVED  FROM  ELEMENT  I


H     =HEAT OF FUSION OF SLAG
H1    =  HEAT  OF  FUSION  OF  IRON
H2    =  HEAT  OF  FUSION  OF  'FEO'
H3    =  HEAT  OF  FUSION  OF  FE3C
H4    =  HEAT  OF  FUSION  OF  AL2O3
H5    =  HEAT  OF  FUSION  OF  SIO2
HTRANS=  HEAT TRANSFER COEFFICIENT


IDR   =WIDTH OF AN ELEMENT IN SLAG
IDT   = LENGTH OF A TIME ELEMENT


K2    =  THERMAL CONDUCTIVITY OF 'FEO'
K3    =  THERMAL CONDUCTIVITY OF FE3C
K4    =  THERMAL CONDUCTIVITY OF AL2O3
K5    =  THERMAL CONDUCTIVITY OF SIO2


N1    =  NO.  OF  TEMP.  INTERVALS  FOR  GG  AND  VG
NO    =  NO. OF NODES
NOS   =  NO. OF NODES IN SLAG
NOT   =  NO. OF TIME STEPS ALLOWABLE


OO    =  THERMAL CONDUCTIVITY OF PARTICLE  PORES
TGV   =  TOTAL  GAS  VOL.  EVOLVED  FROM  PELLET


PS    =  POROSITY OF PARTICLE


Q     =  TEMPERATURE  OF  SPONGE
QR    =  FLOW OF HEAT FOR MELTING PARTICLE


R     =  RADIUS OF PARTICLE
RR    = RADIUS  OF  THERMOCOUPLE  HOLE
```

S = POROSITY OF SLAG SHELL
SS = POROSITY OF LIQ. SLAG

T(N) = TEMP. AT NODE N FOR PAST TIME
TA = TEMP. AT WHICH SOLID-SOLID TRANSFORMATION STARTS
TB = TEMP. AT WHICH SOLID-SOLID TRANSFORMATION ENDS
TFM = VOL. FRACTION OF PARTICLE MELTED
TI = TEMP. OF BULK LIQ. SLAG
TIME = TIME AFTER IMMESION OF PARTICLE
TM = MELTING TEMP. OF PARTICLE
TMS = SOLIDUS TEMP. OF SLAG
TMSP = LIQUIDUS TEMP. OF SLAG
TO = INITIAL TEMP. OF PARTICLE
TR = MELTING RANGE OF SLAG

U = VISCOSITY OF SLAG , POISE

V(N) = VOL. AT NODE N
VG(I) = VOL. OF GAS EVOLVED FROM 1 GRAM OF SPONGE AT TEMP. T(I)
VOL = HALF OF TOTAL VOL. OF EXTERNAL ELEMENT ON PARTICLE AND ADJACENT ELEMENT IN SLAG
VVV = VOL. OF GAS EVOLVED FROM 1 GRAM OF DRI

W1 = WT. FRACTION OF IRON IN D-R PELLET
W2 = WT. FRACTION OF 'FEO' IN D-R PELLET
W3 = WT. FRACTION OF FE3C IN D-R PELLET

X = DIS. FROM FURTHEST ELEMENT TO THE MOVING BOUNDARY
XN = THICKNESS CHANGE IN ONE TIME STEP
XX = THICKNESS OF EXTERNAL ELEMENT OF PARTICLE

YYY = GAS BUBBLING CONTROLLER - 1 . BUBBLING
- 0 . NO BUBBLING

## BIBLIOGRAPHY


1. J. F. Elliott: Proceedings, 34th Ironmaking Conference, AIME, Toronto, Canada, April 1975, vol. 34, pp. 216-227.
2. J. R. Miller: Iron and Steel Engineer, Sep. 1977, pp.45-50.
3. J. M. Bertram: Iron and Steel Engineer, 1972, vol.49, pp. 31-40.
4. T. E. Dancy: Met. Trans., 1977, vol. 8B, pp.201-213.
5. J. R. Miller: Scientific American, 1976, vol. 235, pp. 68-80.
6. Anon: Iron and Steelmaker, Oct. 1976, pp. 12-44.
7. J. R. Miller: Iron and Steelmaker, 1976, vol. 3, pp. 44-46.
8. R. G. Quintero: Iron and Steel Int., 1975, vol. 48, pp. 437-440.
9. J. M. Pena and D. Radke: J. of Metals, 1971, vol.23, pp. 27-32.
10. F. W. Starrat: J. of Metals, 1959, vol. 59, pp. 315-318.
11. C. A. Schroer and D. W. Clark: Iron and Steel Engineer, 1976, vol. 53, pp. 21-25.
12. L. Tellier, I. Mozer, and S. F. Turcotte: Iron and Steel Engineer, 1974, vol. 51, pp. 33-39.
13. P. Kehl: Iron and Steel Engineer, 1973, vol. 50, pp. 35-39.
14. J. E. Bonestell and W. Pietsch: Conf., SEAISI Direct Reduction, Sep. 1977, Bangkok, Thailand.
15. H. D. Pantke: Proceedings, Third International Iron and Steel Congress, TMS-AIME, Chicago, Illinois, April, 1978.
16. N. T. Evans: ibid.
17. R. G. Quintero: ibid.
18. K. A. Kulberg: Iron and Steelmaker, 1976, vol. 3, pp. 35-39.

19. R. J. Oehlberg: Iron and Steel Engineer, 1974, vol. 51, pp. 58-61.

20. J. W. Brown, D. L. Campbell, A. L. Saxton, and J. W. Carr: J. of Metals, 1966, vol. 18, pp. 237-242

21. T. F. Reed, J. C. Agrawal, and E. H. Shipley: J. of Metals, 1960, vol. 12, pp. 317-320.

22. A. Chatterjee and P. K. Chakravarty: Iron and Steel Int., 1977, vol. 50, pp. 245-252.

23. G. Meyer: Iron and Steel Int., 1976, vol. 49, pp. 103-112.

24. A. A. Albert: Conference, Metallurgists, CIM, Vancouver, 1977.

25. A. Barbi: Iron and Steel Int., 1977, vol. 5o, pp. 229-236.

26. A. Chatterjee and P. K. Chakravarty: Iron and Steel Int., 1977, vol. 50, pp. 245-252.

27. J. Mackenzie: J. of Iron and Steel Inst., June 1969, pp. 765-771.

28. D. W. R. George and T. R. Meadowcroft: CIM Bulletin, Jan. 1976, pp. 94-98.

29. W. Pietsch: Conference, AFS East Coast Regional Foundry, Tamiment, Pennsylvania, USA, Nov. 1977.

30. The Making, Shaping and Treating of Steel, H. E. MCGannon, Ed., 1971.

31. J. F. Elliott, J. Nauman, K. Sadrezhaad: Proceedings, 3rd International Iron and Steel Congress, TMS-AIME, Chicago, Illinois, April 1978.

32. H. Knop, H. Nagel and W. Thumm: Int. Iron and Steel Congress, Dusseldorf, 1974.

33. W. Pietsch: SME-AIME Fall Meeting, Denver, 1976.

34. G. Post and D. Ameling: I & SM, April 1975, pp. 43-51.

35. V. F. Knyazev and I. P. Bardin: U.N. Economic Commission for Europe Steel Committee, Bucharest, 1976.

36. U. Pohl and H. K. Schott: ibid.

37. H. Nagel; ibid.

38. A. G. E. Rabiette: Electric Melting Practice, Chapters 2 and 4, J. Wiley, New York, 1972.

39. J. G. Sibakin, P.H. Hookings, and G. A. Roeder: J. of Iron & Steel Inst., Oct. 1967, pp. 1005-1017.

40. J. W. Brown and R. L. Reddy: ILAFA Direct Reduction Congress, Macuto, Venezuela, July 1977.

41. K. R. Bleimann and D. J. Werner: Iron and Steelmaker, 1977, vol. 4, pp. 47-51

42. D. Engledow and F. D. Winter: Ironmaking Steelmaking, 1976, vol. 3, pp. 359-367.

43. J. Celada and R. Quintero: Proceedings, Electric Furnace, pp. 41-46, 1974.

44. J. F. Elliott and F. E. Brantly: I & SM, May 1976, pp. 32-35.

45. J. F. Elliott and J. K. Write: I & SM, May 1976, pp. 32-35.

46. B. Rollinger: I & SM, 1975, vol. 2, pp. 10-17.

47. K. Schermer, Benoni, and Sudafrika: Radex-Rundschau, 1976, heft 2, pp. 675-698.

48. M. Rigaud, A. H. Marquis, and T. E. Dancy: Ironmaking & Steelmaking, 1976, No.6, pp. 366-372.

49. N. Cavagan and T. H. Harris: J. Iron & Steel Inst., 1970, vol. 208, pp. 529-537.

50. J. M. Miller: Blast Furnace and Steel Plant, 1970, vol. 58, part I, p. 408, part II, p. 471.

51. J. L. A. Perez, J. S. Rodriguez, E. A. Bryan, and H. N. Hughes: Iron Steel Eng., 1963, vol. 40, No.8, pp. 69-76.

52. J. Stalhed: J. Met., 1957, vol. 9, pp. 246-249.

53. J. A. Innes and H. F. Melonney: J. of Iron and Steel Inst., Nove. 1969, pp. 1437-1443.

54. A. Barbi: Iron Steel Inst., 1976, vol. 49, pp. 257-262.

55. A. I. Brown and S. M. Marco: Int. to Heat Transfer, 3rd ed., chap. 14, McGraw-Hill, New York, 1958.

56. G. M. Dusinberre: Heat Transfer Calculations by Finite Differences, International Textbook Co., 1961.

57. J. F. Elliott and J. D. Nauman: Proceedings, Metal-Slag-Gas Reactions and Processes, pp. 238-250, Electrochem. Soc., Toronto, Canada, 1975.

58. J. Nauman, Sc.D. Thesis, Mass. Inst. Tech., 1976.

59. J. Nauman, G. Foo, and J. Elliott: Proceedings, Copper Extraction and Refining, pp. 237-258, AIME, Las Vegas, Nevada, 1976.

60. O. Ehrich, Y. Chung, and K. Schwerdtfeger: Int. J. Heat Mass Transfer, 1978, vol. 21, pp. 341-349.

61. J. George and P. S. Damle: Int. J. Num. Meth. Engag., 1975, vol. 9, pp. 239-245.

62. P. B. Grimado and B. A. Boley: Int. J. Num. Meth. Engng., 1970, vol. 2, pp. 175-188.

63. R. I. Pedroso and G. A. Domoto: J. Heat Transfer, 1973, vol. 7, pp. 42-46.

64. C.-L. Huang and Y. -P. Shih: Chem. Engng. Sci., 1975, vol. 30, pp. 897-906.

65. Y. Chuang and O. Ehrich: Int. J. Heat Trans., 1974, vol. 17, pp. 945-953.

66. J. Kern and G. L. Wells: Met. Trans., 1977, vol. 8B, pp. 99-107.

67. Y. Kim and R. D. Pehlke: Met. Trans., 1975, vol. 6B, pp. 585-591.

68. J. F. Elliott: Canadian Met. Quarterly, 1975, vol. 14, pp. 199-204.

69. H. A. Fine, T. Engh, and J. F. Elliott: Met. Trans., 1976, vol. 7B, pp. 277-285.

70. G. Foo, Sc.D. Thesis, Mass. Inst. Tech., 1977.

71. G. Post and D. Ameling: I & SM, April 1975, pp. 43-51.

72. H. S. Carslaw and J. F. Jaeger: Conduction of Heat in Solids, 2nd ed., Oxford Univ. Press, London, 1959.

73. R. L. Gibby and J. L. Bates: Proceedings, 10th Thermal Conductivity Conf., Newton Mass., vol. 4, pp. 7-8, Sept. 1970.

74. T. Murase and A. McBirney: Science, 1970, vol. 170, pp. 165-167.

75. J. L. Bates: Proceedings, 6th International Conf. on Magnetohydrodynamic Electrical Power Generation, vol. 2, Open Cycle Components and Materials, Washington, D.C., June 1975.

76. H. Fujisawa, N. Tuji, H. Mizutani, H. Kanamori and S. Akimoto: J. of Geophys. Res., vol. 73, 1968, pp. 4727-4733.

77. J. F. Elliott, M. Gleiser, and V. Ramakrishna: Thermochemistry for Steelmaking, Addison-Wesley Press, Reading, Mass., 1965.

78. B. B. Mikic and W. M. Rohsenow: J. Heat Trans., vol. 91, 1969, pp. 245-253.

79. M. Ben-Amoz: Int. J. Eng. Sci., vol. 8, 1970, pp. 39-47.

80. G. P. Marino: WAPD-TM-807, UC-25, U.S. Atm. Energy Com., Feb. 1970.

81. A. L. Loeb: J. Amer. Cer. Soc., vol. 37, 1954, pp. 96-99.

82. Y. S. Touloukian, R. W. Powell, C.Y. Ho, and P.G. Klemers, eds. Thermophysical Properties of Matter, Plenum Pub. Co., New York, 1970.

83. J. Kon and A. Fortini: Int. J. Heat, vol. 16, 1973, pp. 2013-2022.

84. Y. E. Lee and D. R. Gaskell: Met. Trans., vol. 5, 1974, pp.853-860.

85. J. Szekely and N. J. Themelis: Rate Phenomena in Process Metallurgy, John Wiley & Sons, Inc., New York, 1971.

86. J. D. Hellums and S. W. Churchill: A.I. Ch. E. Journal, Part I & II, vol. 8, No.5, 1962, pp. 690-695.

87. G. H. Geiger and D. R. Poirier: Transport Phenomena in Metallurgy, Addison-Wesley Co., California, 1973.

88. E. Schmit: Chemie-ing. - Techn., vol. 28, Jahrg. Nr. 3.

89. M. Y. Chow and R. G. Akins: J. Heat Trans., vol. 97, No.1, 1975, pp. 54-59.

90. W. Woodside and J. H. Messmer: J. Appl. Phy., vol. 32, No.9, 1961, pp. 1688-1711.

91. C. Y. Han and P. Griffith: Int. J. Heat Mass. Trans., vol.8, 1965, pp. 887-917.

92. I. Mellan: Industrial Solvents Handbook, Noyes Data Corp., 1970.

93. N. Seving, Ph.D. Thesis, Mass. Inst. Tech., 1976.

94. O. Kubaschewski and E. LL. Evans: Metallurgical Thermochemistry, 3rd ed., Pergamon Press, New York, 1958.